Alma Mater Studiorum

Università di Bologna

DOTTORATO DI RICERCA IN

Scienze Ambientali:

Tutela E Gestione Delle Risorse Naturali

Ciclo XXIII

Settore Concorsuale 04/A4 - GEOFISICA
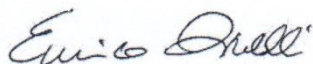**Settore scientifico-disciplinare di afferenza:** GEO/12

"Studio della fascia costiera e dei mari italiani mediante l'analisi integrata di dati da satellite e in situ"

"Satellite and in situ data integrated analysis to study the upper ocean an coastal environment of the Italian seas "

Presentata da: Eleonora Rinaldi

Coordinatore Dottorato   Relatore

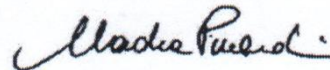Enrico Dinelli   Nadia Pinardi

                                                              Co-relatore

                                                              Rosalia Santoleri

Esame finale anno 2012

Acknowledgment

I am very thankful to Dr. Bruno Buongiorno Nardelli, Dr. Simone Colella and Dr. Gianluca Volpe for their patience and scientific guidance in these years.

A special thank you goes to Dr. Rosalia Santoleri for her help, assistance and scientific support.

I thank all the Group for Satellite Oceanography at CNR for making the workplace a friendly place, as well as for their willingness to share experiences and knowledge.

I thank Dr Nadia Pinardi for her insightful scientific discussions.

Thank you to my family for having always believed in me.

This thesis is dedicated to Andrea, Fabrizio and Lucrezia who will be born soon. They make my life happy.

Index

Abstract

The thesis objectives are to develop new methodologies for study of the space and time variability of Italian upper ocean ecosystem through the combined use of multi-sensors satellite data and in situ observations and to identify the capability and limits of remote sensing observations to monitor the marine state at short and long time scales. Three oceanographic basins have been selected and subjected to different types of analyses.

The first region is the Tyrrhenian Sea where a comparative analysis of altimetry and lagrangian measurements was carried out to study the surface circulation. The results allowed to deepen the knowledge of the Tyrrhenian Sea surface dynamics and its variability and to defined the limitations of satellite altimetry measurements to detect small scale marine circulation features. Channel of Sicily study aimed to identify the spatial-temporal variability of phytoplankton biomass and to understand the impact of the upper ocean circulation on the marine ecosystem. An combined analysis of the satellite of long term time series of chlorophyll, Sea Surface Temperature and Sea Level field data was applied. The results allowed to identify the key role of the Atlantic water inflow in modulating the seasonal variability of the phytoplankton biomass in the region. Finally, Italian coastal marine system was studied with the objective to explore the potential capability of Ocean Color data in detecting chlorophyll trend in coastal areas. The most appropriated methodology to detect long term environmental changes was defined through intercomparison of chlorophyll trends detected by in situ and satellite. Then, Italian coastal areas subject to eutrophication problems were identified. This work has demonstrated that satellites data constitute an unique opportunity to define the features and forcing influencing the upper ocean ecosystems dynamics and can be used also to monitor environmental variables capable of influencing phytoplankton productivity.

Introduction

The oceans cover over 70% of Earth's surface and representing over 95% of the biosphere they contribute to the mitigation of climate change. The oceans are the main reserve and distributor of heat and salts, they affect the weather, modulate evaporation, precipitation and vapour in the atmosphere. The intensification of human activities in coastal areas, in combination with climate changes that are occurring on a global scale, is dramatically altering the biodiversity of marine environments. The forecast of global change include both direct and indirect effects on the structure and functioning of the oceans, including the alteration of the circulation of water masses (Shaffer et al.,2000) and changes in the composition of living communities.

In recent decades the planet's temperature is increasing (IPCC, 2007), this increment of the temperature is caused by the progressive increase of anthropogenic CO_2 (a greenhouse gas) concentration in the atmosphere (Cox et al., 2000; IPCC, 2001; Sarmiento et al., 2004). The oceans play a fundamental role in the carbon cycle as the concentration of CO_2 is in dynamic equilibrium with that in the atmosphere: an increase in the atmospheric concentration of CO_2 enhances the ocean absorbing capacity. The exchange of CO_2 between atmosphere-ocean occurs through the so-called biological pump. Its refers to the sinking of organic matter from the surface productive layers to deep waters in the oceans.

The efficiency of the biological pump is linked to the photosynthesis process that in the marine environment is performed by phytoplankton (i.e., the unicellular microscopic algae living in the upper layer of all water bodies across the world). The phytoplankton through photosynthesis, allows the transformation of inorganic carbon into organic carbon and its storage in biomass. The speed with which this biomass is created and made available to the successive trophic levels is called primary production. Quantifying the carbon flux into the ocean through the marine primary productivity, and understanding the mechanisms that might control it, are of crucial importance for defining the planet's carbon budget and its link to climate change.

In recent years the science has intensively concerned to understand what are the processes that regulate the global carbon cycle and how the CO_2 fluxes between the atmosphere and other compartments of the planet vary over time. Moreover a lot of effort has been made to understand the physical processes affecting the spatial distribution and temporal development

of phytoplankton biomass. The growth-limiting factor of phytoplankton is the availability of light and nutrients (Parsons et al., 1983). Those depend in turn on physical processes such as general ocean circulation, deep water formation, mixed-layer dynamics, upwelling and the solar cycle (Behrenfeld et al., 2006). It is so obvious the importance of study and understand the phenomena that determine the nutrient enrichment in the surface layers of water as the Sea Surface Temperature and the marine circulation. This later other than have influence on nutrient budget are able to condition the dynamics of the biomass of some pelagic fish species (Cutitta et al.,2003, Garcia Lafuente et al.,2003). A detailed knowledge of the marine circulation is therefore of crucial importance for the correct management of fisheries activities and more generally for the study of the pollution dispersion and transport.

Satellite data represent an essential observational tool which offers an unique perspective on the natural environment. Thanks to the synoptic view and the high sampling frequency and high spatial resolution, remotely sensed data have been successfully used to provide unique and important information on surface phytoplankton distribution, Sea Surface Temperature and sea surface currents. However, the satellites investigate only the first layer of the sea, furthermore, the presence of clouds over the area of acquisition affects the availability of satellite data in the visible and infrared bands. The integration between in situ measurements and satellite observations permits to overcome the inherent limitations of both methods of data collection. Indeed, the in situ measurements, are able to sample the entire water column and to be operational even when the satellite due to cloud cover, is not able to give information about the sea area investigated. Nevertheless, due to the fact that they are point data, the coverage of a large portion of the sea requires long operation times.

The two main objectives of this work are:

1) to develop new methodologies for studying the space and time variability of Italian upper ocean ecosystem through the combined use of multi-sensors satellite data and in situ observations;

2) to identify the capability and limits of the of remote sensing observations to monitor the marine state at short and long time scales.

Three different oceanographic basins have been selected and subjected to different types of analysis.

The first region examined is the Tyrrhenian Sea. This basin has been chosen because all the previous studies indicate that the Tyrrhenian basin is an extremely active region of the Mediterranean Sea, characterized by a rich mesoscale dynamics. Moreover, even if the Tyrrhenian Sea is a basin of transition for the water masses that through it reach the north

western regions of the Mediterranean Sea, all the previous study result do not allow an adequate evaluation on the role of this basin plays in the general Mediterranean Sea circulation. The peculiarity of the study done in this thesis is a comparative analysis of altimetry and lagrangian measurements. This method allows to complement and compare the information provided by two datasets separately and aiming to quantify the impact of the different sampling strategy of the two instruments. The purpose of this analysis was to deepen the knowledge of the Tyrrhenian Sea surface dynamics and its variability.

The channel of Sicily was chosen because it plays a key role for the exchange of water masses and their physical-biochemical properties between the Eastern and the Western Mediterranean. Thus, it represents a crucial area for both understanding the basin scale variability and for the important fishery activities carried out by the countries bordering the Channel. The study on this region aims to identify the spatial-temporal variability of phytoplankton biomass and to understand the impact of the upper ocean circulation on the marine ecosystem. To achieve this objectives an combined analysis of the satellite of long term time series of chlorophyll (the most widely used proxy for the study of the distribution of phytoplankton biomass), Sea Surface Temperature and Sea Level field data was applied.

The last region examined is the Italian coastal marine system. Despite the ecologically and socio-economically importance of this area there is a strong scientific consensus that coastal marine ecosystems, along with the goods and services they provide, are threatened by anthropogenic and global climate change. This thesis explores the potential capability of Ocean Color data in detecting chlorophyll trend in coastal areas, indeed remotely-sensed data provides a method to examine trends in the coastal environment without the necessity of in situ sampling observations. It should be noted that, despite the fact that the Sea-viewing Wide Field-of-view Sensor (SeaWiFS) provides ten years of nearly continuous, consistent and reliably-calibrated record of remotely-sensed chlorophyll, in coastal waters remotely-sensed data are less accurate than in the open ocean due to increased turbidity in coastal waters and possible the bottom reflectance problems. For this reason, before to determine the trend of chlorophyll through the satellite data a comparison between them and in situ data was made.

The thesis is organized as follows: chapter 1 presents and overview of the Mediterranean Sea circulation and reviews the present main knowledge physical and biological oceanography of the three study areas. In Chapter 2, the basic physical principles of ocean remote sensing are described. Moreover a short state of the art of satellite oceanography is presented. Chapter 3 presents the comparison between langrangian and altimeter data in the Tyrrhenian Sea and the surface circulation as revealed by both dataset is described. Chapter 4 shows the

phytoplankton biomass space-time variability in the Sicily Channel and its dependence from physical forcing as Sea Surface Temperature and surface geostrophic circulation. In Chapter 5 the analyses to detect chlorophyll trends along the Italian coasts from Ocean Colour data is investigated. Moreover the phytoplankton trends along the Italian coast was discussed. Finally, Chapter 6 draws the main conclusions of this thesis.

Chapter 1

Italian seas and coasts

This chapter overviews the state of the art of the Italian Sea oceanography and of the study regarding the chlorophyll trend along the Italian coasts.

First an overview of the Mediterranean sea oceanography is presented, then the state of the art of each geographic area examined in this thesis is discussed.

1.1   The Mediterranean Sea

The Mediterranean Sea (MED) is a semi-enclosed basin connected to the Atlantic Ocean through the Gibraltar Strait. It is divided into two main sub-basins, the Eastern (EMED) and Western (WMED) Mediterranean by the strait of Sicily. Its circulation is schematically decrypted as a three-layer system: the surface layer, that is 50-200 m thick, the intermediate layer, that occupies a thickness between 200 and 600 m and the deep layer (Lacombe and Tchernia, 1972; Lacombe et al., 1981).

The Atlantic Water (AW) enters through the Strait of Gibraltar at the surface, this "sweet" water east of the Strait due to evaporation and mixing increases its salinity migrating to the Levantine Basin (Fig 1.1 a). The temporal scales of this thermohaline circulation is approximately 100 years (Roether and Schlitzer,1991). During winter, when strong winds intensify evaporation producing a process of vertical convection, in correspondence of the Rhodes cyclonic gyre the MAW sinks give origin to the Levantine Intermediate Water (LIW) (Malanotte-Rizzoli e Hecht,1988; Lascaratos et al., 1993) (Fig 1.1 b).

Different processes of transformation of surface water in deep water characterize the EMED and WMED, however in both basin these process have a sub basin scale and they are characterized by cyclonic circulation (Fig 1.1 c). (Gascard, 1978; Anati, 1981).

In particular, in the EMED the increase in density, which determines the sinking of surface waters, is due to the increase of salinity resulting from the evaporation. An exception is represented by the Adriatic Sea, in which the deep water is originating by a cooling process due to the Bora, a particularly cold and dry wind that blows with extraordinary intensity. This dense water flows along the Italian coast and it mixes with LIW in the Ionian, giving rise to one of the main sources Mediterranean abyssal water. Another site of formation of

intermediate and deep water in EMED is located in the northern Aegean in correspondence to the vortex in the south of Rhodes, as written previously.

In the WMED the deep water is formed by heat loss and subsequent sinking of the waters due to the presence of cold winds. This phenomenon occurs in the Gulf of Lion due to the Mistral wind (Benzohora e Millot,1995; Millot,1999;Rhein et al.,1999), and in the Thyrrhenian Sea (Hopkins,1985).
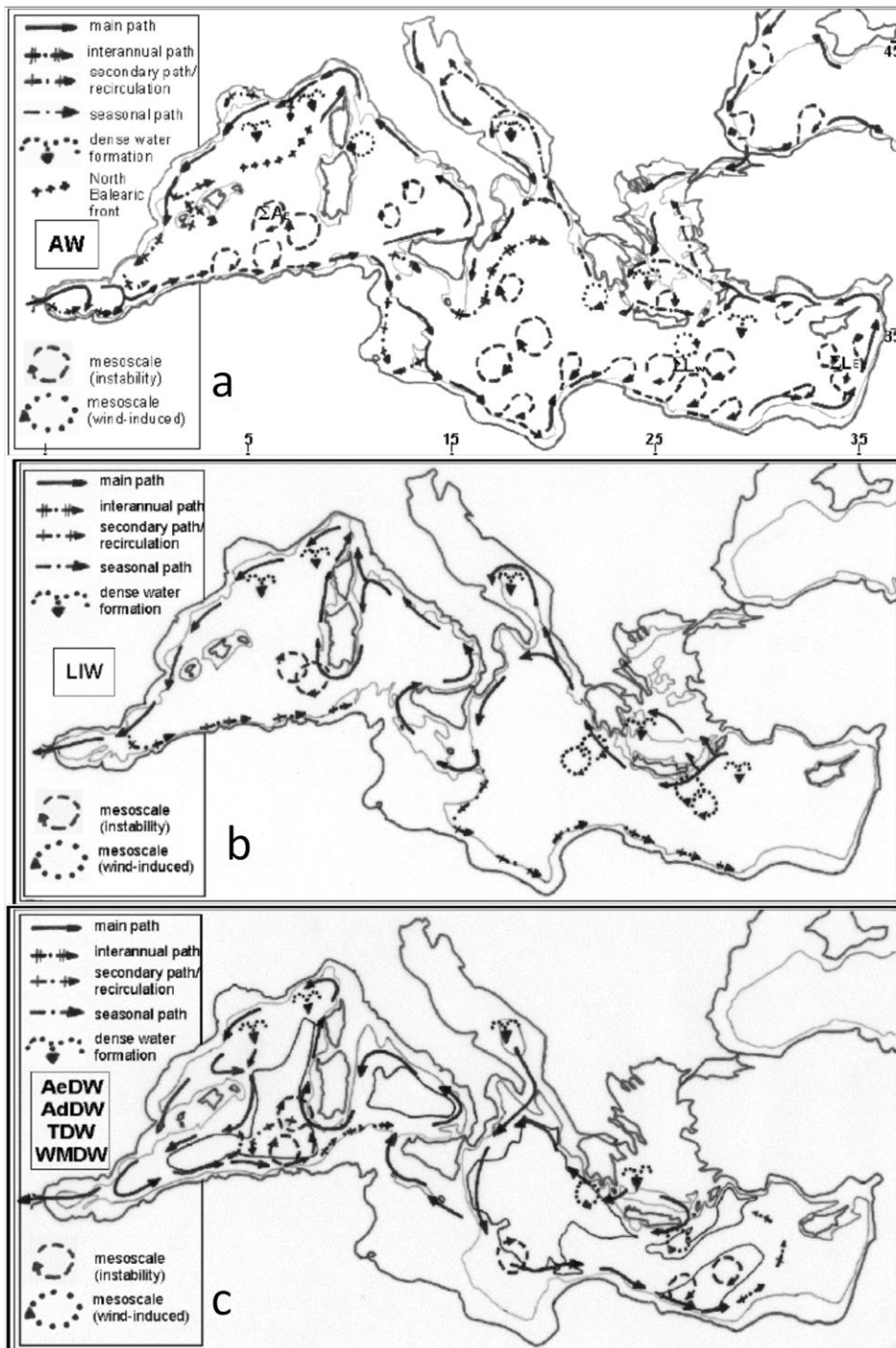
Figure.1 Schemes of the Mediterranean Sea surface layer(a), intermediate layer (b) and deep layer (c) (from *Millot, Taupier, 2004*).

1.2   The Tyrrhenian Sea

Although the main characteristics of the Mediterranean Sea are well known, our knowledge of the processes taking place in one of its sub-basins, the Tyrrhenian Sea, is not yet fully exhaustive.

The Tyrrhenian Sea is one of the major sub-basins of the Mediterranean. It has a triangular shape and a very complex bathymetry and is connected to the outer Mediterranean Sea with the Corsica Channel (north) and a broad opening to the south-west, between Sardinia and Sicily (Fig 1.2). This basin plays an important role in the transformation of the main Mediterranean intermediate and deep waters (Astraldi and Gasparini, 1994, Gasparini et al., 1999, Sparnocchia et al., 1999) occasionally resulting in the formation of Tyrrhenian dense water (Astraldi and Gasparini, 1994).

Figure 1.2 Bottom topography of Tyrrhenian Sea.

Even though the first investigations on the Tyrrhenian date from hundred years ago (Nielsen, 1912) and the basin was the object of a thorough investigation carried out in the framework of the International Geophysical Year (Aliverti et al.,1968), direct measurements of velocities and transports in the Tyrrhenian Sea are still very sparse. Available information are mainly based, on one hand, on the in-situ measurements collected in the north part of the basin during "TEMPO" surveys in the late '80s/early '90s (Astraldi and Gasparini, 1994, and Marullo et al., 1994) and by the limited data collected at its southern entrance by Sparnocchia et al.(1999).

These data allowed a satisfactory hydrological characterization of the Tyrrhenian Sea, even though the mechanisms of observed long term changes still have to be fully understood. On the other hand, the informations on the circulation in the basin, especially at the surface, are much less accurate. The traditional concept (Millot, 1987 and 1999) of a cyclonic circulation at all levels appears to be far too schematic: recent Eulerian (for the deep layer, P. Falco, personal communication on unpublished data) and Lagrangian studies (we refer in particular to the MedArgo data regarding the intermediate water circulation, Poulain et al., 2007) show a remarkable and unexpected complexity. northern portion of the basin where TEMPO data were available, whereas the southern part has not been practically explored.

In the past, efforts have been concentrated on some elements of the surface dynamics of the the northwest Tyrrhenian is dominated by the presence of an important feature, the North Tyrrhenian Cyclone (NTC, see Marullo et al., 1994), induced by strong north-westerly winds channelled by the Strait of Bonifacio, presenting a strong seasonal variability and affecting the coastal currents flowing along the north-eastern flank of the basin. Past observations show that this northern gyre, whose dimensions are of the order of 100 km, displays a strong seasonal dependence in size and position. During winter it is stretched along the meridional direction in the western part of the basin, while in summer it is zonally oriented (Artale et al.,1994, Astraldi e Gasparini, 1994) capturing a weak flow along the Italian Peninsula (Fig 1.3 a,b)
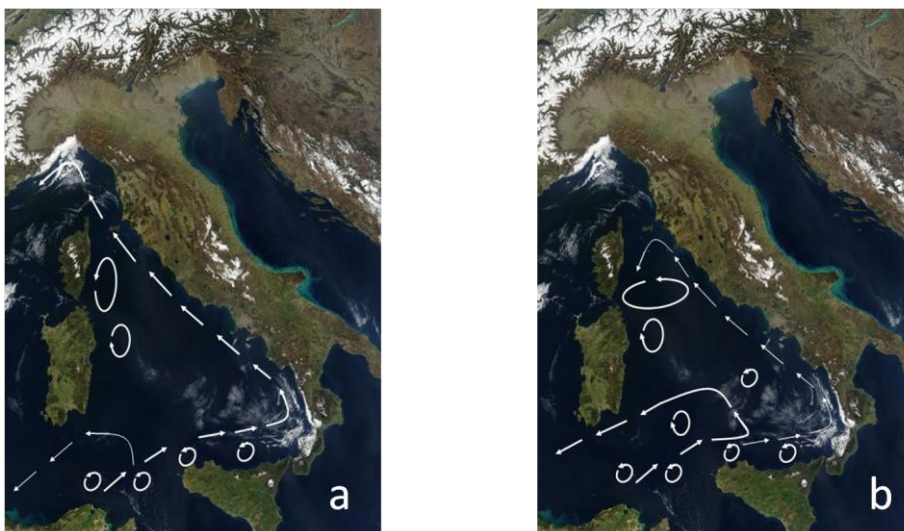

Figure 1.3 Reconstruction of the surface circulation of Tyrrhenian Sea during winter-spring (a) and in summer-autumn (b)

n summer, both cyclonic and anticyclonic eddies with characteristic length scales of 30-40 km are nested within the larger gyre (Artale et al.,1994). Marullo et al (1994), on the basis of AVHRR thermal images analysis, suggested that the NTC in summer consists of a cold water filament originating from the Strait of Bonifacio and extending eastward, rather than being a well organized cyclonic structure. Despite this different interpretation of the NTC structure past studies agree that the change of NTC orientation (zonal/meridional in summer/winter) is due to the strengthening of the current that drives the circulation through the Corsica Channel. South of the NTC, an anticyclonic gyre (NTA, North Tyrrhenian Anticyclone) is present. The generation and evolution of these gyres is also controlled by the strong wind events affecting the Strait of Bonifacio, and specifically by the wind stress curl associated with the easterly winds, and its associated Ekman pumping (Crepon et al., 1989; Artale et al. 1994).

The seasonal variability of the northern Tyrrhenian is also mirrored in the water exchange between the Tyrrhenian and the Ligurian Sea, mainly driven by steric effects, which dominate in the winter season (Astraldi and Gasparini, 1994; Marullo et al., 1994; Vignudelli et al., 1999; 2000), with an interannual variability possibly linked with regional teleconnection phenomena, namely the North Atlantic Oscillation (Vignudelli et al., 1999).

In the southern part of the basin, the dynamics are conditioned by the exchanges through the straits of Sicily and Sardinia. Surface water of Atlantic origin (AW) enters the Tyrrhenian Sea off the northern Sicilian coast. (see, e.g., Krivosheya and Ovchinnikov, 1973). It is believed to flow eastwards along the northern coast of Sicily, following an overall cyclonic pattern, proceeding along the western coast of Italy and then entering the Ligurian Sea through the Corsica Channel (Aliverti et al. 1968; Elliot et al., 1978; Tait, 1984). Using Lagrangian data collected in the Straits of Sicily in the 1990s, Poulain and Zambianchi (2007) recently showed that waters coming from the Algerian Current indeed flow north-eastwards into the Tyrrhenian, along the Sicilian coast. Their analyses clearly indicated that this flow returns southbound on the western side of the Sardinian Channel and forms a rather stable cyclonic gyre.

1.3   The Sicily Channel

The Sicily Channel divides the Mediterranean Sea into two sub-basins, the eastern and the western, thus representing a crucial area for both understanding the basin scale variability (Astraldi et al., 1999), and for the important fishery activities carried out by the countries bordering the Channel. The main characteristics of the Channel of Sicily circulation are well known, while the biological processes taking place in the channel and the spatial and temporal distribution and variability of the chlorophyll field still need investigations.

The average depth of the Sicily Channel is less than 300 m, with maximum values not exceeding 1500 m (Figure 4).
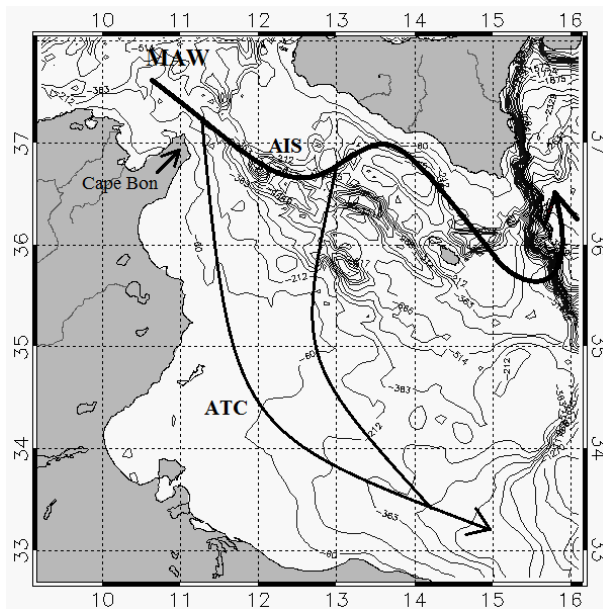
Figure 1.4 Reconstruction of the Sicily Channel surface circulation

From a dynamical point of view, the Sicily Channel can be schematically considered as a two-layer system: a surface (up to ~200 m depth) and fresher water mass (relative to the Mediterranean resident water masse) of Atlantic origin (Modified Atlantic Water, MAW) flowing eastwards, and the saltier Levantine Intermediate Water (LIW) flowing westwards. Once the MAW enters the Channel, near Cap Bon (Figure 4), it splits into two veins, the Atlantic Tunisian Current (ATC) that circulates close to the Tunisian coasts (Beranger et al., 2004, Pierini and Rubino, 2001) and the Atlantic Ionian Stream (AIS, Robinson et al., 1999), that flows into the central and northern region of the Channel (Poulain and Zambianchi, 2007) describing a cyclonic gyre around the Adventure Bank named ABV (Robinson et al., 1999).

South of Pantelleria Island, the AIS often bifurcates: a principal vein flows north-north-eastward, while a weaker stream directly flows along the Tunisian shelf (Lermusiaux et al., 2001). In summer the first veins of the AIS above descript is constrained in the centre of the channel by the up-welling front originating in the southern coasts of Sicily due to with local wind (Buongiorno Nardelli et al., 1999, Marullo et al., 1999a,b Le Vourch et al., 1992; Kostianoy, 1996; Piccioni et al., 1988, Sorgente et al., 2003; Béranger et al., 2004). On the contrary down welling processes are founded along the eastern coast of Tunisia on the opposite side of the Strait (Agostini and Bakun, 2002). The up-welling front is characterized by jets and filaments that are usually observed off-shore of Mazzara del Vallo and Capo Passero, see Figure 1.5 (Buongiorno Nardelli et al., 1999). During winter, the AIS extends in a wider region because in this season the up-welling is restricted both spatially and temporally.
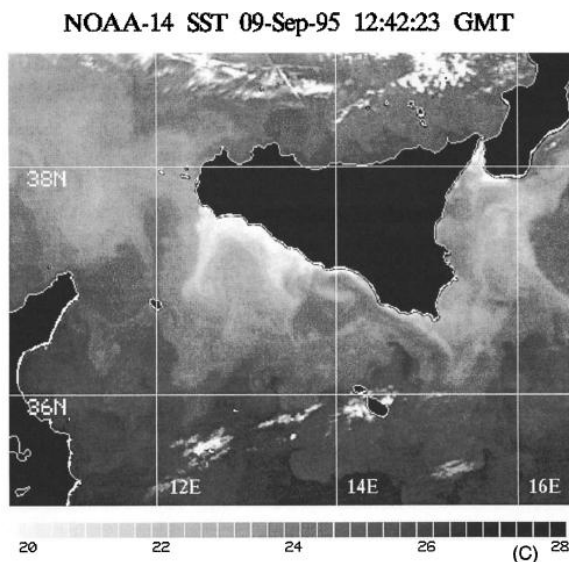
Figure 1.5 AVHRR images on 9 September 1995 in which are visible the coastal upwelling in the northern part of the channel and two filaments near Mazara del Vallo at 37.3°N, 13.5°E. (From Buongiorno Nardelli et al., 1999)

Off shore Cape Passero the AIS follows a cyclonic vortex called Ionian Shelf Break Vortex (IBV), (Lermusiaux,1999; Robinson et al., 1999; Lermusiaux and Robinson, 2001). Another cyclonic vortex called Messina Rise Vortex, MRV, is found south of Messina. At the eastern boundary of these latter two vortices the Ionian slope fronts, ISFs, are present and active at different locations and depths (Lermusiaux, 1999 and Lermusiaux and Robinson (2001).

From the biogeochemical point of view the eastern and the western regions of the Mediterranean Sea have already been shown to have an order of magnitude difference in the surface chlorophyll concentration (Santoleri et al., 2008,Volpe et al., 2011) along with different seasonal cycles: the eastern basin presents a seasonal cycle similar to that of the sub-tropical gyres, whereas the western basin phytoplankton dynamics can be associated with that of the north Atlantic with a pronounced spring bloom (D'Ortenzio and Ribera d'Alcalà, 2009). Based on SeaWiFS data, the entire Sicily Channel is characterized by phytoplankton biomass values ranging between 0.04 and 0.5 mg CHL m^{-3} at sub-basin scale (the entire sub-basin can be considered as a mesotrophic area), with a spatial variability on a daily basis encompassing 3 orders of magnitude (roughly between 0.01 and 10 mg CHL m^{-3}) on a daily basis. In general, maximum (minimum) values recur during winter-spring (summer) in correspondence of periods of low (high) water column stratification. From the visualization of daily SeaWiFS data, higher and nearly invariant values throughout the year are found in coastal areas, whereas off-shore region exhibit a more pronounced variability. Moreover, specific oceanographic features, such as wind-induced coastal upwelling, frontal meanders and instabilities significantly modulate the local distribution of phytoplankton biomass. In fact, the most productive area of the Channel has been generally associated with the up-welling that occurs along the south-eastern coasts of Sicily, at Cape Passero as demostrated by the value of fluorescence found in this area by Lafuente et al (2002) see fig 1.6.

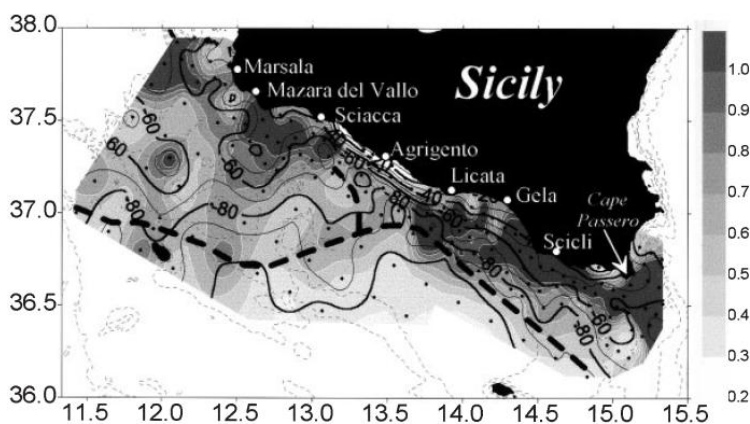Figure 1.6 Depth of the maximum of fuorescence (meters, labelled contours) and numerical value of this maximum during the period 24 June-14 July 1998 (from Lafuente et al 2002)

1.4   Ocean Colour Chlorophyll trends along the Italian coasts

The achievement of a good ecological status in European waters by 2015 is the intent of the Water Framework Directive (WFD) 2000/60. Since the publication of the WFD the European States need an effective monitoring system of the coastal waters. The problem of protection and of a compatible development of coasts necessarily requires a physical and bio-ecological definition of this term, indeed, the coastal areas can be placed in a wide range of definitions so a definition universally valid is difficult to found. The different definitions of coastal take into account separately geomorphological criteria, hydrographic criteria, the economic dynamics or criteria for the distribution of vegetation. For example, the simplest definition refers to the area between the high and low tide, while biologically the bound of the coastal areas is made to coincide approximately with the depth range of 50 m (euphotic zone), in other words how far the Posidonia can survive.

From the Ocean Colour (OC) point of view the waters are usually divided into two categories: case 1 waters, that are those waters in which the optical properties are dependent on the phytoplankton and on the degradation products their associated and case 2 waters in which other substances, such as resuspended sediments, terrigenous particles, yellow substance or anthropogenic materials, range independently from the concentration of phytoplankton and they determine the optical properties of the body of water. Case 1 waters are associated with the open sea waters while case 2 waters are associated with shelf and coastal waters.

The coastal waters represent only a small fraction of natural waters on the planet. However they play a role of great importance from the ecological, social and economic point of view. Indeed about 60% of the world population lives in coastal areas and about 90% of the catch comes from coastal areas. The strong anthropization, the irrational exploitation of resources and the changes in climate, are causing a strong modification of the coastal areas and they represent a continuo threat to the biodiversity of these areas. The eutrophization is the principal risk for the coastal water, it was defined by Nixon (1995) as an increase in the rate of supply of organic matter to an ecosystem'. The degenerative process is caused by the enrichment of water by salts, primarily nitrogen and phosphorus, leading to increased algal productivity and the production of a quantity of biomass greater than that can be used by

herbivorous organisms, this can lead to a reduction of dissolved oxygen when the organic matter decomposes.

For these reasons monitoring of coastal chlorophyll-a (Chl-a) concentration, considered as a proxy of phytoplankton biomass, can be an efficient tool to evaluate the Italian environmental policy taken to reduce the release of nitrogen and phosphate on the coastal water.

The Mediterranean Sea is characterized by a general decreasing trend in Chl concentration (Behrenfeld and al, 2006 Doney 2006and Greget et al., 2003). Behrenfeld et al. (2006) have linked the decreasing trend in ocean primary production to the climatic changes that determine a surface warming, resulting in an increase in the density contrast between the surface layer and underlying nutrient-rich waters. This in turn leads to enhanced stratification, which suppresses nutrient exchange through vertical mixing. Barale et al., (2008) have attributed the negative trend to the increased nutrient-limitation, resulting from reduced vertical mixing due to a more stable stratification of the basin, in line with the general warming trend of the Mediterranean Sea. However they found positive trend of Chl in some coastal area, they have associated this hotspots continental runoff and to a growing "biological dynamism" at these sites.

Actually the studies regarding the Chl-a trend along the Italian coast are principally concentrated in the north of the Adriatic Sea. Obviously this is due to the presence of the outflows of Po, which affects the amount of nutrients in this region. A recent study based on satellite data demonstrate that in the last decade there is a decrement of the Chl-a surface concentrations specially in the western area of the basin that is generally more eutrophic respect to the centre and the eastern coast in which the negative trend is less marked (Mozetič et al., 2010). This negative trend is justified by the reductions observed in the outflows of the Po (Zanchettin et al. 2008) and Isonzo (Comici and Bussani 2007) rivers and by the fact that phosphorus being banned by Italian law in the mid-1980s and this , could have had a strong influence on nutrient concentrations in the coastal area (de Wit and Bendoricchio 2001).

On the contrary increasing trend of productivity were found in the Middle and Southern Adriatic (Marasoviæ, et al., 1995). More recently, Matarrese et al (2009) analyzing Chl-a Modis data in the Soutern Adriatic Sea found a positive trend in Taranto Gulf and along the Margherita di Savoia coasts. These trend are mostly due to the meteorological forcing, which influenced oceanographic phenomena like water stratification, upwelling, stronger inflows of Mediterranean water into the Adriatic (Morovic et al., 2004).

Chapter 2

Satellite Oceanography

This thesis analyzes chlorophyll, sea surface temperature and sea level height products derived by satelllite data acquired by both passive and active sensors. These satellite data are produced by specialized processing chains which use specific algorithm for the parameter retrievals. Even if the retrieval of the parameters is out the scope of the thesis, this chapter introduces the basic physical principles of ocean remote sensing. This preliminary step is particularly useful and important to recognize the complexity of the measurement techniques and data processing used to retrieve the geophysical products used in this thesis and to understand some problems encountered in the analysis of the satellite data products. Then potential use of satellite data to infer the upper ocean dynamics and to study the seasonal and interannual variability of the ocean field is review in order to show state of the art of satellite oceanography.

2.1   Principles of oceanography satellite

The first artificial satellite was launched in 1957 by the Soviet Union, and in 1964 there was a first conference in which the possibility of conducting oceanographic observations from space is discussed. To observe the oceans from space allows the synoptic view in two dimensions with high spatial resolution and it makes possible to measure large areas also isolated of ocean for long periods.

The remote sensing sensors measure the electromagnetic radiation emitted or reflected by the area observed at frequencies established (Fig 2.1). The satellite sensors can be of two types: active and passive. The active sensors produce the radiation that are reflected from the surface and then analyzed by the same sensor. Differently, the passive sensors measure the reflection (or emission) of natural radiation on the Earth surface to certain wavelengths.
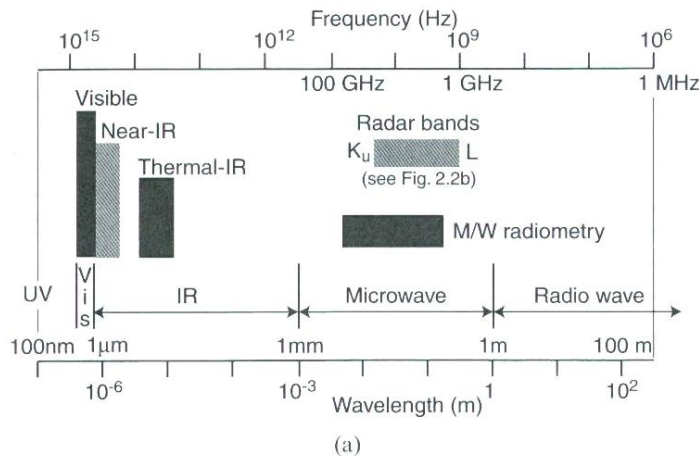
Figure 2.1 Spectrum bands used for remote sensing (Robinson 2004)

2.1.1   Ocean Colour

The relevant parameters for the OC are the **Irradiance**, the **Radiance**, the **Reflectance** and the **Transmittance**.

The **Irradiance**, E, is defined as the amount of radiant energy intercepted by a surface area element. It denotes the light arriving on a surface area and has units of W m-2.

The **Radiance**, L, is the measure of the light leaving a surface per unit solid angle in a given direction. The radiance has units of W sr-1 m-2.

The **Remote Sensing Reflectance** of a water body, Rrs, is defined as the Radiance to Irradiance ratio, that is the amount of light leaving the surface vertically upwards weighted by the amount of light entering the surface from all directions. The spectral shape of Rrs defines the so-called ocean colour.

The **Transmittance** ,T, is the fraction of radiation that passes through a medium which absorbs uniformly.

Only a small percentage of the signal received from the sensor comes from the ocean. Indeed the 80-90% of the signal is due to the interaction of the electromagnetic waves with the constituents of the atmosphere as molecules (Rayleigh) and particles (Austin, 1974 ; Hooker et al., 1992).

Figure 2.2 shows the radiance that reaches the sensor at the top of the atmosphere and it is made of various contributions as proposed by Gordon (1978, 1981). T'LW is the water-

leaving radiance inside the Instantaneous Field Of View (IFOV) plus the radiance that arise the sensors from the external water of the IFOV but that is captured as a result of scattering of the atmosphere. L_R and L_A are the radiances due to the molecular scattering (Rayleigh) and aerosol scattering respectively.
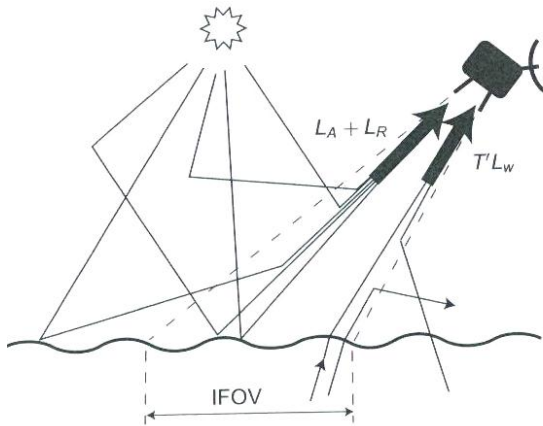
Figure 2.2 Optical pathways to an ocean colour sensor

Defining L_S as the total radiance received to the sensor, we can write:

$$L_S = L_A + L_R + T\ L_W \qquad\qquad 1.1$$

L_R can be estimated with sufficient accuracy for remote sensing applications using the theory of Rayleigh (Gordon et al., 1988a) while the estimate of L_A presents greater difficulties due to the fact that the concentration and distribution of aerosols in the atmosphere are very variable in space and time.

One of the possible techniques for determining L_A is include one or more bands in the near infrared in the spectrum. Indeed at this wavelength L_W is considered to be negligibly small and it is possible to calculate L_A using the models of radiative transfer which evaluate the aerosol properties spectral dependence. The contribution of L_A in the visible band channel is computed with a 5% uncertainty (*Gordon and Wang*, 1994). Therefore the water-leaving radiances can be evaluated and used to measure the ocean chlorophyll concentration through the ocean colour algorithms. These relate the surface chlorophyll concentration to the blue-to-green reflectance ratio (see *Morel and Maritorena*, 2001; *O'Reilly et al.*, 1998; 2000), in general, the higher the chlorophyll concentration the lower is the B/G ratio. In this thesis I used data in which the chlorophyll values were obtained with MedOC4 (*Volpe et al.*, 2007) ocean colour algorithm. *Volpe et al.* (2007) have shown that MedOC4, compared with other global algorithms, produces more realistic values in the Mediterranean differing from *in situ*

measurements by about 35% and therefore within the 35% SeaWiFS mission uncertainty target.

The OC data analyzed in this thesis are the L3 data acquired and processed by the Group for Satellite Oceanography (GOS) at the Istituto di Scienze dell'Atmosfera e del Clima of the Italian National Research Council, Rome. The L3 data contain chlorophyll data remapped on the area of interest.

2.1.2   Sea Surface Temperature

At the base of infrared remote sensing is the concept that all bodies having a temperature above 0° K emit spontaneously electromagnetic radiation due to thermal agitation of their atoms or molecules. It is possible to measure the Emittance, M(λ,T), definted as the radiant flux emitted by the surface of a body per second per unit area, through Planck's Law:

$$M(\lambda,T) = C_1/\lambda[exp(C_2/\lambda T) - 1]10^{-6}$$

Where λ is the wavelength in meters, T is the temperature in degrees Kelvin, and C1 and C2 are two constants with values equal to 3.74x10-16 Wm2 and 1.44x10-2 mK respectively. With this formula we obtain the emittance of a black body, ie a perfect emitter of thermal radiation, in Wm2 µm-1

The spectral emissivity, denoted by ε (λ) is the fraction of energy radiated by a body respect to the energy radiated by a black body which is at the same temperature. The Wien's law determines the the position of the peak of the emittance:

$$\lambda_{max} = \frac{2897}{T} \mu m K^{-1}$$

The temperature of radiance is definite as the thermometric temperature that the body would have if it were a black body (with absorption equal to one) and located close to the measuring instrument. The peak of emission of the sea surface temperature is between 9 and 11 µm, moreover the radiance changes rapidly as a function of temperature, this makes the thermal infrared an excellent region for the monitoring of sea surface temperature. The radiance temperature of the SST is usually lower than the real because of the components of the atmosphere. In the range of infrared wavelengths of interest for remote sensing, the components of the atmosphere absorb and re-emit radiation as a function of their

concentration and according to the temperature of the atmosphere, generally this is less than that of the sea and it causes a shift of the peak emission to greater wavelengths.

The maximum transparency of the atmosphere occurs in two windows of infrared between 3.5 - 4.1 and 10-12.5 μm. To measure the SST is mainly used the last window, this is due to the fact that the sea surface has the maximum emission in this wavelength. Moreover the reflected solar component is negligible and the reflectance of the sea surface is lower than that to 3.7 μm, making the atmospheric component reflected irrelevant. For this reason the use of 3.7 μm window, is limited to nighttime hours.

The peak emissivity in the infrared wavelength is between 0.98 and 0.99 (Masuda et al., 1988), but it is sensitive to the view angle and to the wind speed, moreover it varies if an organic film is present on the surface. Assuming that the surface emits radiation as a black body, the mistakes are in the order of 0.1-0.2 ° K and they can be corrected inside the algorithm for atmospheric correction.

One of the atmospheric correction algorithms used is based on the method of split-window and it is finalized at the correction of the absorption due to atmospheric water vapor. The principle behind the split-window technique is the proportionality between the atmospheric attenuation and the difference between two radiance measurements made in adjacent thermal channels each subject to different absorption (Tbi, Tbj).

The thermometric temperature Ts is obtained by a linear relation from a measured brightness temperatures in channels 4 and 5

$$T_s = aT_{bi} + b(T_{bi} - T_{bj}) + c$$

The coefficients used in the formula depend on the channels used, on the atmospheric absorption and on the surface emissivity. They are calculated depending on the specific region and on weather conditions of the day examined (McMillin and Crosby, 1984).

Moreover, the daily data are strongly influenced by the presence of cloud cover. To prevent that data being contaminated by clouds a threshold of brightness temperature is established, below it the pixel is assumed to be affected by clouds. This is possible becouse the temperature of the clouds is much lower than that expected for SST in a given geographical area. The comparison with the climatology of the SST in the region of study for that time of year is done with a brightness temperature in the band of 12 μm, if the difference exceeds the threshold, the pixel is classified as cloudy. Once the pixel is classified as cloudy, it is assigned a value which corresponds to claim that the data does not contain useful information for the

study. The cloud free data arrays are processed by multichannel algorithm to obtain SST estimation for each location.

The SST dataset used in this thesis is the optimally interpolated (OISST) re-analysis product based on Pathfinder SST time series (Marullo et al. 2007). These are multisensors SST data and they represent the foundation temperature that is "the temperature measured or estimated at the base of the diurnal thermocline" (Robinson 2004). Marullo et al. (2007) estimated the mean bias error of OISST product equal to 0.04°C and the standard deviation 0.66°C .

Moreover, they evaluated the sensitivity of OISST accuracy to seasonal factors lower than 0.3°C and they did not evidence significant sensor drifts, shifts or responses to anomalous atmospheric events

2.1.3   Sea Surface Height

The altimeters measure the distance from the surface to the satellite from the time of return of the signal emitted, knowing the parameters of the orbit of the satellite is possible to estimate the height of the sea. This depend on the total amount of mass along the entire water column and by the volume that it occupies. So the sea level variations measured by altimeter include both baroclinic terms and barotropic components, even when the tides and the inverse barometer effect have been filtered.

The sensor measure the effective level of the sea mediated on the area illuminated by the antenna. However the estimate is affected by the contamination of the electromagnetic signal transmitted/reflected from the atmosphere (but also the roughness of the surface). So despite the choice of frequencies in which the atmosphere is essentially transparent, there is a reduction in the speed at which the signal travels, that results in an overestimation of the range (h). The error on the range estimate is

$$\Delta h = \int_{0}^{h} (n-1) dz$$

Where n is refractive index of the medium.

The refractive index of the earth's atmosphere varies as a function of temperature and density of gases present in the troposphere. Assuming valid the hydrostatic equilibrium and the ideal gas law, the vertically integrated delay on the signal can be considered only function of the atmospheric pressure to the ground. Generally this data is obtained from meteorological

models. Moreover, also the water vapor affects the speed of propagation of light in the atmosphere. The correction is obtained either from measurements of emission on characteristic frequencies of the water vapor or from models.

Addictionally, the height of the sea surface is measured respect to the ellipsoid that does not coincide with the geoid (the earth's equipotential surface) but it may deviate several meters over distances of a few kilometres. Obviously this can be a source of error. Unfortunately, the components of the geoid for the oceans are know on lengths of waves of thousands of kilometers, and there is no measure of the geoid with the spatial resolution needed for the study of marine circulation. For many application of altimeter data, for example to estimate the geostrophic speeds from the horizontal gradients of elevations, it is necessary to remove the geoid from the data.

To do this the mean level over the time of the sea is assumed as an equipotential surface. This is calculated through the repeat track analysis method that consists in to calculate on a regular grid the the average of measurements obtained from different cycles of the satellite on a given number of years, this mean is then subtracted from the single pass.

An additional source of error derives from the shape of the sea waves. Indeed the wave crest reflects less than the cable. This results is a general lowering of the mean surface estimated.

A further contribution to the height of sea came from the tidal. The satellites periods of repetition are chosen to not sample the sea surface on multiple frequencies of the tidal signal.

Finally, the sea level responds isostatically to changes in atmospheric pressure, so an increase in pressure of 1 hPa determines a lower of the surface of about one centimeter. The formula gives the corrections to apply to the data

$$Inv\_bar = - 9.948 \ (Patm - 1013.25)$$

This hypothesis is not valid for phenomena that occur on time scales comparable to that of isostatic adjustment.

The altimeter dataset analyzed here are Mediterranean Absolute Dynamic Topography and absolute geostrophic velocities distributed by AVISO (Archiving Validation and Interpretation of Satellite Oceanographic Data). The MADT is the addition of a mean dynamic topography (MDT) to the sea level anomalies (SLA), as detailed in Rio et al. (2007), the accuracy (RMS error) for the MADT is of the order of 3 cm. For a more complete description of the dataset used in this thesis see sections 3.1.3 and 4.1.3.

2.2 Use of satellite data to infer information on the upper ocean circulation and dynamics

The Advanced Very High Resolution Radiometers (AVHRR) on board the National Oceanic and Atmospheric Administration (NOAA) have provided the most reliable global ocean measurements of SST whit high spatial and radiometric resolution, regular sampling and synoptic perspective over two decades (Barton, 1995, Kidwell, 1998; Goodrum et al., 2000). A technique widely used in physical oceanography to analyze satellite SST data is the EOF analysis. This technique has been largely used to obtain the dominant patterns of residual variance in AVHRR images time series (Kelly, 1985, 1988; Laggerloef and Berstein, 1988; Fang and Hsieh, 1993; Gallaudet and Simpson, 1994). In 1999 Marullo et al., using EOF have analyzed ten-year of AVHRR-SST in the Eastern Mediterranean Sea to quantify the interannual variabilities in its different sub-basin. More recently (2011) the same author et al. has applied EOF to study the SST multidecadal variability in the Mediterranean Sea and to explore possible connections with other regions of the global ocean.

Satellite altimetry provides a great opportunity to study the dynamics of the sea due to the fact that altimeter data extend over the past 15 or more years. This have been widely used in the study of ocean circulation and to understand its variability (Kelly and Gille, 1990; Le Traon and De Mey, 1994; Challenor et al., 1996, Strub et al., 2000, Korotaev 2003, Birol et al., 2010).

The first study of circulation using TOPEX/POSEIDON sea level variability (SLV) in the Mediterranean Sea was done by Larnicol et al. (1995) who identified the main areas of high variability and they have concluded that T/P is able to measure the main features of the large-scale surface circulation. Ayoub et al. (1998) have improved considerably the resolution over the Mediterranean merging ERS 1 and T/P data giving a more complete description of the Mediterranean variable surface circulation. Moreover, the global mapping techniques, developed by Le Traon et al. (1998) and Ducet et al. (2000) and follow to create data by SSALTO/DUACS, have allowed basin-wide studies of the circulation variability (Larnicol et al. 2002, Pujol and Larnicol 2005). In addition, the contemporary availability of up to five altimeters (T/P, ERS-2, EnviSat RA, Jason-1 and GFO) has enhanced the capability of multimission altimeter datasets to capture the mesoscale structures. Pascual et al. (2007) have demonstrated that to detect the mesoscale circulation at least three altimeters are needed.

Moreover they show that a four-altimeter configuration permits a mapping of sea level and velocity with a relative accuracy of 6% and 23 %, respectively, and increase the average eddy kinetic energy over the basin by 15% with respect to a two configuration.

Over the last few years many scientists have used the altimeter data combined with in situ data or ocean circulation model to study the circulation in the Mediterranean Sea (Rio et al., 2007, Bouffard et al., 2008, Jordi et al., 2009, Ruiz et al.,2009, Bouffard et al., 2010). Vignudelli et al. (2000) have examined water transport anomalies from a currentmeter and altimeter-derived sea level differences in the Corsica Channel to study the variability of the flow between the Tyrrhenian and Ligurian Seas. Few studies have specifically applied the altimeter data in the Tyrrhenian Sea, Vignudelli and coautors (2003) have examined its circulation analyzing the results from XBT and alimeter data of single sensor T/P while more recently Budillon et al., (2009) have analyzed altimetric data with two hydrographic cruises to monitor hydrographic conditions of the Tyrrhenian Sea. Altimeter data have also been widely used as input for the EOF technique see for example Toole and Siegel 2001,Cazenave, et al., 2002, Volkov and Denis L., 2005, Alvera-Azca´rate, et al.,2009.While, more recently, Ioannone et al.,(2010) have investigated the variability of the sea surface structure of the northern Ionian Sea analyzing, through EOF, altimeter remotely-sensed Sea Level Anomaly (SLA) maps.

Since October 1978, when the Coastal Zone Color Scanner radiometer (CZCS) was launched, ocean colour satellite data have provided unprecedented high space-time resolution information on the surface distribution of phytoplankton biomass in the ocean. The results obtained with the CZCS have encouraged the use of satellite data and driven several space agency to approve different missions. Among all sensors that have provided data on OC (The Ocean Color and Temperature Sensor (OCTS), SeaviewingWide Field-of-view Sensor (SeaWiFS), Moderate Resolution Imaging Spectroradiometer (MODIS), Global Imager (GLI), and Medium Resolution Imaging Spectrometer (MERIS)), the SeaWiFS has provided the longest time series of data. Moreover due to its frequent global coverage its data are the data used in most published results.

Ocean color data have become an important tool to study the primary production and the phytoplankton distribution (Toole and Siegel 2001, Yoder & Kennelly 2003, Wilson and Coles 2005, Garcia and Garcia 2008,Iida 2007). The spatial and temporal distribution of phytoplankton is nowadays quite well-understood on a climatological basis, resulting in a well-defined zonation of the world oceans, the so-called bio-provinces (Longhurst, 1998). The temporal evolution of the phytoplankton spatial patterns has recently been investigated by

Henson et al. (2009). They found a good correlation in the position and spatial extension of the transition zone between the subpolar and subtropical regions with an extensively used climatic index, the North Atlantic Oscillation Index (NAO).

In addition, the biology of the oceans is dependent on physical properties as temperature, salinity, light, and on dynamics as mixing, upwelling, advection, of the water masses. The use of satellite data has allowed a better understanding of the links between biology, physic and dynamics of the ocean. Many studies have used statistical analysis techniques to connect the biological variability with physical dynamics (Wilson and Adamec, 2001, 2002, Palacios 2004). For example, using the semivariogram approach from geostatistics applied to SeaWifs Data, Doney et al (2003) characterize for the first time the global patterns of mesoscale ocean biological variability. While, Wilson and Coles (2005) have analyzed the correlation between different parameters of the Sea (in particular they study climatological satellite observations of sea surface height, sea surface temperature, upper ocean chlorophyll-a, the mixed-layer depth and the thermocline depth) to quantify the broad-scale spatial and temporal relationships.

Santoleri et al (2003) have analyzed three years of SeaWiFS data and the results of a one-dimensional (1-D) coupled physical-biological model to understand the relation between atmospheric forcing and interannual variability of the surface spring bloom in the south Adriatic Gyre. While, Pascal et al., (2002) have compared altimetry, SST and conductivity-temperature-depth (CTD) data to analyze a mesoscale anticyclonic eddy in the Balearic Sea. Moreover, Iudicone et al., (1998), examining the mesoscale features of the circulation detected by the altimeter and contemporaneous AVHRR thermal imagery in some basin of the Mediterranean Sea, found a relation between Sea Level Anomalies (SLA) and gyres and eddies observed in AVHRR images. More lately, for the first time Volpe et al (2011) have applied EOF decompostition to Chl, SST and Mediterranean Absolute Dynamic Topography (MADT) satellite weekly time to find the link between biotic and abiotic factors in the Mediterranean Sea at different space and time scales.

Chapter 3

Lagrangian and Eulerian observations of the surface circulation in the Tyrrhenian Sea

This chapter focuses on the study of the Tyrrhenian Sea circulation. The analysis of the state of the knowledge of the Tyrrhenian sea circulation (section 2) clearly showed that only the mean large scale surface circulation is well known. On the contrary, the variability of the main features modulating the Tyrrhenian large scale current system still needs investigation and little is known about the energy involved in mesoscale processes. As a consequence, in this chapter we try to fill this particular gap through the analysis of satellite altimeter measurements and Lagrangian surface data.

The circulation is described first by a set of 53 surface drifters deployed in the area between December 2001 and February 2004. In order to supplement the drifter data with continuously and uniformly sampled observations, and to characterize the seasonal, as well as higher frequency variability of the surface circulation, the Lagrangian analysis was associated to simultaneous satellite remotely-sensed altimeter, covering the period 2001-2004.

Indeed, on one hand, satellite data can provide long-term, synoptic and global estimates of key parameters of the oceans, but they still need to be validated by available *in situ* measurements. On the other hand, dynamical structures with very fast propagation velocities or short life duration cannot be studied by means of altimeter data that can only monitor processes at temporal scales longer than ~ 10 days. On the contrary, Lagrangian data provide information on short term variability of the surface field but can be intermittent in space/time due to the limited number of drifters available.

While both Lagrangian and altimeter data have been extensively used in the past to study the Mediterranean ocean surface circulation separately (e.g. Larnicol et al. 2002; Iudicone et al, 1998; Buongiorno Nardelli et al. 2002, Pujol and Larnicol, 2005, Poulain and Zanbianchi 2007), here more than three years of Lagrangian data acquired in the Tyrrhenian Sea from 2001 to 2004 are presented and analysed together with coincident altimeter data. Trajectory

analysis and different kinds of pseudo-Eulerian statistics applied to the Lagrangian and to satellite data are thus analysed to identify the mean patterns of the Tyrrhenian Sea circulation as well as the variability of its basin, sub-basin and mesoscale structures.

The method chosen here, namely comparing filtered drifters statistics with re-sampled altimeter data over drifters trajectories (see section 3.3) represents an innovative approach that served to complement and compare the information provided by two datasets separately and helped to quantify the impact of the different sampling strategy of the two instruments, as well as the dynamical limitations of altimeter derived velocities in representing the ocean surface circulation.

3.1   Data

3.1.1 Drifting buoy data-set

The in situ data used in this study were obtained from 53 satellite-tracked modified CODE drifters deployed in the Tyrrhenian Sea and contributing data from December 2001 to February 2004. This Lagrangian experiment was organized in the framework of the "Programma Ambiente Mediterraneo" initiative, funded by the Italian Ministry for Research, with additional funding obtained from the U.S. Office of Naval Research.

The modified CODE drifters have the same structure of the original ones, conceived for and used in the Coastal Dynamics Experiment (CODE) in the early 1980's (Davis, 1985). They consist of a vertical, 1 m-long plastic tube, containing the electronics and the transmission package and antenna, with four sails extending radially from the tube over its entire length, which maximize the surface current drag. The total vertical extent of the system is about 1 m. The buoyancy is provided by four small floating spheres tethered to the upper and outer extremities of the sails.

Comparison with current meter measurements (Davis, 1985) and surface ocean dye experiments (D. Olson, Personal Communication) show that velocities estimated from CODE drifter trajectories are accurate to about 3 cm/s, even under strong wind conditions.

All drifters were tracked by the Argos Data Collection and Location System. In order to explore the most efficient transmission duty cycle in terms of cost-effectiveness and at the same time accuracy of velocity derivation, various transmission duty cycles were tried for this study. The raw drifter data were first edited for spikes and outliers (Poulain et al., 2004). They

were then interpolated at 2 hour intervals using a kriging technique, and low-pass filtered (36 hour cut-off) to remove high frequency current components. Finally, the low-pass time series were sub-sampled every 6 hours and the surface velocities have been estimated through centred finite differencing of the filtered positions.

The Tyrrhenian Lagrangian experiment consisted of 6 successive deployment episodes. Deployment time and location as well as drifter lifetimes are summarized in Table I (Appendix A), and deployment locations are also shown in Figure 3.1. Drifter deployments had been originally planned so as to take advantage of the Tyrrhenian coastal current, allegedly a swift current flowing along the western coast of the Italian Peninsula from the extreme South (Calabria) all the way northeastward to the Corsica Channel. Therefore most of the drifters have been launched in the southeastern region of the Tyrrhenian. The total number of observation days gathered in this experiment is around 5000 drifter-days, and the average lifetime of drifters amounts to 90 days approximately (Table I).
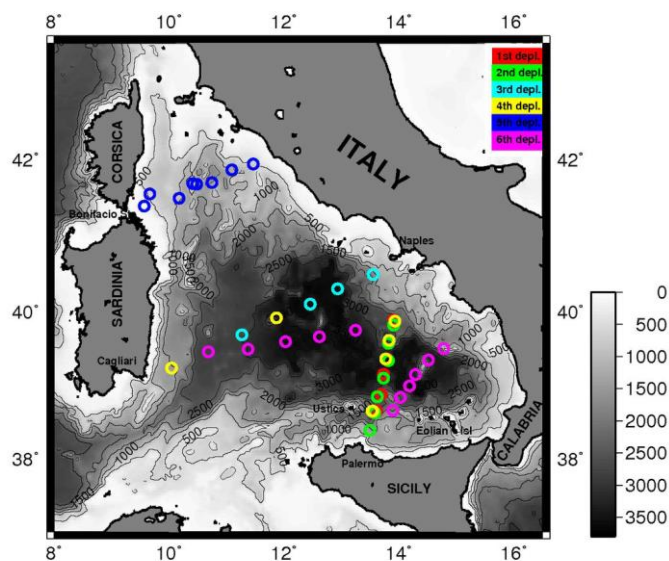
Figure 3.1 Map of the Tyrrhenian Sea with its bathymetry and the different drifter deployment locations (see also Table 1, appendix A, for information on the individual deployments).

In figure 3.2 the spaghetti diagram of all drifter trajectories is shown and in figure 3.3 the relative drifter data density (in 0.5° x 0.5° bins) in the Tyrrhenian. The absolute maximum of data density is located in the southeastern portion of the basin. This is partly due to the

deployment locations, and mostly to the circulation in that area, which yields a longer renewal time for surface water there rather than in other sub-basins. Another (relative) density maximum is displayed in correspondence to the southward current flowing along the Sardinian coasts, and a further, very weak maximum in the area south of the Corsica Channel.
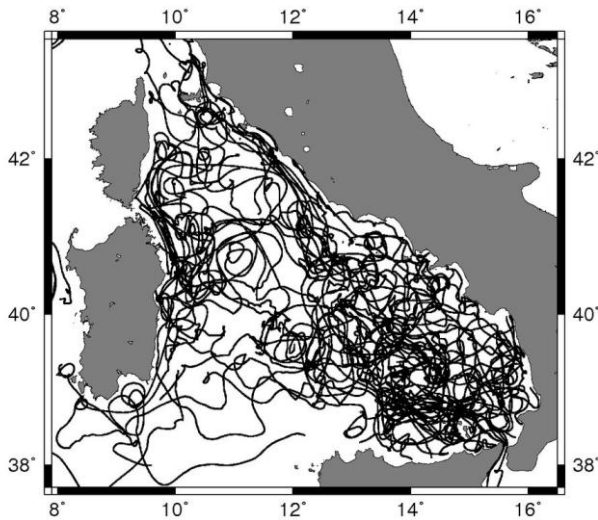
Figure 3.2 Composite of all trajectories of drifters deployedin Tyrrhenian Sea from 2001 to 2004 analyzed in this study.
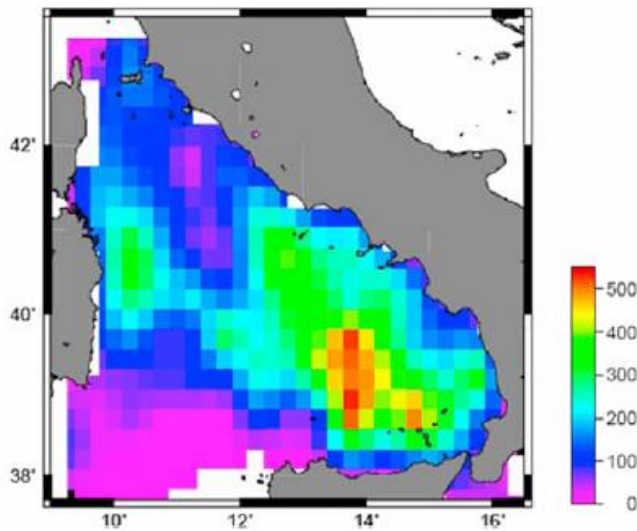
Figure 3.3 Drifter data density in 6 hourly data points.

Pseudo-Eulerian statistics have been computed from this dataset (for the definitions of mean kinetic energy MKE, eddy kinetic energy EKE and of the variance ellipses see Emery and Thomson, 1998; Poulain and Zambianchi, 2007).

The pseudo-Eulerian approach is a classical tool utilized in the study of Lagrangian data and consist of subdividing the domain under observation into regions (bins) within which the flow

is assumed to be homogeneous and stationary, and by computing the mean field as the average of all the velocity measurements available in the bin (Swenson and Niiler, 1996; Poulain, 2001; for a thorough methodological discussion see Bauer et al., 1998). The bin size has to be selected so as to contain a large number of measurements to ensure robustness of the inferred statistical quantities; at the same time bins have been kept small enough to achieve an appropriate space resolution, and to avoid an excessive smoothing of the mean field and the consequent erroneous inclusion of a portion of it in the residuals. In this study bins of 0.25° x 0.25° are used.

3.1.2 Wind data

In order to evaluate the Ekman component from the velocity field deduced by drifters, we have used the operational analysis of wind data provided by the European Centre for Medium-range Weather Forecast (ECMWF) for the period relative to the drifter measurements.

The ECMWF wind data are relative to a height of 10 m above the sea surface and have a spatial resolution of 0.5 x 0.5 degree and temporal resolution of six hours. Wind-driven currents estimated from wind data on the basis of Ekman's theory have been evaluated using drifter data by several authors (see, e.g., the recent examples by, Ralph and Niiler, 1999; by Rio and Hernandez, 2003; and the application to the eastern Mediterranean by Poulain et al., 2009, which summarizes earlier efforts on this issue). Here we have used the general formula for the Mediterranean proposed by Mauri and Poulain (2004):

$\boldsymbol{U}$wind-driven (cm/s) = 1.2 exp($-i$24º) $\boldsymbol{U}$wind (m/s)

The wind data have been interpolated at the time of observation and at the drifter positions using a bilinear scheme. The Ekman component has then been removed from drifter velocities, and the resulting Ekman-corrected drifter observations have undergone the same binning above described for the original drifter data.

3.1.3 Altimeter data-set

The altimeter data considered are the updated Mediterranean Absolute Dynamic Topography (MADT) maps from four altimetric satellites Jason-1, Envisat or ERS-2, Topex/Poseidon and Geosat Follow-On GFO, (TOPEX/POSEIDON was substituted by Jason since June 2002, and ERS2 by ENVISAT since July 2003), covering the period of the Tyrrhenian Lagrangian experiment (from January 2001 to December 2004). The altimeter products were produced by Ssalto/Duacs and distributed by Aviso, with support from Cnes (http://www.aviso.oceanobs.com/duacs/).

These altimeter data are interpolated by AVISO over a regular 1/8° grid on a weekly basis, using an optimal interpolation method that merges the data coming from the diverse altimeter missions, directly adjusting the residual long wavelength errors (Ducet et al. 2000). The covariance function used by this interpolation procedure is shaped as:

$$C(r,t) = \left[1 + ar + \frac{1}{6}(ar)^2 - \frac{1}{6}(ar)^3 \right] e^{-ar} e^{\left(\frac{t}{T}\right)^2}$$

where the parameters a and T practically lead to space and time decorrelation scales of about 100 km and 10 days, respectively.

Finally, the Absolute Dynamic Topography is computed adding a mean dynamic topography (MDT) to the sea level anomalies (SLA). The method applied to calculate the MDT was developed and described by Rio and Hernandez (2004) and has been specifically applied to the Mediterranean data by Rio et al. (2007).

From the MADT, we estimate the surface velocities assuming the geostrophic approximation, which enables to obtain the surface velocity from the gradients of the ocean topography. In order to be consistent with the procedure used for drifter data, we applied the pseudo-Eulerian approach also to altimeter data, so that the altimeter geostrophic velocities were first binned over the same 0.25° x 0.25° grid used for Lagrangian data and then used to compute the statistics.

3.2   Analysis of the surface circulation

3.2.1 Surface circulation revealed by drifters trajectories

The general picture of the surface circulation coming out of the drifter trajectories can be outlined as follows (see Figures 3.2 and 3.4): once the surface waters penetrate into the Tyrrhenian, they typically undergo a northward deflection in correspondence to complex bathymetric features of the Sicilian shelf break (fig 3.4e). Rather than continuing cyclonically along the Sicilian and then along the Italian continental coastline, the core of the surface transport off North-West Sicily is thus displaced offshore. The shelf area next to the Sicilian coast West of the Eolian Islands is characterized by recirculations rather than by the expected eastward zonal flow (see Fig 3.4a, 3.4d and 3.4f). In particular, the trajectories show the presence of a southern anticyclonic recirculation and of a northern cyclonic one, connected to the coastal flow further north (Fig 4d and 4f), whose presence had been suggested in the geostrophic flow computations by Krivosheya and Ovchinnikov (1973), but never substantiated by current data.

The coastal current in the eastern zone of the Tyrrhenian results quite unstable in its southernmost portion, and often branches westward, originating a complex flow pattern in the south-central Tyrrhenian basin. Moreover, this current is characterized by recirculations with scales ranging from 20 to 100 km and more, some of which are transient and some of which turn out to be quasi-permanent features of the velocity field (fig 3.4d). In particular, the drifter data show the presence of a strong and recurrent anticyclonic circulation in the centre of the Southern Tyrrhenian very well caught by drifters 33204 and 34447 (Fig 3.4b). I will refer to it, in analogy with the above mentioned NTA and NTC, as South Tyrrhenian Anticyclone (STA), which is further investigated in the following with the aid of altimeter data.

The eastern coastal current becomes a steady and recurrent feature of the surface Tyrrhenian circulation only north of the Gulf of Naples (Fig 3.2 and Fig 3.4 a,c,d). From there on, it flows close to the coast all the way to the Corsica Channel, occasionally changing direction with local recirculations which bring its waters into marginal sub-basins (bays and gulfs) or into the offshore regions (Fig 3.4c,f). I have to point out that the drifter trajectories make it through the Corsica Channel into the Ligurian Sea only in winter in agreement with the increase of the Corsica Chanel outflow observed by currentometer records collected in that

area (Vignudelli et al., 1999 and 2000). This indicates that the northward coastal flow undergoes seasonal variability.

In the northern Tyrrhenian, the return circulation is ensured by the NTC and by its southern counterpart, the NTA, which also in our data show some degree of seasonal variability, possibly contributing to the variability of the through flow across the Corsica Channel (Fig 3.4c and e). After tracing the two vortices, the southward flow closing the broad cyclonic circulation in the direction of the Sardinia Channel also "leaks" into the basin, nourishing several recirculations (fig 3.4e). Given all the above, the flow in the interior of the basin is dominated by transient and only occasionally quasi-steady vortices, and, despite the vicinity to the Sardinia Channel, it is very difficult to identify a mean flow pattern in the southern section of the Tyrrhenian (fig 2), as mirrored in the pseudo-Eulerian statistics (see below).
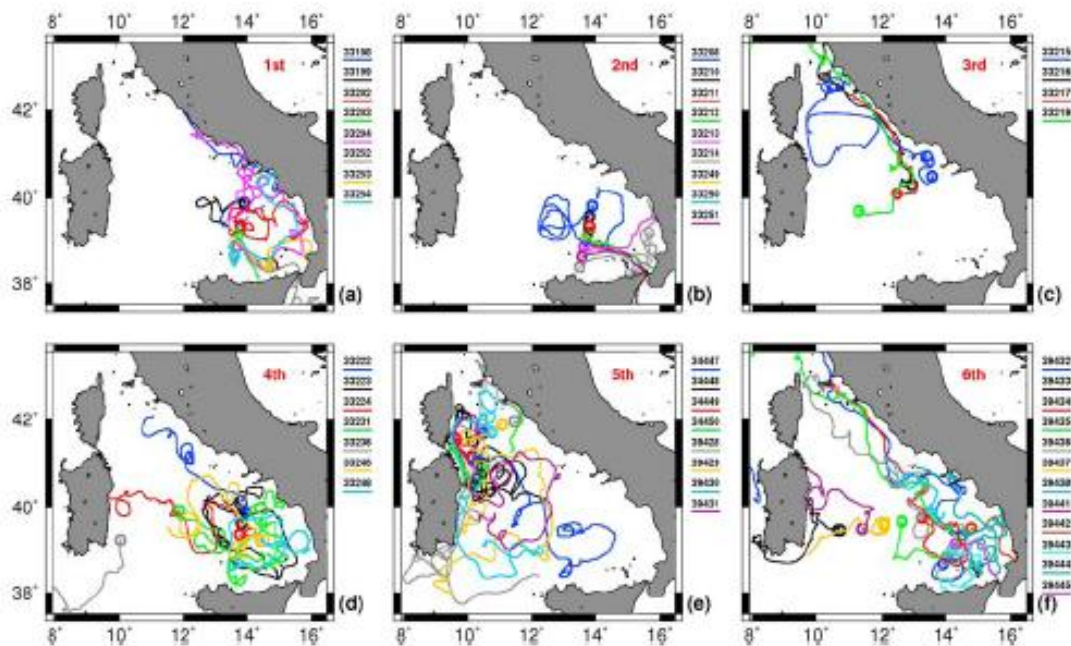
Figure 3.4 Drifter trajectories for the different deployments: (a) 1st, (b) 2nd, (c) 3rd, (d) 4th, (e) 5th, and (f) 6th deployments (see also Table 1 for information on the individual deployments; here we show only trajectories longer than 10 days).

The separation of the Tyrrhenian circulation in two regimes is clearly shown in the portions of trajectories plotted according to the drifter speed (Figure 5). Figure 5 nicely displays the deductions drawn from the trajectory analysis: the slowest speeds (less than 15 cm/s) dominate the central-southern area of the basin; speeds between 15 and 25 cm/s are clearly associated with mesoscale and sub-basin recirculation structures, and are ubiquitous in the whole Tyrrhenian; fastest speeds are associated with the (northern) Tyrrhenian coastal

current, as we would like to define it from now on, with the Corsican-Sardinian coastal current, i.e. the southward coastal current flowing along the western boundary of the basin, and also limited to the northern part of it, and occasionally with the jet-like flow of AW directed between Ustica and the Eolian Islands.

Given the limited number of instruments available for this experiment, it is not possible to adequately describe the exchange between the Tyrrhenian and the neighbouring basins.
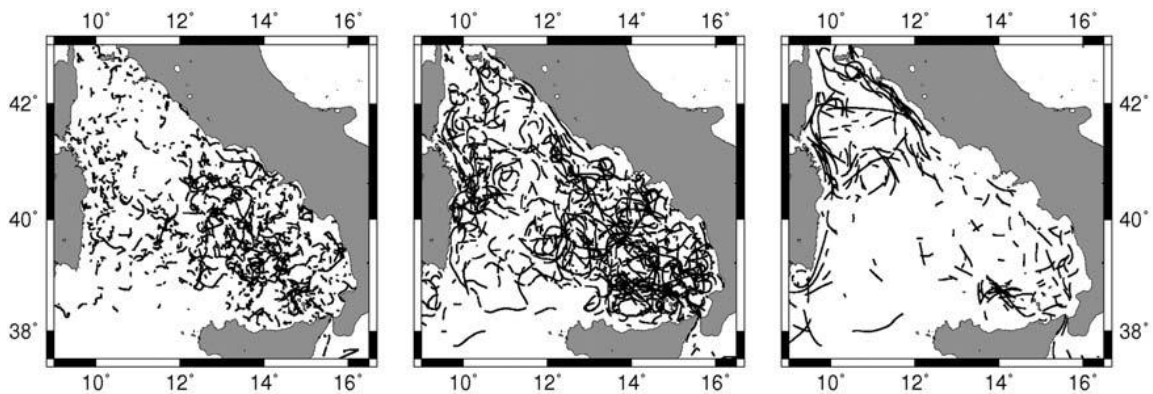
Figure 3.5 Segments of trajectories corresponding to different drifter speed ranges: (left) lower than 15 cm/s, (middle) between 15 and 25 cm/s, and (right) higher than 25 cm/s.

As to the northward outflow of surface Tyrrhenian water through the Corsica Channel, it is worth noticing, however, that only four out of ten drifters approaching the channel flowed through it into the Ligurian Sea. The outflow described by these four drifters occurred between mid November and mid December of two different years, confirming the seasonal character of the flow in that area, possibly driven by the steric difference between Tyrrhenian and Ligurian Sea level (Vignudelli et al., 2000).

On the opposite side of the basin, various drifters deployed in the Southern Tyrrhenian were stranded in the close vicinity of the Strait of Messina, or even crossed it and entered the Ionian Sea. This happened in three out of four southern deployments, and in particular to one over eight drifters deployed during the 1st deployment episode, five over nine in the 2nd, one over nine in the last one.

Three out of the seven drifters approaching the Strait of Messina eventually crossed it and made it into the Ionian Sea. This pathway from the Tyrrhenian to the Ionian Sea was also recently inferred in transmitter-equipped Caretta caretta turtle trajectories (Bentivegna et al., 2007). The drifter data for the first time made a direct observation of this flow.

3.2.2   Pseudo-Eulerian analysis of drifter data

In figure 3.6 I show the maps of pseudo-Eulerian statistics relative to the drifter data which will be compared in the following sections with analogous quantities drawn from altimeter data. The maps of MKE and the mean flow (Figure 3.6a) well reproduce the general pattern of the circulation described in section 3.1.1. The highest levels of MKE are observed in correspondence to the cyclonic sub-basin circulation between Sardinia and Sicily and in the northern regions of the basin in correspondence of the NTC and in the NTA. Moreover the value of some bins in the Corsica Channel (levels of energy greater than 200 cm^2/s^2 and speeds above 20 cm/s) reveal the energetic character of the seasonal flow in this area. In the south-eastern region of the Tyrrhenian Sea, it is not possible to identify a clear mean flow, the highest values of MKE being found near the Eolian Islands.

Similarly to what was found for the MKE, high values of EKE (Figure 3.6b) prevail in the northern part of the basin, where the variance ellipses show a large degree of anisotropy in correspondence of the northern Tyrrhenian coastal current and on the edges of the two main structures, NTC and NTA. A very high variability is also displayed in the south-eastern region of the basin, which is particularly remarkable since MKE values in that area are low, thus leading to a strong increase of the EKE/MKE ratio. In this section of the basin the EKE map displays a circular area, between 12-16°E 38-40.5°N, with values greater than 150 cm^2/s^2 along the edges of the structure and lower values at its centre. Probably, this distribution is due to the variability of STA, of the current flowing off the northern coast of Sicily and of the cyclonic and anticyclonic recirculations west of Eolian Islands.

Figure 3.6. Pseudo-Eulerian statistics from drifter data. (a) Mean kinetic energy with superimposed themean flow vectors. (b) Eddy kinetic energy with superimposed the variance ellipses. (c) MKE and mean flow vectors obtained smoothing fields shown in Figure 3.6a. (d) EKE and variances ellipses obtained smoothing fields shown in Figure 3.6b.

3.2.3 Overview of the surface circulation as described by the altimeter data

This subsection describes the surface circulation traced by the altimeter data (Figure 3.7 a and 3.7b). In the mean field, the NTC anticlockwise rotation emerges as the prominent structure of the circulation in the northern region of Tyrrhenian Sea. The eastern boundary of this gyre is represented by the coastal current leaving the Tyrrhenian Sea through the Corsica Channel.

The NTA acts as the southern boundary of the NTC, but it is distinguished by lower values of energy than the NTC. The westward flow of the NTA meets a double core cyclonic gyre that extends as far south as 38°N capturing the major portion of the AW entering the basin. The presence of this gyre can explain the outflow in the western side of the Sardinia Channel observed in hydrological measurements (Sparnocchia et al 1999 and Astraldi et al. 2002). The highest values of MKE (>135 cm^2/s^2) for this feature are associated with the southward flow along the Sardinian coast and with the southern area of this vortex (MKE >300 cm^2/s^2).

A minor portion of the AW is captured by the STA, the anticyclonic vortex between 12-13 E and 39-40 N, having a circular shape with a diameter of ~100 km and MKE level of around 70 cm^2/s^2. An anticyclonic circulation prevails near the northern coast of Sicily, and higher energy is observed in its eastern zone where it encounters another gyre having a cyclonic rotation that extends until 40° N. Offshore the Gulf of Naples, a second anticyclonic recirculation is present. The presence of this series of eddies means that the AW entering in the Tyrrhenian Sea in the eastern part of the Sardinia Channel, rather than flowing cyclonically along the Sicilian and Italian coasts is shifted offshore, creating a more complex surface circulation in the whole southeastern domain of the basin.

Qualitatively, the EKE map shows a distribution similar to that of the MKE, with maxima in correspondence of the divergence zone of the NTC and NTA (EKE > 135 cm^2/s^2), along 38°N and along the eastern side of the cyclonic gyre in front of the Calabrian coast (between 15°-16°E 38°- 40° N) where the eccentricity of variance ellipses shows that the variability of the mean flow is prevalently oriented along the northwest-southeast direction.

The central area of the Tyrrhenian Sea is characterized by low values of EKE except for the area occupied by the STA. Over the whole basin, the MKE is generally higher than the EKE.
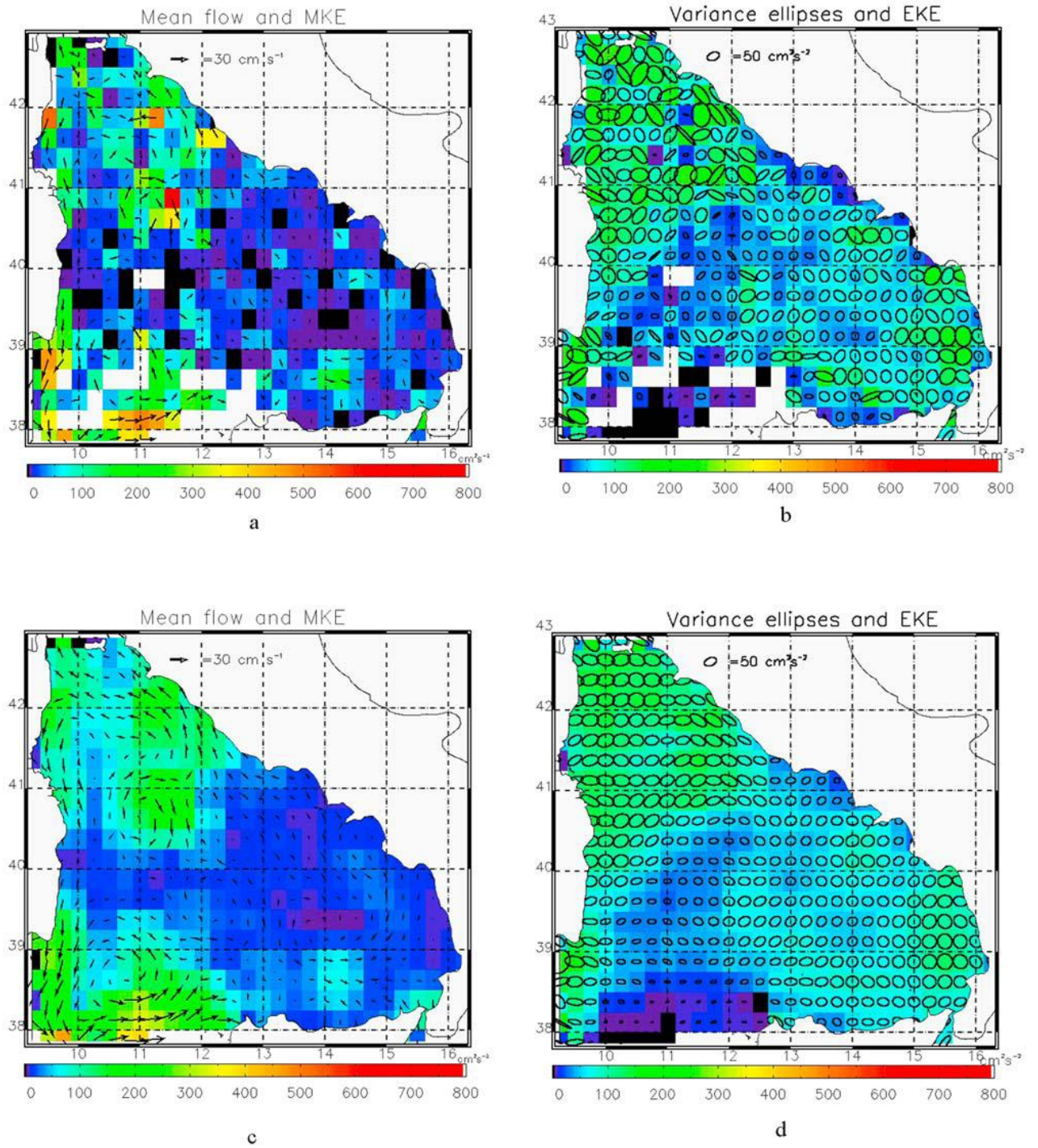
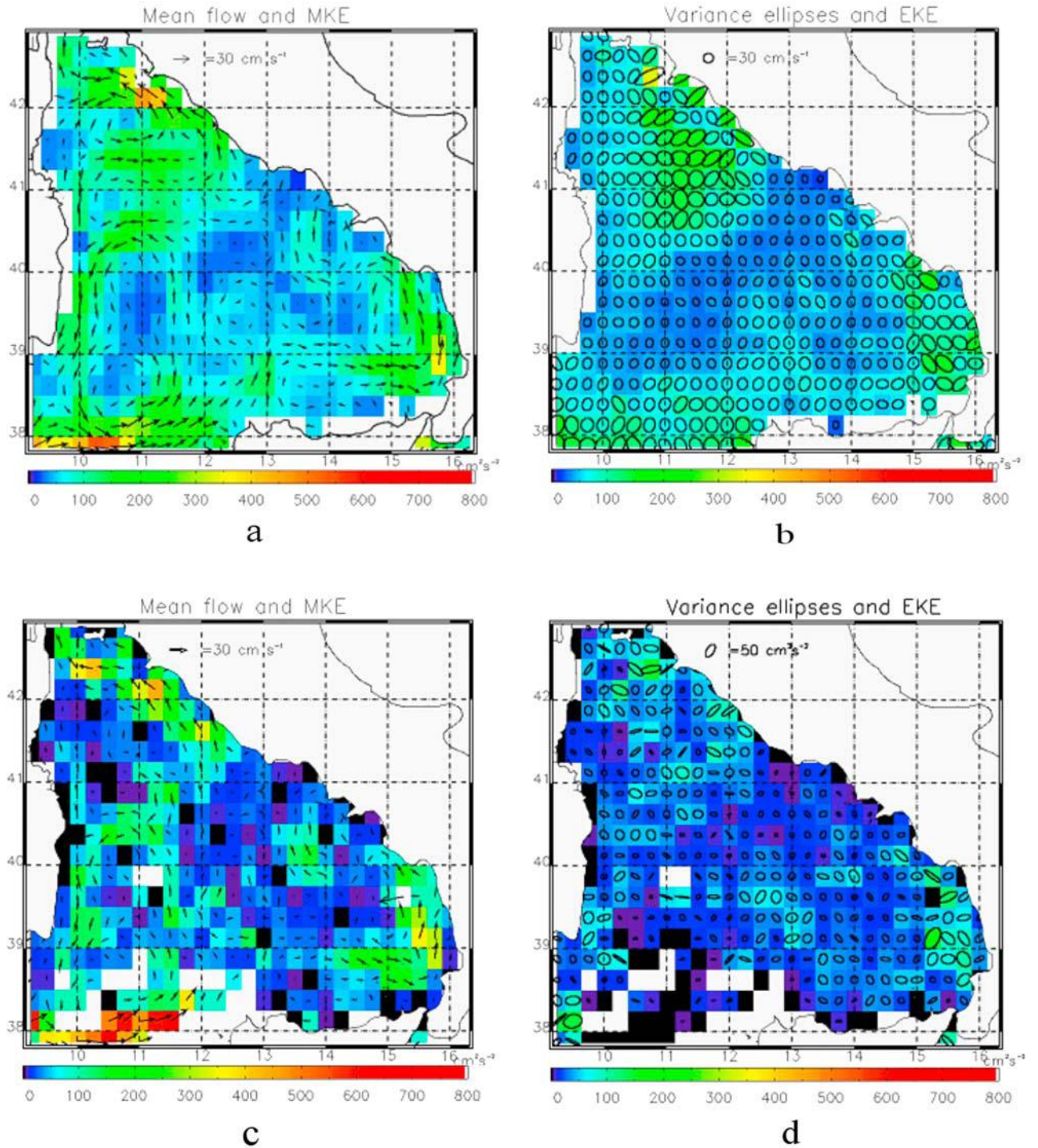Figure 3.7. Pseudo‑Eulerian statistics from altimeter data. (a) Mean kinetic energy with superimposed the mean flow vectors. (b) Eddy kinetic energy with superimposed the variance ellipses. (c) MKE and mean flow vectors computed using altimeter data sampled in correspondence of the drifter measurements. (d) EKE and variances ellipses computed using altimeter data sampled in correspondence of the drifter measurements.

3.3 Joint pseudo-Eulerian analysis of altimeter and drifter data

Even if altimeter measurements are by definition Eulerian and consequently Eulerian statistics might be easily computed from them, in the present analysis the same kind of averaging and binning procedures have been performed on both altimeter and drifter data (thus we will call both pseudo-Eulerian in the following). This choice was driven by the necessity to evaluate the limits and representativeness of both datasets in terms of dynamical and/or sampling factors. In fact, original altimeter data are collected along tracks that are located several kilometres apart, with an instantaneous field of view of ~9 km, and a repetitivity ranging between 10 days and 35 days. These data are then used to obtained interpolated fields, as described in section 2.3. On the opposite, drifter data are characterized by a purely Lagrangian sampling, with large data gaps both in space and time. However, they also provide different measurements of the surface circulation in terms of dynamical components, for example including or not the ageostrophic components of the flow.

The maps of MKE and the mean flow estimated from drifter data and from altimeter are shown in Figures 3.6a and 3.7a, respectively. Despite the fact that the general pattern of the circulation shown in the two maps is quite similar, the energy levels are rather different. In general the value of MKE is slightly greater for the altimeter data than for drifters (basin averages are 99 cm^2/s^2 and 74 cm^2/s^2, respectively). In the southeastern area of the basin, the MKE levels appear higher when estimated from the altimeter than from drifter data but the contrary occurs in the western region in correspondence of the NTA and in the western side of NTC.

On the other hand, the two EKE maps (presented in Figure 3.6b and 3.7b) are quite different both in terms of structure and orientation of the variance ellipses and in terms of energy values. Energy levels computed from the altimeter are lower than those obtained from drifters almost everywhere (except in the region of divergence of NTC and NTA, 11°E-41°N where the EKE levels of the two maps appear quite comparable). Indeed the average EKE of drifters is 73 cm2/s2 while the average EKE of altimeter is 67 cm^2/s^2.

A possible source of the observed discrepancy might be represented by the fact that the altimeter-based dynamic topography actually leaves out the scales of variability that are

significantly smaller than the decorrelation length (~ 100 km) used by the optimal interpolation algorithm.

Moreover, the differences are possibly due to the fact that, despite the 36 hours trajectory filtering removes part of the ageostrophic components of the current, the drifter velocities still contain an ageostrophic component due to the wind-driven Ekman transport, to cyclostrophic balance and/or to rapidly evolving mesoscale features. These components cannot be detected by altimetry, given that the geostrophic approximation has to be assumed in order to estimate velocities from measured surface elevation (see section 3). For that reason, as part of our analysis, the Ekman component has been estimated from the ECMWF wind data and subtracted from the drifter velocities.

However, the MKE and EKE statistics calculated from corrected velocities (not shown) do not show large differences from a qualitative standpoint, with respect to those computed from uncorrected data: the mean flow pattern, the eccentricity of variance ellipses as well as the general distribution of MKE and EKE are very similar. The impact of the Ekman correction is of the order of 20% on the EKE (in agreement with the order of magnitude discussed by Mauri and Poulain, 2004; see also Poulain et al., 2009) and twice as much on the MKE. The corrected trajectories have thus been used hereafter.

The latter value, however, is not surprising, as the mean circulation is not directly related to the instantaneous or short-term wind forcing (see again, Mauri and Poulain, 2004). This is the case of the NTC and the NTA: they are induced by the wind but in fact represent the effect of geostrophic adjustment over much longer time scales (Crepon et al., 1989); for this reason in the area downwind the Strait of Bonifacio, i.e. in the Tyrrhenian zone where winds are generally the most intense, the MKE relative difference shows only a marginal maximum. On the contrary, maxima of this difference are found in correspondence of subareas of the southern part of the basin, where the mean surface velocity field is much weaker and more subject to the short-term wind effect.

In order to better check on the consistency between the Lagrangian measurements and the altimeter dataset, and to evaluate how much of the observed differences can be related to dynamical processes, the pseudo-Eulerian statistics derived from the drifters have also been spatially smoothed. The data have been smoothed using a moving average with a square boxcar. The dimension of the boxcar has been chosen to be as comparable as possible to the scales of spatial decorrelation used in the optimal interpolation of altimeter data (~100 Km). The resulting fields are shown in Figure 3.6c and 3.6d.

Lagrangian and Eulerian observations of the surface circulation in the Tyrrhenian Sea

The smoothing does not modify significantly the average of the MKE and of the EKE (73 cm^2/s^2 and 66 cm^2/s^2 respectively). On the western side of the basin (west of 12 °E), the smoothed drifter data (Figure 3.6c) display approximately the same qualitative (spatial distribution of local energy minima and maxima) and quantitative (actual MKE values) patterns shown by the altimeter data of Figure 3.7a. This agreement is evident for the eastern side of NTC, in which the highest value of energy (~170cm^2/s^2) characterizes the current along the Italian coast; the same values of MKE are observable in the Corsica Channel. Nevertheless, the westward flow just above 41°N observed in the altimeter data is not visible in the smoothed drifter field. On the eastern side of the Tyrrhenian Sea the value are still quite different. This is probably due to the fact that in the western area of the basin the circulation is characterized by sub-basin scale structures, while in the eastern region the circulation is more irregular and dominated by the mesoscale field. So the differences can be due to the different capacity of the instruments to sample the mesoscale dynamics.

The values of the smoothed EKE estimated from the drifter dataset are also in this case larger than the altimeter EKE ones, in fact the relative difference between altimeter and smoothed maps is of the order of 43%. The correlation between altimeter and drifters EKE maps and between altimeter and smoothed drifters maps is very similar (of the order of 0.37, we computed the Pearson correlation coefficient estimating its confidence levels with the Student-T test) .Finally, to further investigate if the differences between altimeter and drifters are due to different sampling capability and/or to dynamics, the pseudo-Eulerian statistics have been estimated from altimeter data resampled along drifter trajectories (Figures 3.7c, 3.7d).

The MKE map of altimeter data sampled over drifters is quite similar to the drifters MKE maps, the value of the mean MKE is comparable to the mean MKE of drifters data (88 cm^2/s^2 and 84 cm^2/s^2 respectively); moreover the correlation between the two patterns is of the order to 0.7 with a significance of 99%. This value of correlation is very different from the correlations found between all combinations of previous MKE maps (altimeter-drifters and altimeter-smoothed maps), that never exceeded 0.4.

On the opposite, the levels of re-sampled altimeter EKE, the size and the orientation of the variance ellipses are still very different. The average altimeter EKE is still very low (29 cm^2/s^2) with respect to the EKE computed from the drifters, moreover the variance ellipses are more regular and smaller than those from both smoothed data and drifters. On the other hand the correlation for the EKE maps is 0.45 with a significance of 99%.

Even though the differences observed can still be partly imputed to the different intrinsic space-time sampling capability of the two instruments (drifters are smoothed spatially but not temporally, while altimeter data, though representative of a particular day, are obtained interpolating data collected at different times, that are then smoothed through statistical interpolation), the above analysis indicates that a significant part of the drifters EKE is possibly associated with ageostrophic signals. In any case, however, our results suggest that any research involving interpolated altimeter data (as modelling validations, for example) should carefully take into account that altimeter data may be biased in terms of energy involved in the variable processes.

3.4   Seasonal variability

In order to characterize the main seasonal variability of the circulation in the Tyrrhenian, the mean flow, MKE and EKE were computed from the four year altimeter dataset separately for winter (from November to April) and summer seasons (from May to October). These two extended seasons were defined by subdividing the year in all possible couples of six-month periods and selecting the two periods showing the maximum difference between each other. The resulting definition turned out to coincide with the choice made for the Tyrrhenian Sea by Marullo et al. (1994) and for the central Mediterranean by Poulain and Zambianchi (2007).

The analysis shows (Figure 3.8) that the NTC is stronger in summer than in winter. From May to October it extends over the entire width of the basin, velocities and MKE levels much higher than in winter (reaching values above 200 cm^2/s^2) characterize the southern section of the cyclone. In contrast, from November to April, the NTC is confined between 10°E and 11° E and 41.5°-42.5°N, while a strong and wide northward current is observed along the Italian peninsula at the same latitudes. This current is not clearly visible in summer, when the inflow of the AW at 12.5°E appears weaker and mainly captured by the STA and by the eddy centred at 40.25°N- 14°E.

The structure and intensity of the NTA are linked to that of the NTC. In summer, when the NTC has an elongated shape around 41.5° N, the NTA has a zonally oriented ellipsoidal shape and it is more intense. In this period, sea-surface heights display a strong gradient and the MKE levels reach the value of 250 cm^2/s^2. On the contrary, during winter, the NTA takes a circular form and presents MKE values of around 100 cm^2/s^2 only along its eastern and southern boundaries.

Lagrangian and Eulerian observations of the surface circulation in the Tyrrhenian Sea

The seasonal variability of the EKE is coherent with the pattern and position of these two structures. A large area of high variability occupies the entire region north of 45.5N and reaches value of the order 180 cm^2/s^2 while in winter the maximum of EKE (130 cm^2/s^2) is positioned in correspondence to the eastern boundary of the NTC and NTA.

The two-core cyclonic structures present along the southeastern coast of Sardinia and elongating southwards in the Sardinia channel (located in the area 10°-12° E, 38°-40° N) have the same variability of the two gyres in the north. In summer, it is characterized by higher values of MKE and the cyclonic eddy in the south of Sardinia is more intense. In the entire region off of Sardinia, Fig 8 shows similar pattern of the variance ellipses and similar values of EKE in both winter and summer indicating that the EKE seasonal signal is very limited.

On the contrary, the flow features in the southern Tyrrhenian are weaker in summer than in winter. While the shape and position of the STA and of the eddies centred at 40.25°N- 14°E and 15°E-39.5° N are unchanged from one season to the other, from November to April, they display higher values of MKE and stronger gradient of sea-surface heights. The EKE shows a very similar pattern in both seasons even if higher values are observed in winter, probably due to the intensification of the AW inflow.

Even though the analysis on altimeter data was performed over only 4 years and the drifter trajectories are relatively sparse, the seasonality shown in the north Tyrrhenian by remote sensing and drifter data is in good agreement with former analyses (Marullo et al., 1984; Vignudelli et al., 1999 and 2000), which leads us to believe that the Tyrrhenian indeed has a strong seasonal variability. This analysis also revealed that the seasonal signal mainly affects the mean pattern of the circulation instead of modulating its variable eddy field.
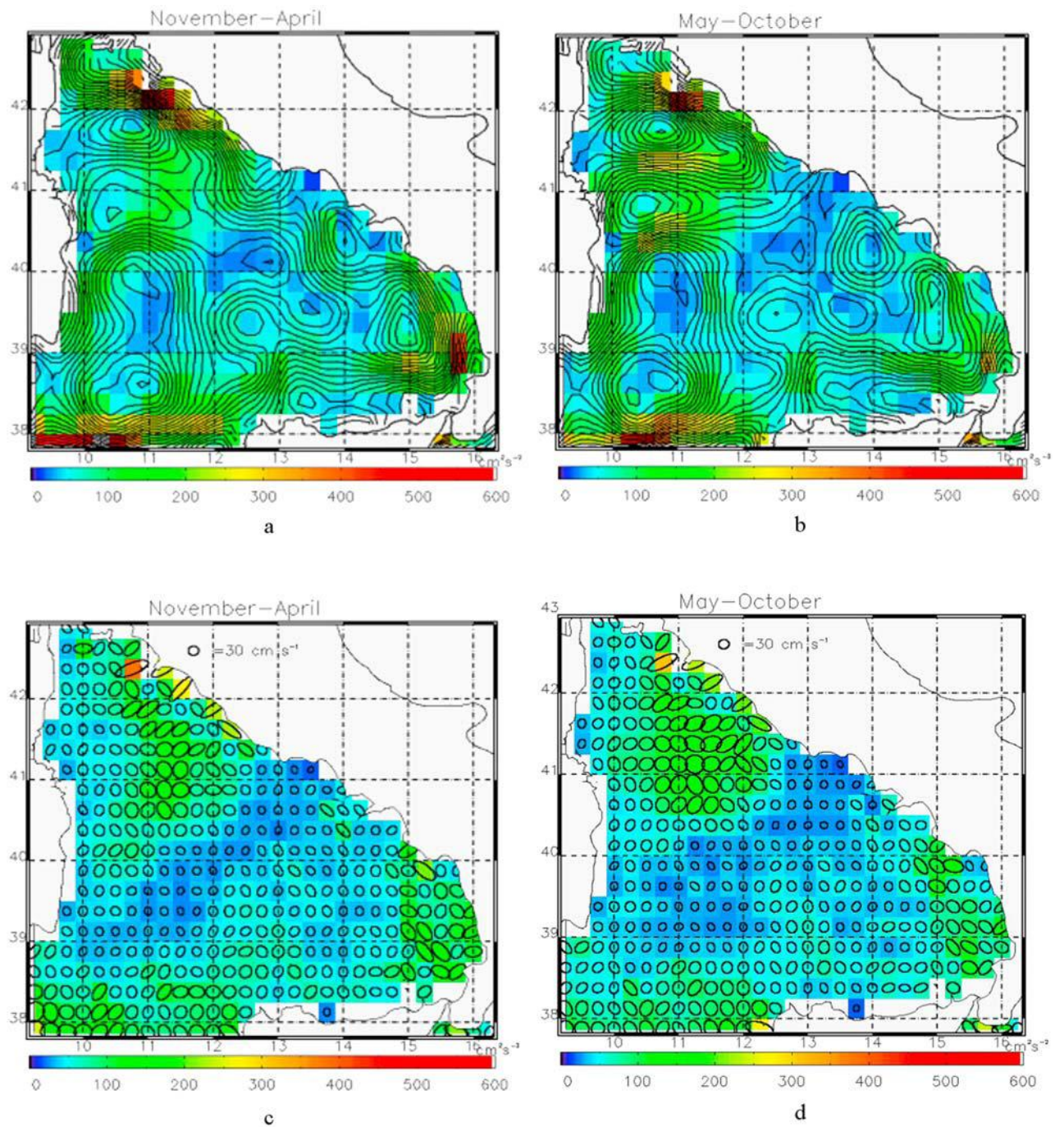
Figure 8. Seasonal variability of the Tyrrhenian Sea circulation from altimeter data. Mean kinetic energy with superimposed the mean flow vectors in (a) winter and (b) summer. Eddy kinetic energy with superimposed the variance ellipses relative in (c) winter and (d) summer.

3.5   Conclusions

The study of the Tyrrhenian surface and near surface circulation was performed analyzing 53 CODE drifters and 4 years of altimetric data. The analysis of individual drifter trajectories together with pseudo-Eulerian statistics calculated using both datasets has provided a new insight about the Tyrrhenian Sea mean surface circulation and associated variability.

The circulation pattern resulting from this study is very different from that described in the literature, and new structures of the circulation are identified. In contrast to the classical view of circulation, the trajectory analysis and the pseudo-Eulerian statistics describe a circulation which only in a very broad sense can be considered as 'overall cyclonic', modulated by a series of mesoscale/sub-basin structures, of both transient and semi-permanent nature. The importance of these structures overcomes by far the mean flow pictures, especially in the southern sub-basin.

Among these structures, besides the already known NTC and NTA, new structures of the circulation have been identified, specially in the southern region of the basin.

In particular, between 12°-13° E and 39°-40° N, an anticyclone gyre (STA) has been observed in both dataset as a persistent feature of the circulation. Moreover, in the south eastern region of the basin the incoming flow is deviated offshore from the Sicilian coastline by the presence of an anticyclonic gyre and it is trapped by a second cyclonic gyre located in front of the Calabrian coast. Finally, our analysis shows that the bifurcation of the AW at the southern entrance of the basin is due to the presence of the double core cyclonic structure described in section 3.2.3.

A certain degree of seasonal variability was detected in the altimeter data. In particular, the circulation features in the western side of the basin appear to be stronger in summer than in winter. In contrast, the STA and the circulation in the south eastern region are more intense in winter than in summer. This seasonal signal affects the general pattern of the flow and the associated MKE instead of the eddy field, which is less variable with the season almost in all the basin, with the exceptions of the area occupied by the NTC and the region offshore the south eastern boundary, where higher differences are found.

This observed seasonal signal seems more strongly influenced by the inflow and outflow at the main open boundary of the basin, than by the local variability of the wind field. The maximum MKE in the southern part of the basin is in phase with the outflow at the Corsica channel, consistently with Astraldi e Gasparini (1992) hypothesis that the intensification of

the Tyrrhenian Sea western current is ruled by the winter surface buoyancy fluxes in the Ligurian-Provencial basin. This process also requires the increase of the inflow at the southern entrance of the basin, as visible in Figure 8, in order to compensate the increasing of outflow. This hypothesis has also been confirmed by modelling studies of the Mediterranean Sea by Artale et al (2002).

Moreover, the winter increase of the Tyrrhenian outflow is known to be responsible to the NTC dislocation towards Corsica and its meridional orientation. Since the NTC-NTA system is driven by the wind stress curl at Strait of Bonifacio, observed all year round (Artale et al 1994), it is not surprising that these features are always present in our data.

The apparent contradictory seasonal maximum EKE in the summer season when northwestern winds are less intense with respect to the winter season can be attributed to the same process. In summer, when the outflow is minimum, the basin can respond to local forcing and internal dynamics, and the variability of the wind stress at the Strait of Bonifacio can drive a higher variability in the strength and position of the NTC, as observed also in the infrared imagery by Marullo et al (1994) and Perilli et al (1995).

The pseudo-Eulerian statistics computed with the two datasets highlighted the sampling and dynamical differences between drifter and altimeter measurements. The MKE levels of energy are quite similar when comparing the altimeter data sampled over drifter trajectories with the spatially smoothed pseudo-Eulerian statistics derived from drifter. However, the variance ellipses and the EKE levels computed from altimeter measurements are always smaller than those from drifters. Consequently, it is possible conclude that, even though altimeter data obviously ensure a wider and more regular sampling, they are missing a considerable part of the signal, at least when considering the standard interpolated products.

Chapter 4

Phytoplankton distribution and variability in the Sicily Channel as seen by remote sensing data

In this chapter I present the study performed on phytoplankton biomass space-time variability in the Sicily Channel. The aim of this work is to infer on the relative importance of the upper layers mixing and horizontal and vertical advection, associated with the surface circulation and with the recurrent wind-driven upwelling along the southern coasts of Sicily (see Chapter 2) in controlling the biological variability over time scales, in a key area as the Sicily Channel.

Given their high resolution spatial and temporal coverage, satellite data represent the best data choice for exploring these issues. Indeed, in upwelling systems, in which colder and nutrient-richer waters reach the surface from below, the sea surface temperature (SST) can represent a good proxy of the nutrient enrichment process in surface waters (Strickland et al., 1970; Traganza et al. 1983; Siliò-Calzada et al., 2008). Therefore, when upwelling is the dominant process driving phytoplankton variability, one would expect a negative correlation to occur between SST and CHL.

On the other hand, the analysis of the sea level (SL), and in particular of the surface Kinetic Energy (KE) associated with water mass movement, can provide a first order insight into the circulation patterns that may affect the phytoplankton dynamics shedding light on the role of water mass advection in the regulation of phytoplankton space-time variability.

Consequently, in this work satellite data will be used to infer on both biological (ocean colour data) and physical (SST and SL) processes.

4.1   The Data

The dataset analyzed in this work covers the time period spanning from January 1998 to December 2006. Weekly fields, averaged over 8-day, at 1/16° spatial resolution were analyzed.

The Sicily Channel domain was obtained for the three datasets (Chl, SST and KE) by extraction from each of the weekly fields. Since, on one side, ocean colour data quality may be affected by bottom reflection or sediment resuspensions, and on the other because continental shelf dynamics is beyond the scope of this work, all pixels with a bathimetry less than 50 m have been masked out.

 The following paragraphs summarize the main steps adopted to obtain them.

4.1.1   Chlorophyll data

The CHL dataset used in this work is the extraction of the Sicily Channel domain (Figure 1.4) from the DINEOF-interpolated SeaWiFS dataset used by Volpe et al. (2011), with the same algorithm (MedOC4, Volpe et al., 2007) and same temporal (8-day) and spatial (1/16°) resolutions. To account for the log-normal CHL distribution, weekly-1/16° fields were obtained by averaging the base-10 log-transformed chlorophyll values (Volpe et al., 2011); thus data presented in this work are the Log10(CHL).

4.1.2   SST

The SST dataset used in this work is the extraction of the Sicily Channel domain from the optimally-interpolated (OI) SST dataset used by Volpe et al. (2011) and developed by Marullo et al. (2007), with the same temporal (8-day) and spatial (1/16°) resolutions.

The OISST re-analysis is based on Pathfinder SST time series and has an accuracy of ~0.6°C and a mean bias error of ~0.04°C with respect to in situ measurement. The sensitivity of OISST accuracy to seasonal factors is lower than 0.3°C and no significant sensor drifts, shifts or responses to anomalous atmospheric events were evidenced (Marullo et al. 2007).

4.1.3 Kinetic Energy

We used the surface velocity (U and V components) Ssalto/DUACS MADT (Mediterranean Absolute Dynamic Topography) product, distributed by AVISO (Archiving Validation and Interpretation of Satellite Oceanographic Data), and consists of the geostrophic velocities derived from the delayed time optimally interpolated ADT, which is obtained from TOPEX/POSEIDON, Jason 1 and ERS1-2, ENVISAT measurements (T/P was substituted by Jason since June 2002, and ERS2 by ENVISAT since July 2003). In the AVISO MADT product, the data provided by the different altimeters are inter-calibrated through a global crossover adjustment of the along-track measurements, referencing all other sensors to T/P (or Jason). Standard instrumental and geophysical corrections are applied (for a more in depth description, see Le Traon and Ogor, 1998).

The Absolute Dynamic Topography product is then computed by adding a synthetic mean dynamic topography (MDT) obtained by merging satellite and *in situ* data to the sea level anomalies (SLA). The method applied to calculate the MDT was developed by Rio and Hernandez (2004) and has been specifically adapted to the Mediterranean data by Rio et al. (2007).

The Kinetic Energy has been calculated as:

$$KE = \frac{1}{2}\left(U^2 + V^2\right)$$

where U and V are the meridional and zonal geostrophic current components computed from the sea surface slope as measured by satellite altimeters (Fu and Cazenave 2001). KE data were remapped on the same 1/16° resolution grid as CHL and SST data, with the same temporal binning.

4.2   Methods

This work aims at assessing the degree of co-variability and at pointing out a cause-effect relationship between biological (CHL) and physical variables (SST and KE. One way of isolating single processes and determining the dominant modes of variability of either physical or biological variables is to apply the empirical orthogonal function (EOF) decomposition to such time series.

Phytoplankton distribution and variability in the Sicily Channel as seen by remote sensing data

The purpose of the EOF decomposition is to find the signals (functions/modes) that explain the maximum variance within in a time series (Lorenz, 1956). The original data can thus be interpreted as a (linear) combination of empirical modes, also known as principal components, which often reflects the variability associated with specific physical (or biological) processes, or to their interaction. EOF analysis represents an efficient tool to describe the ocean physical and biological variability, as demonstrated by the growing number of studies that have used it (e.g. Gallaudet and Simpson, 1994; Marullo et al., 1997; Buongiorno Nardelli and Santoleri 2004, 2005; Buongiorno Nardelli et al. 2003, 2010; Iida and Saitoh, 2007; Katara et al., 2008; Garcia and Garcia, 2008; Primpas et al., 2010).

The method is based on a decomposition of a multivariate data set into an uncorrelated linear combination of separate functions of the original variables ranked by variance. The purpose of EOF is to find the signals that explain the maximum variance in a time series.

Data are represented by a data matrix X(t, s) representing the value of the field X at time t and spatial position s. For satellite data, X is a matrix with dimension MxN, where M is the number of spatially distributed points (sea points) and N is the number of points over time (number of images). To calculate EOF, the mean field (calculated over the whole time series) is removed from each variable $\mathbf{x}$(t). Then the data are organized in a matrix where the rows contain the temporal realizations and the columns identify the spatial data points, so time is incorporated in the state vector and I use EOF to refer to the "temporal" patterns.

Once the anomaly data matrix is determined, the temporal covariance matrix is thus defined as:

$$S = \frac{1}{n} X^T X$$

This matrix is symmetrical and therefore diagonalizable with the Singular Value Decomposition (SVD) method (Press et al., 1992, Golub and van Loan,1996). SVD returns the eigenvector of S (the k'th EOF is simply the k'th eigenvector u_k of S) and the eigenvalues of S.

The eigenvalues give a measure of the importance of each mode. Infact they represent the variance explained by the corresponding mode and are usually normalized to get a percent of the total variance. Eigenvalues and eigenvectors are generally sorted in decreasing order so that the first modes explain the major part of the fields variance.

Results from the EOF analysis have to be interpreted as variability maps with respect to the fields' 2D average values. In other words, the projection of the anomaly field X onto the k'th temporal EOF u_k is given by:

Phytoplankton distribution and variability in the Sicily Channel as seen by remote sensing data

$$a(x, y, t) = \sum_{i=1}^{n} P_i(x, y) \cdot A_i(t)$$

where and Pi and Ai are the EOF spatial patterns and temporal amplitudes for each of the n modes, respectively.

The temporal evolutions of the principal EOF modes of any single variable are used as input to a cross-correlation analysis to allow for i) quantitatively determining the degree of co-variability between biotic and abiotic parameters, and ii) offering a quantitative means for discussing the results.

As consequence of the latter, only the most correlated pairs of modes will be here analysed and discussed. The co-variability between CHL and SST, and KE is assessed through both spatial and temporal lagged correlation analyses.

All correlation values were tested for significance using the Student's T distribution. Student's T test needs, as input, the correlation value (the significance of which we want) and the number of degrees of freedom to evaluate the T parameter that is than compared against those in statistical tables.

An important point is that, when the cross-correlation is computed between two highly auto-correlated time series, the number of degrees of freedom generally used (i.e., N-1 with N = the length of data vectors) is inadequate to represent the effective number of independent observation required by the test. In this respect, and following Volpe et al. (2011, and references therein), the number of effective independent observations, N*, was evaluated for each time lag and for each pair of modes as:

$$N^* = \left(\frac{1}{N} + \frac{2}{N^2} \sum_{lag=1}^{lag=N} (N - lag) \cdot r_{xx}(lag) \cdot r_{yy}(lag) \right)^{-1}$$

where N is the length of the EOF amplitude data variable, and rxx and ryy are the auto-correlation terms of each EOF amplitude data variable.

4.3   Results

The inference on the physical mechanisms (through the analysis of SST and KE) that can potentially explain the biological variability (CHL), is first evaluated on a climatological level (e.g. comparing the $\overline{X}$ derived from the three datasets, Section 4.3.1), and then through a rigorous correlation analysis between different spatial patterns and amplitudes (e.g. comparing the patterns and temporal amplitudes for each of the modes the three data time series, Section 4.3.2).

4.3.1   Climatological coupling between Chl, and SST and KE

Despite the low range of variability, the CHL average map exhibits a quite clear zonation with the up-stream MAW-impacted system being generally more productive than the down-stream one (Fig 2.1a). Coastal areas around Cape Bon and Sicily appear to be the most productive.

The KE average map shows maxima in correspondence of the Algerian Current System and off Cape Passero, this latter producing the well-known homonymic filament (Fig 2.1b). In general, the MAW path (as already described in section 1.3 and schematically shown in Fig 1.4) is well-depicted with all the meanders and gyres associated with it.

The SST average map shown in Fig 2.1c highlights an overall meridional gradient, with the southern part being warmer than the northern part. This temperature pattern is a sign, on one hand, of the mean effect of the latitudinal variations in the heat fluxes (driven by the insolation), and, on the other, of the different water masses present in the surface layer.

The instantaneous correlations among these three average fields prompt for the critical role played by the surface thermal field which can represent a strong constraint to phytoplankton growth (r=-0.86). Although not statistically supported (r=0.37), it is reasonable to deduce that KE plays a stimulating role only in highly dynamics systems such as the Algerian Current and the Cape Passero filament, where CHL shows its maxima (≥ 0.1 mg m-3).

An interesting feature is given by the two minima in the SST and KE maps in correspondence of the local maximum of CHL close to the Sicily coast: this represents the area where upwelling plays a major role by supplying nutrients to the upper lit layer allowing for high phytoplankton biomass abundances.

Phytoplankton distribution and variability in the Sicily Channel as seen by remote sensing data
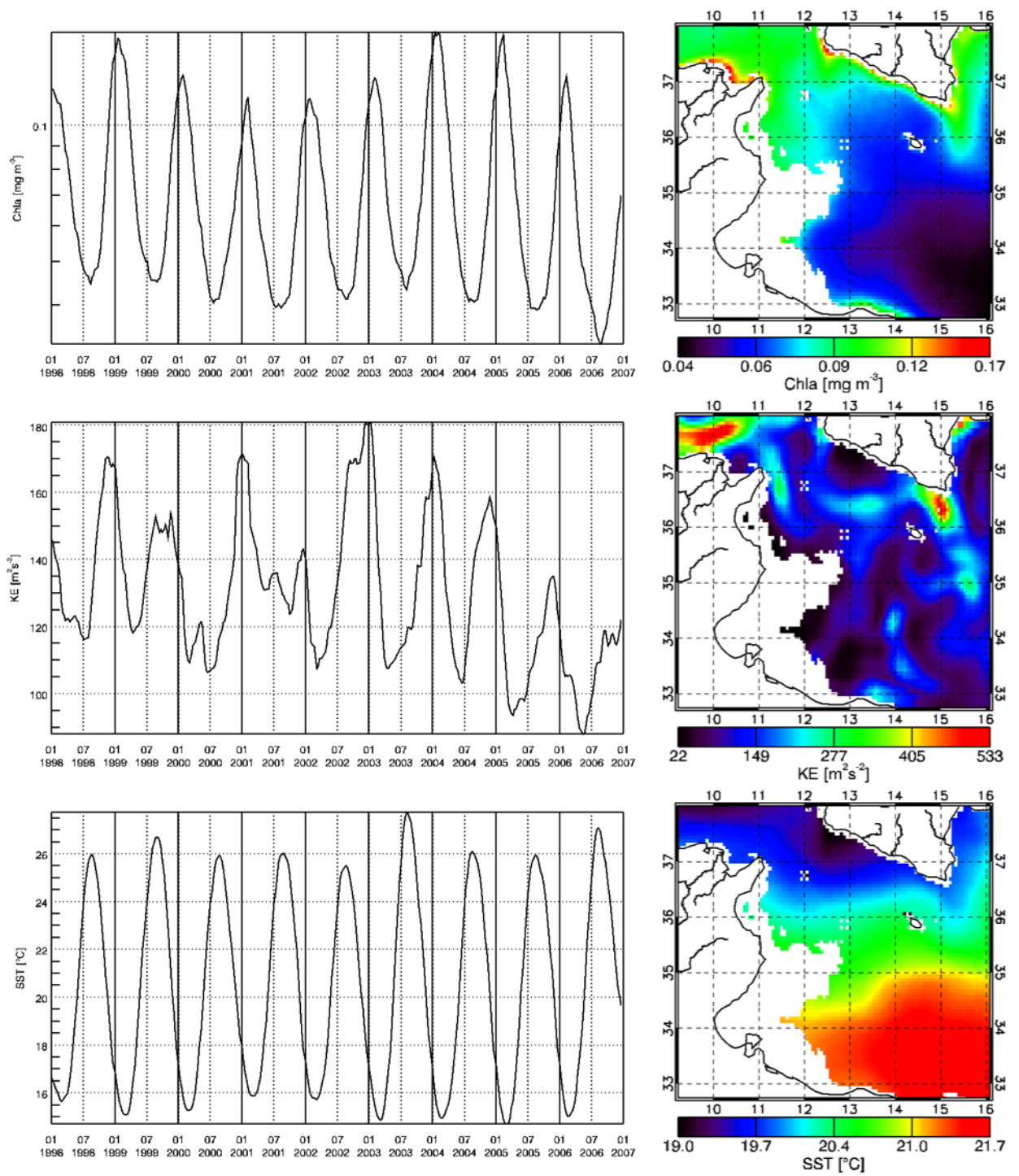

Figure 2.1. Left panels: time evolution of basin scale weekly averages for CHL (upper), KE (middle) and SST. Right panels are the temporal averages over the entire time series (1998-2006). Areas with bottom depth shallower than 50 m are masked out and not taken into account for the evaluation of the time evolution plot

4.3.2   EOF analysis

4.3.2.1   The role of Modified Atlantic water over the CHL seasonal variability (1st CHL mode)

The first CHL mode explains 79% of total variance (Fig. 2.2 a-b). The spatial pattern shows positive values everywhere, meaning that seasonal variations occur simultaneously within the entire channel. The strongest signals, however, are present at the strait entrance, downstream Cap Bon, and also off-shore Cape Passero (Fig 2.2 a) .

 Corresponding EOF amplitude displays a clear annual cycle: the highest signal is generally observed from November/December to March, whereas the lowest values are recorded from June to October (Fig 2.2 b). Interannual variations are also evident, with CHL maxima generally decreasing until 2002. The bloom lasted for a shorter time in 2001 and 2003 with respect to the previous years. The signal then increased up to 2005 and decreased again during 2006.

This mode is strongly related to the first mode of KE (Fig. 3 c-d). In fact, it displays a maximum temporal correlation of 0.70, with a time lag of roughly two months. It is important to remember that to make sure the statistically significant correlations found are not due to auto-correlation but due to "real" relationships, autocorrelation was taken into account by evaluating the effective number of independent observations N*(the number of degrees of freedom) in the significance test, as described in section XX. Moreover, even if the temporal correlation between the first modes of Chl and SST is higher than the correlation between Chl and KE the corresponding spatial correlation the is almost zero, while the correlation between Chl and KE spatial patterns attains around 0.48 (Table 2.1). So the Chl variability explained by this mode is linked to the KE rather than to the SST.

The first mode of KE (Fig 2.2 c-d), representing 15% of KE total variance, describes the annual variations of the MAW inflow and AIS intensity and displacement, which fairly agree with what is known from both in situ and modelling studies (e.g. Robinson et al.1999).

The pattern of the MAW entering the Strait is coherent with what observed by Astraldi et al. (1999) from the analysis of moored currentmeter data. In particular, during the fall-winter season, the flow is more intense. At this time, MAW enters the channel flowing mainly along

the Tunisian coast, while only a smaller portion goes into the Tyrrhenian Sea. On the opposite, during summer, the MAW mainly flows along the south-western coasts of Sicily.

The high temporal correlation between the first modes of Chl and KE and the analysis of the two patterns suggest that the advection of MAW (which is richer in chlorophyll and nutrients than the resident waters) from the northern African coasts has a significant impact on the phytoplankton biomass inside the Channel.

The time delay between the increased advection (in fall/beginning of winter) and the stronger phytoplankton variation (winter/early spring) can then be related to the fact that the CHL concentration in the advected waters also changes with the season, the bloom being favoured by late-winter-early spring conditions. Thus the combination of flow intensity and CHL concentration variations in the advected waters leads to the observed variability inside the Channel.

Additionally, the AIS is more intense during winter also near Cape Passero. In that area, the high chlorophyll coastal waters are advected offshore in a sort of filament while the front between the Atlantic and Ionian waters weakens, driving a lower cross-shelf transport, during summer. In this period, the main flow turns directly northward around Cape Passero.

The significant correlation between the first modes of Chl and KE thus suggests that approximately 80% of the phytoplankton variability inside the Channel is related to the advection of the MAW from the North Africa coasts.

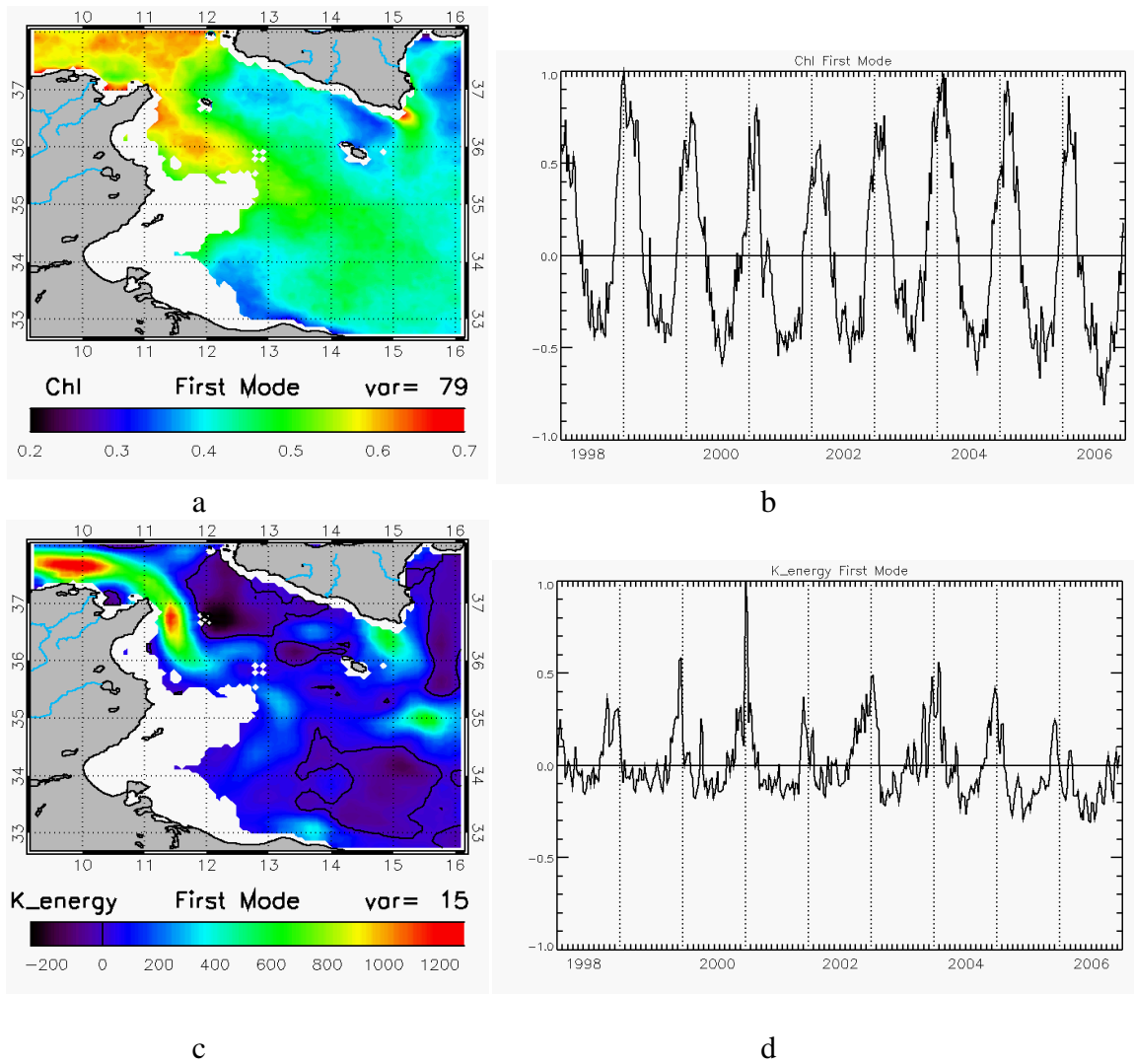Phytoplankton distribution and variability in the Sicily Channel as seen by remote sensing data

a

b

c

d

Figure 2.2 first LCHL(a-b) and Kinetic Energy EOF mode (c-d). Units are in Log10(mg m-3) for LCHL and cm s-1 for KE. Temporal amplitudes and spatial patterns are normalized on the spatial pattern maximum value for each mode. The percentage of total variance explained by the single mode is superimposed to pattern maps.

4.3.2.2 Role of the stratification process on the CHL variability at annual scale (2nd CHL mode)

The pattern of the second CHL mode, explaining 3% of the total CHL variance, shows two regions of opposite sign, with positive (negative) anomalies present in the northern (southern) regions of the Channel (Fig 2.3 a). This pattern reminds the mean SST distribution as visible in fig. 2.3 c, which reflects the typical AIS undulation around the Adventure Bank and the Maltese Bank (Lermusiaux et al., 2001).

Corresponding CHL amplitude shows both high frequency and interannual signals (Fig. 2.3 b), with recurrent spring peaks following negative winter minima in the northern region of the Channel (positive values in Fig 2.3 a), and coastal winter maxima along the Tunisian coasts (negative values in Fig 2.3 a). In 1998, 2002 and 2004, the spring bloom was practically absent, while it was at its maximum in 1999, 2000 and 2005. In the other years, the spring bloom was not particularly marked.

This mode is correlated to the 2nd mode of SST with a temporal correlation of 0.52 (with a lag of roughly five months) and a spatial correlation of -0.92

This second mode, representing 1% of SST variance, displays two regions of opposite sign. Specifically, the northern part of the channel is characterized by negative values while the southern region is characterized by positive values (fig 2.3c).

The temporal amplitude presents the maximum values during 1998 and 2003 (fig 2.3d).

The correlation between these two modes suggests that the phytoplankton responds to stratification-mixing succession as already pointed out by Doney (2006), but with a timing that is very similar to that identified by Volpe et al. (2011) when analysing DWF areas and corresponding spring blooms. In practice, the lower stratification observed along the Sicily coast in autumn/winter (partly due to the simultaneous displacement of the MAW in the southern part of the channel as shown by KE mode 1, but also to the more intense winter mixing), drives a flux of nutrients from the deeper layers to the surface. When re-stratification starts, the favourable conditions for the consumption of these new nutrients drive an increase in the CHL concentration.

In some sense, if CHL mode 1 displays a spring maximum related to the horizontal advection by the MAW of both CHL and nutrients in the centre of the Channel, this second mode

identifies the areas where spring bloom intensity can be related to the only nutrient repletion driven by winter mixing.

Nevertheless, it has to be stressed that the SST amplitude presents a more evident annual signal with respect to the CHL amplitude (with a comparable interannual variability).

a   b

c   d
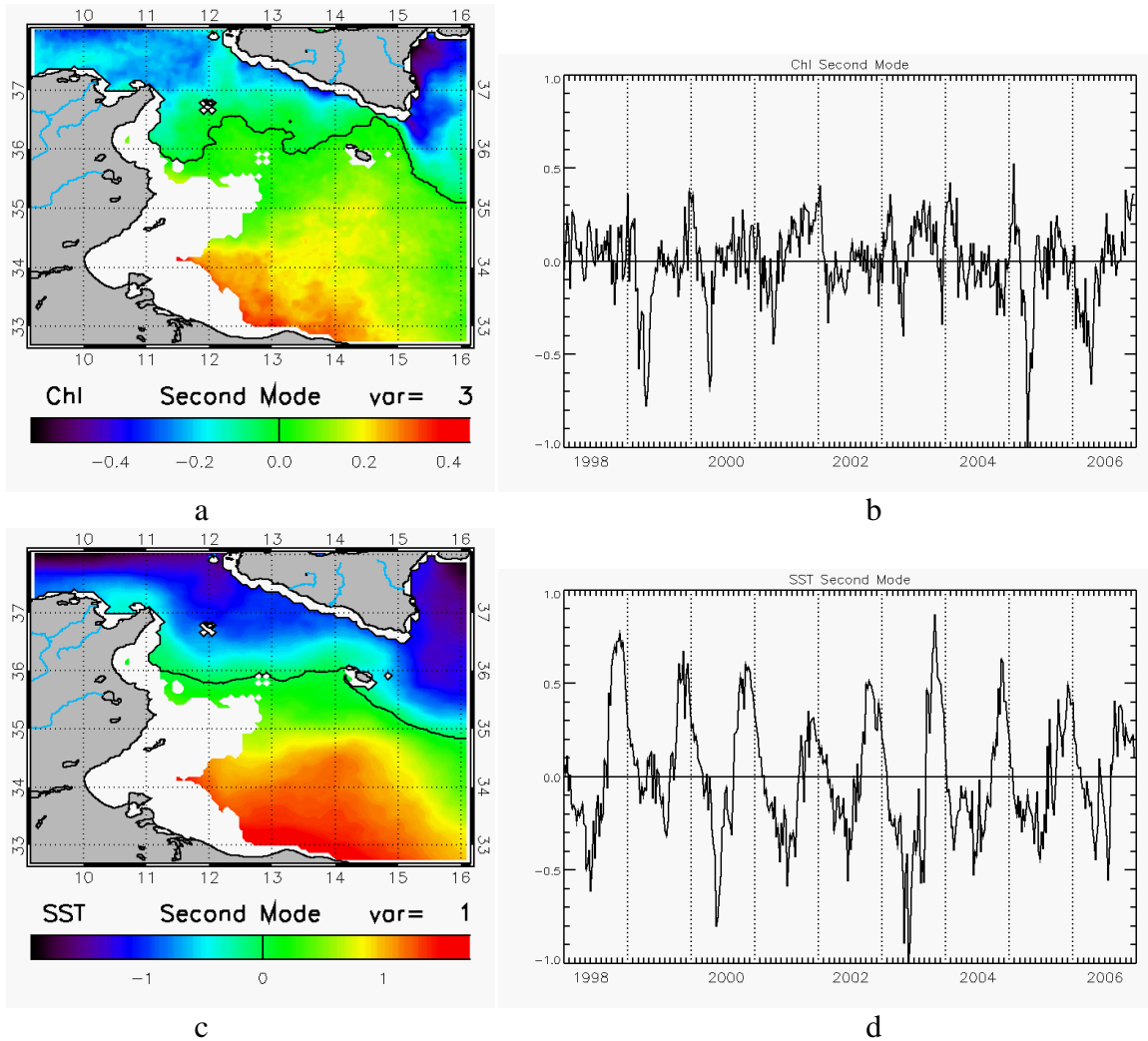
Fig 2.3 Second Chl (a-b) and SST EOF mode (c-d). For details see fig2.2.

4.3.2.3 Response to high frequency atmospheric events (3rd CHL mode)

The third CHL mode (2% total variance) presents a secondary annual signal (as compared to the first CHL mode), with positive anomalies along the African coasts and in the whole western sector of the Channel during the fall season, corresponding to negative anomalies in the Ionian Sea, and opposite anomalies in spring (Fig 2.4 a,b).

The pattern of this CHL mode is strongly correlated to that of the third SST mode (Fig 2.4 c,d spatial correlation ~0.78), but temporal correlation is very low, as the two amplitudes display very different behaviours, the SST mode showing much higher frequency variations than CHL.

As hypothesized by Buongiorno Nardelli et al. (2010) when investigating the causes of SST variability in the Black Sea, this kind of SST responses, namely characterized by high frequency but quite large scale, is likely to be related to the air-sea interactions associated with rapidly changing atmospheric conditions.
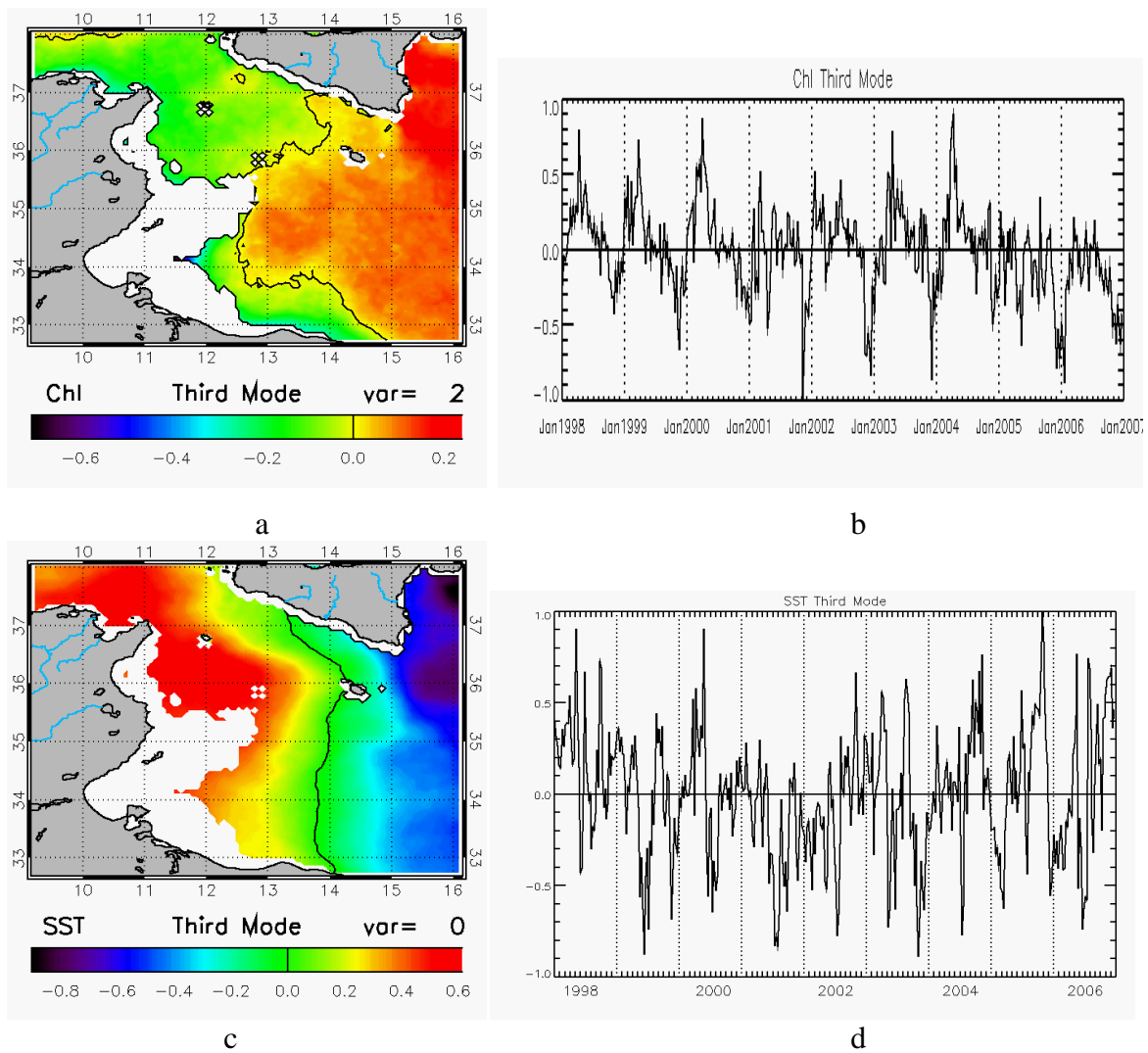
Fig 2.4 Third Chl (a-b) and SST EOF mode (c-d). For details see fig2.2.

4.3.2.4 Response to Coastal upwelling (4th CHL mode)

The fourth CHL mode explains a very small percentage of the total covariance (1.24%), however, it is this mode that more clearly reminds the pattern associated with the well-known coastal upwelling in the area south of Mazara del Vallo.

Corresponding amplitude, though characterized by an irregular evolution from year to year, generally displays positive values during summer, and negative anomalies in autumn (which correspond to positive anomalies along the coasts of Tunisia).

If we compute the correlations between this mode and the first SST one, we get very low values, mainly because of the different response in the SST pattern South of 35° N. However,

if we repeat the computations limiting to the northern part of the Channel, the relation between the two variables appears much more evident, reaching values of about -0.74.

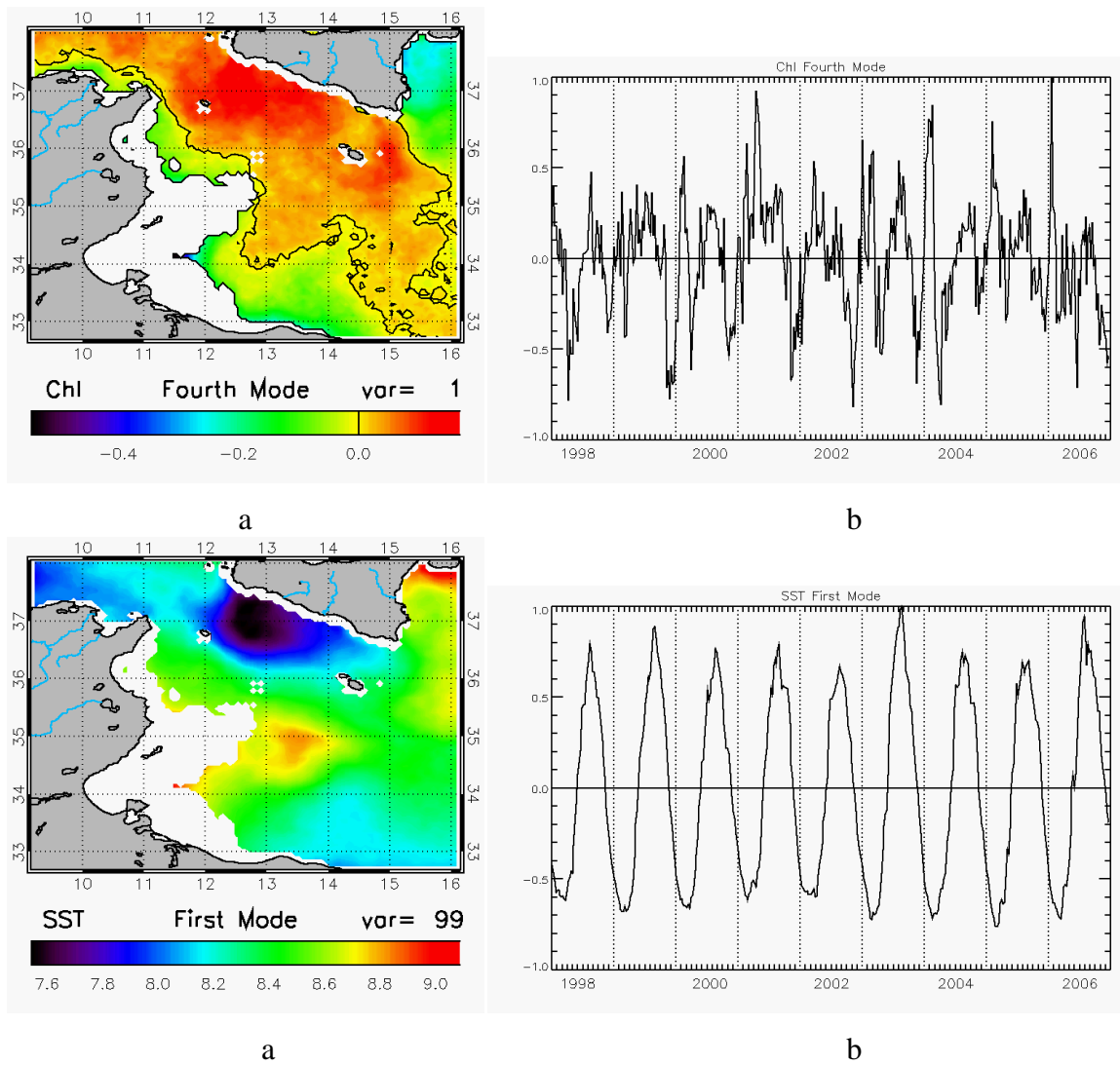a   b

a   b

Fig 2.6 Chl (a-b) and first SST EOF mode (c-d). For details see fig2.2.

Variable 1 (mode#)	Variable 2 (mode#)	Time r	Time lag	Confidence Level	N	N*	Space r
LCHL 1	KE 1	0.70	1.7 months	99.50%	399	14	0.46
LCHL 2	SST 2	0.52	5.4 monts	99.50%	385	42	-0.92
LCHL 3	SST 3	0.2	0	99.50%	405	149	0.78
LCHL 4	SST 1	0.2	4 monts	95%	390	49	-0.02

Table 2.1

Space-time correlation between two variables. Variable 1 follows variable 2 in the temporal correlation analysis with a time lag as defined in the relevant column. The mode to which the correlation refers is indicated next to the variable name. N indicates the length of amplitude vectors, and N* indicates the number of effective independent observations used in the significance test (T-Student) as the number of degrees of freedom.

4.4   Conclusions

The identification of the physical processes that have influence on the phytoplankton variability in the Channel of Sicily was performed applying the EOF analysis to 9 year of Chlorophyll, Sea Surface Temperature and Sea Level data.

Using the result of EOF to calculate the spatial and temporal correlation analyses, this technique has helped us to identify the different mechanisms that drive the Chl variability in the Channel. This analysis showed that the Chl variability is linked, with different time scales, both to the kinetic energy, and therefore to the circulation in the Channel, both the SST and then to the stratification processes that occur in this region.

The high temporal and spatial correlation (0.70 and 0.46 respectively) of the first modes of Chl and KE (that respectively explain the 79% and 15% of total variance) suggests that, at seasonal scale, the phytoplankton variability is principally driven by the MAW advection of water rich in chlorophyll and nutrients from the North Africa coasts.

The time delay of two months between the enhance of MAW transport and the increase of biomass may be justified by the fact that for the phytoplanktonic bloom both nutrients and right lighting conditions are necessary and this combination occurs during spring.

Our results highlighted that at annual scale the Chl variability is linked to the water column stratification and mixing. Indeed, the second CHL mode, explaining 3% of the variance, has an high correlation with the second SST mode that represents 1% of SST variance (time correlation of 0.52 with a lag of five months and spatial correlation of -0.92). This result is in

accord with the result of Doney (2006) and Behrenfeld et al. (2006) even if the time lag similar to that found by Volpe (2011) highlights that the process of mixing-stratification is particularly important for nutrient enrichment along the Sicilian Coasts, that are less affected by the 'horizontal' enrichment of nutrients due to the MAW transport.

Contrary to what was expected this study shows that only a small part of the Chl variability in the Channel is linked to the nutrient enrichment due to the coastal upwelling.

Chapter 5

Ocean Colour Chlorophyll trends along the Italian coasts

This chapter describes the work done to develop and define an appropriate environmental indicator for Italian coastline using Ocean Colour data. Five non parametric methods have been selected to evaluate trends from long time series of OC data. Trends detected by OC data have been compared with trends obtained through *in situ* data to select method to be used to detect long term trends. This comparison allowed to select the most suitable method to apply to the entire OC dataset. Finally the resulting chlorophyll trends along the Italian coasts has been discussed.

5.1   Data

5.1.1   *In situ* dataset

In-situ Chl-a data used in this work are part of the EEA Eionet and ICES network. The dataset consists of 200 coastal stations along the Italian coastlines, with exception of Calabria and Sicily in which no *in situ* measurements are available, see fig 5.1. The stations are sampled with a weekly or biweekly frequency and the overall measurements cover the period 1998-2009. These measurements are part of the Italian contribution to EEA Eionet dataset, and are acquired by the different regional environmental agencies in the framework of Italian coastal monitoring National Program. Even if this Eionet dataset is the only one covering the entire Italian coast water for a sufficient long spanning time, a careful analysis of the data shows several problematic issue that need to the taken into account. First, no all the stations present the same temporal coverage. Indeed many stations are sampled for fewer years, other stations have not temporal continuity coverage and finally many of them are not sampled in all the months of each year. Second important limitation is that the Chlorophyll data have maximum two significant digits, moreover, the information on the sensor used to acquire data are not

available and no information are provided on the calibration procedure used to convert the flourimeter measurements into chlorophyll. So this type of data cannot be used to quantify the errors associated to OC chlorophyll estimates, for this reason I limit their use only to evaluate consistency between in situ and OC trends.
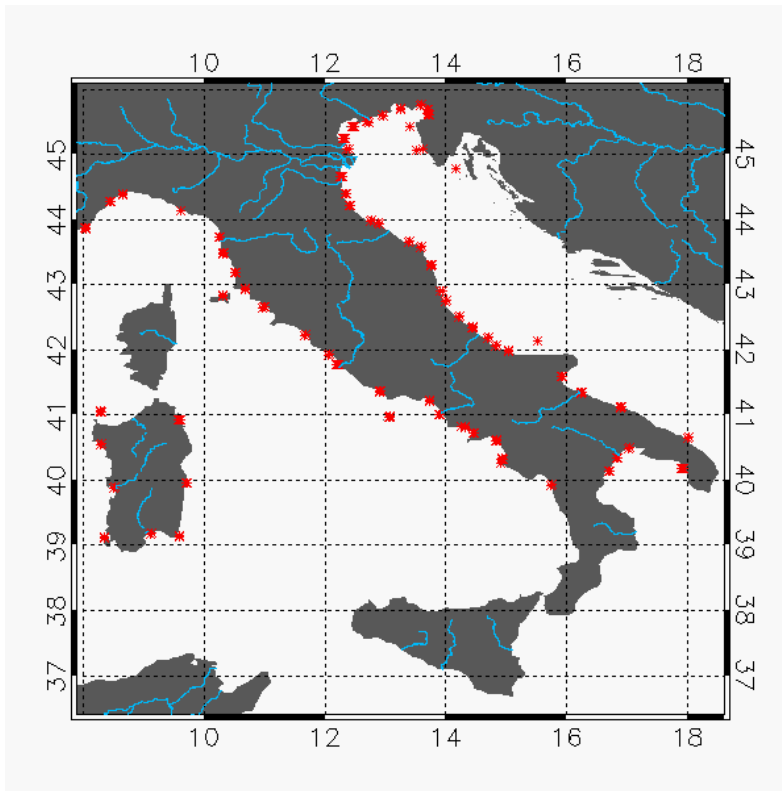
Figure 5.1 Eionet and ICES *in situ* station analyzed in this work.

5.1.2   Ocean Colour dataset

In this work the OC data used are the two OC Mediterranean re-analysis datasets produced by CNR-ISAC. The Mediterranean re-analysis consist in full SeaWiFS time series processed consistently with up-to-date knowledge on satellite sensor calibration, characterization and attitude, complete (as far as possible) ancillary data sets, latest versions of models and algorithms. These re-analysis products are associated with the latest reprocessing version of the NASA software (SeaDaS 6.1), so it is the regional Mediterranean counterpart of the last NASA SeaWiFS re-analysis.

The dataset includes two chlorophyll products: the Mediterranean regional Chlorophyll product and the Mediterranean merged Case1-Case2 chlorophyll product. Both dataset cover

the time period spanning from 1997 to 2009 with a daily temporal resolution and a spatial resolution of 1 Km.

5.1.2.1   OC Mediterranean re-analysis product

This product is obtained processing the entire row SeaWiFS sensor dataset acquired by the receiving station HROM at Istituto di Scienze dell'Atmosfera e del Clima (Rome, Italy) up to L3 applying the MedOC4 ocean colour algorithm for chlorophyll retrieval.

The MedOC4 algorithm has been validated with a large in-situ bio-optical dataset for the Mediterranean area, and its performance has been compared with global algorithms such as OC4v4 for SeaWiFS, the results show that MedOC4 performs better than OC4v4, diverging from *in situ* measurements by about 35% and therefore within the 35% SeaWiFS mission uncertainty target (Volpe et al., 2007).

5.1.2.2   Merged Case 1- Case 2 chlorophyll product

The Case1/case2 product is obtained using two different bio-optical algorithms for open ocean (case1) and coastal turbid water (case2). So in principle, this product should improve the quality of the chlorophyll satellite estimates in proximity to the coast.

The exact identification of the two water types relies on the method described in D'Alimonte et al. (2003), and which takes account of the whole light spectrum from blue to NIR bands for both two water types from *in situ* data. For the computation of these two average spectra two distinct datasets were used, for Case1 and Case2 waters the MedOC4 (Volpe et al., 2007) and CoASTS (Berthon et al., 2002, Zibordi et al., 2002a) datasets are used, respectively.

5.2   Methods

Four non parametric methods to evaluate trends have been selected and evaluated. Only non parametric tests are selected because these are more suitable for non-normally distributed data and for dataset containing data gaps. The most commonly non parametric statistical tests used to assess the significance of trend in hydro–metereological time series are: Ordinary Least Square Regression, Spearman partial rank correlation test, Mann-Kendall test (used by EEA) and Seasonal Kendall Test. For Mann-Kendall and Seasonal Kendall I used the Sen's method to evaluate the slope of the trend.

All the tests analyzed in this study were applied to entire dataset of OC, to entire *in situ* dataset and to the OC data sampled in correspondence to each *in situ* station. More in details the information on location and acquisition time of each in situ measurements are used to select OC chlorophyll data having minimum distance with the corresponding *in situ* data allowing to build new OC dataset. This new dataset has been used as reference to compare the OC and the *in situ* trends in order to avoid differences introduced by discrepancy on space-time sampling strategy. Moreover, to evaluate the sensibility of the tests to the input data sample, all considered tests were applied to the monthly mean data. Only the Mann-Kendall and Ordinary Least Square regression methods were applied both to the daily data and to the monthly mean after removing seasonal signal. Finally the Mann-Kendall was applied to the average of months from May to September (summer season, as done by the EEA for *in situ* dataset, hereafter referred to as summer trend).

To remove the seasonal signal monthly mean anomalies were produced removing from each month the monthly climatological field. For both dataset we used the satellite monthly climatological mean, this is due to the fact that the *in situ* dataset have not enough data to compute the monthly climatology for each station.

5.2.1 Ordinary Least Square regression

Ordinary Least Square regression (OLS) is the simplest method used to test if a trend is present in a time series. This method is based on the statistical formula:

$$Y_i = \alpha + \beta_i + \varepsilon_i$$

Where Yi is the response for year i, α is the intercept, β is the slope and εi are random errors.

The slope and the intercept are evaluated trough the method of least squares. Their values are obtained by the formula:

$$\beta = \frac{\sum (i-\bar{i})(Y_i-\bar{Y}_i)}{\sum (i-\bar{i})^2} \qquad \alpha = \bar{Y}_i - \beta_i \qquad SE(\beta) = \sqrt{\frac{\sum (Y_i-\alpha-\beta_i)^2}{(n-2)\sum (j-\bar{j})^2}}$$

The standard error of the slope is given by:

To reject the null hypothesis (no trend is present in the time series) 0 should not be included in the interval:

$$\beta \pm t_{a,n-2} SE(\beta)$$

$t_{\alpha/2}$ is computed from the t-distribution table using an alfa significance level is a priori specified and n-2 degrees of freedom.

5.2.2 Mann-Kendall test

The Mann-Kendall (M-K) test is the most widely used test for detecting trends in a time series.

The MK test is based on the test statistic S and var(S) definited as

$$S = \sum_{i=1}^{n-1} \sum_{j=i+1}^{n} \text{sgn}(x_j - x_i)$$

$$VAR(S) = \frac{1}{18}\left[n(n-1)(2n+5) - \sum_{p=1}^{q} t_p(t_p-1)(2t_p+5) \right]$$

Where n is number of data and x is data point at times i and j (j > i), g is the number of tied groups (a tied group is a set of sample data having the same value), and p t is the number of data points in the pth group.

If xj >xi S is incremented by 1 on the contrary if xj < xi S is decremented by 1. The final value of S, that is determined by the sum of all increments and decrements, establishes that an increasing trend is present in the time series if the value is positive, on the contrary if the S value is negative there is a decreasing trend.

The statistical significance of the test is computed using the Z value defined as:

$$Z = \begin{cases} \dfrac{S-1}{\sqrt{VAR(S)}} & if \quad S > 0 \\ 0 & if \quad S = 0 \\ \dfrac{S+1}{\sqrt{VAR(S)}} & if \quad S < 0 \end{cases}$$

72

the null hypothesis is accepted if $|Z| > Z_{1-\alpha/2}$, where $Z_{1-\alpha/2}$ is obtained from the normal cumulative distribution tables.

5.2.3 Seasonal Kendall test

The Seasonal Kendall (SMK) test is a modification of the Mann-Kendall test and it is particularly adapt to test trend in case of presence of seasonality in the time series. In the SK test the test statistic S and VAR(S) are computed independently for each month or season, the seasonal statistics are then added, and a Z statistic is computed.

5.2.4 Sen's Method

For both M-K and SK the slope of the trend is determined using the Sen's method.
The magnitude of the slope β is estimated by the median of the slopes after computing the slope of each data pairs

$$\beta = Median\left[Q_k = \frac{X_j - X_i}{j - i}\right]$$

A confidence interval is developed by estimating the M1 and M2 :

$$M_1 = \frac{N - C}{2} \qquad M_2 = \frac{N + C}{2}$$

Where N and C are derived from:

$$N = n(n-1)/2 \qquad C = Z_{1-\alpha/2}\sqrt{VAR(S)}$$

Finally, the slopes corresponding to M1 and M2+1 are chosen as the lower and upper confidence limits, respectively.

5.2.5 Spearman partial rank correlation test

The Spearman partial rank correlation test (SPRC) has been developed to verify the existence of a relationship between two variables, in this case Chl (S) and time (T), after removing the effects of seasonality (M) from the time series. The statistic test for the SPRC method is calculated by:

$$\rho_{STM} = \frac{\rho_{ST} - \rho_{SM}\rho_{TM}}{(1-\rho_{SM}^2)^{1/2}(1-\rho_{TM}^2)^2} \quad \text{where:} \quad \rho_{xy} = 1 - \frac{6\sum_{i=1}^{n}(R_i^{(x)} - R_i^{(y)})^2}{n^3 - n}$$

And $\rho_i(x)$ is the rank of the variable X at time i.

The null hypothesis affirms that there is not relationship between the two variables. To test this hypothesis the test statistic t is calculated thought the formula proposed by Mcleod et al., (1991):

$$t = \frac{(n-2)^{1/2}\rho_{STM}}{(1-\rho_{STM}^2)^{1/2}}$$

The t distribution with n-2 degrees of freedom is used to compute the corresponding p value. If $|t| \geq t_{1-a/2,n-2}$ the null hypothesis is rejected. If ρ_{STM} is positive the trend is confirmed as an increasing trend, on the contrary if ρ_{STM} is negative the trend is definite a decreasing trend.

5.3   Results

5.3.1   Comparison between *in situ* and OC data

5.3.1.1   Results in the test area

As a first step of this work all methods (§ 5.2) were applied over a test area covering the North Adriatic Sea (NAdrS) (Fig 5.2). This sub-region has been choosen, since it is characterized by Po river discharges, by the presence of eutrophication problems and by the presence of both case-1 (open water) and case-2 (coastal water) waters, which affect the quality of OC retrieval. Moreover in this area OC data are already validated in open ocean and coastal water against *in situ* measurements acquired by the scientific community.

The test area presents 46 coastal stations. In order to compare methods, at each stations the standard deviation (σ) of the re-sampled OC data is computed, then I have created three subset of data, the first containing only the *in situ* data and the corresponding satellite data that fall within the range of a standard deviation, the second containing the data that fall within the range of two standard deviations, and the last containing the data that fall within the range of three standard deviations. Therefore the tests were applied separately for each subset of dataset. This type of analysis aims to identify an in situ and OC colour reference dataset that minimize the error introduced by the acquisition and processing methods.

Furthermore, the decision to use a procedure instead of another is based on the consideration of the power and of the efficiency of a method. The power is the probability that a test will reject the null hypothesis, e.g. no trend, when the alternative hypothesis is true, the efficiency is measured via estimation error. So, for all methods the significance of the detected trend and the error bars have been determined.
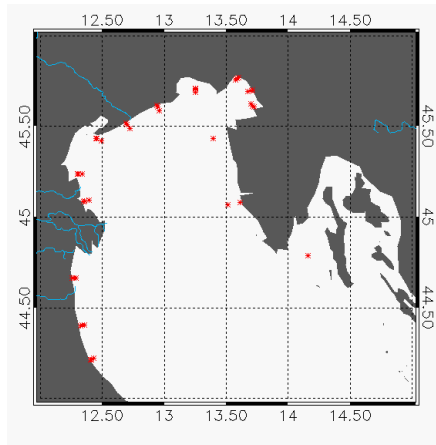
Figure 5.2 North Adriatic Sea *in situ* station analyzed in this work.

Table 5.1 synthesizes the result of the comparison between OC and *in situ* data; the following is a description of the columns present in the table.

- ✓ Column A: name of the test applied;
- ✓ Column B: OC product used as input (MedOC4 refers to the standard MED product and Case1-2 represents the merged case1/2 product);
- ✓ Column C: range of standard deviation considered;
- ✓ Column D: number of stations in which both *in situ* and OC data detect a trend with significativity greater than 50%;
- ✓ Column E: number of stations in which the trend is positive or negative both for *in situ* and OC data;
- ✓ Column F: number of stations that have the same sign of the trend in both datasets and in which the error bars of the trend calculated from *in situ* and OC data are overlapped;
- ✓ Column G: is the ratio between Column E and Column D, it represents the percentage of stations in which the satellite and in situ trends are in agreement.
- ✓ Column H: is the ratio of Column F and Column E; this column shows the percentage of number of stations in which both the sign and the errors of OC and *in situ* trend are consistent.

75

- ✓ Column I: is the ratio between Column F/ Column D; this column shows percentage the number of stations with consistent results on the total number of stations. This column provides an overall information on the success of the method and will used with Column G and H to identify the different performances among the selected methods.

- ✓ Column J: number of station in which *in situ* and OC data detect a trend with opposite sign;

- ✓ Column K: number of station in which *in situ* and OC data detect a trend with opposite sign but in which the error bars of the trends calculated from *in situ* and OC data overlap;

- ✓ Column L: is the ratio between Column J and Column D, it represents the percentage of stations in which the satellite and in situ trends are in disagreement.

- ✓ Column M: is the ratio of Column K and Column J; this column shows the percentage of number of stations in which the sign of OC and *in situ* trend are in disagreement but the errors of the trend overlap.

- ✓ Column N: is the ratio of Column K and Column D this column shows percentage the number of stations in which *in situ* and OC trends are in disagreement but the error bars of the trend are in agreement on the total number of stations

NAdrS													
A	B	C	D	E	F	G	H	I	J	K	L	M	N
Test applied	OC dataset	Sigma	Number of station	Stations with same sign of trend	Stations with same sign of trend in which the error bars overlap	% E/D	% F/E	% F/D	Stations with opposite sign of trend	Stations with opposite sign of trend in which the ranges overlap	% J/D	% K/J	% K/D
Montly trend (input data: montly mean)													
M-K	MedOC4	1	22	22	8	100	36,3636	36,36364	0	0	0	0	0
M-K	CASE 1-2	1	28	28	19	100	67,8571	67,85714	0	0	0	0	0
OLS	MedOC4	1	22	22	16	100	72,7273	72,72727	0	0	0	0	0
OLS	CASE 1-2	1	17	17	14	100	82,3529	82,35294	0	0	0	0	0
S-M-K	MedOC4	1	14	14	14	100	100	100	0	0	0	0	0
S-M-K	CASE 1-2	1	13	13	11	100	84,6154	84,61538	0	0	0	0	0
SPRC	MedOC4	1	34	29	12	85,29412	41,3793	35,29412	5	0	14,70588	0	0
SPRC	CASE 1-2	1	43	36	14	83,72093	38,8889	32,55814	7	0	16,27907	0	0
M-K	MedOC4	2	30	28	13	93,33333	46,4286	43,33333	2	0	6,666667	0	0
M-K	CASE 1-2	2	26	26	10	100	38,4615	38,46154	1	0	3,846154	0	0
OLS	MedOC4	2	20	20	12	100	60	60	0	0	0	0	0
OLS	CASE 1-2	2	21	21	15	100	71,4286	71,42857	1	0	4,761905	0	0
S-M-K	MedOC4	2	14	14	14	100	100	100	0	0	0	0	0
S-M-K	CASE 1-2	2	13	13	11	100	84,6154	84,61538	0	0	0	0	0
SPRC	MedOC4	2	45	36	16	80	44,4444	35,55556	9	0	20	0	0
SPRC	CASE 1-2	2	45	34	14	75,55556	41,1765	31,11111	11	1	24,44444	9,090909	2,222222
M-K	MedOC4	3	24	23	9	95,83333	39,1304	37,5	1	0	4,166667	0	0
M-K	CASE 1-2	3	26	25	9	96,15385	36	34,61538	1	0	3,846154	0	0
OLS	MedOC4	3	20	19	11	95	57,8947	55	1	0	5	0	0
OLS	CASE 1-2	3	20	19	13	95	68,4211	65	1	0	5	0	0
S-M-K	MedOC4	3	14	14	14	100	100	100	0	0	0	0	0
S-M-K	CASE 1-2	3	13	13	11	100	84,6154	84,61538	0	0	0	0	0
SPRC	MedOC4	3	45	33	10	73,33333	30,303	22,22222	12	2	26,66667	16,66667	4,444444
SPRC	CASE 1-2	3	45	34	14	75,55556	41,1765	31,11111	11	1	24,44444	9,090909	2,222222
Montly trend (input data: montly deseasonalized mean)													
M-K	MedOC4	1	20	20	12	100	60	60	0	0	0	0	0
M-K	CASE 1-2	1	25	21	11	84	52,381	44	4	0	16	0	0
OLS	MedOC4	1	17	17	15	100	88,2353	88,23529	0	0	0	0	0
OLS	CASE 1-2	1	14	14	12	100	85,7143	85,71429	0	0	0	0	0
M-K	MedOC4	2	23	22	8	95,65217	36,3636	34,78261	1	0	4,347826	0	0
M-K	CASE 1-2	2	28	27	16	96,42857	59,2593	57,14286	1	0	3,571429	0	0
OLS	MedOC4	2	16	16	8	100	50	50	0	0	0	0	0
OLS	CASE 1-2	2	22	21	14	95,45455	66,6667	63,63636	1	0	4,545455	0	0
M-K	MedOC4	3	25	23	2	92	8,69565	8	2	0	8	0	0
M-K	CASE 1-2	3	23	21	6	91,30435	28,5714	26,08696	2	0	8,695652	0	0
OLS	MedOC4	3	16	16	8	100	50	50	0	0	0	0	0
OLS	CASE 1-2	3	25	23	14	92	60,8696	56	2	0	8	0	0
Daily trend (input data: daily mean)													
M-K	MedOC4	1	26	26	13	100	50	50	0	0	0	0	0
M-K	CASE 1-2	1	29	28	19	96,55172	67,8571	65,51724	1	1	3,448276	100	3,448276
OLS	MedOC4	1	20	20	16	100	80	80	0	0	0	0	0
OLS	CASE 1-2	1	21	21	19	100	90,4762	90,47619	0	0	0	0	0
M-K	MedOC4	2	28	27	11	96,42857	40,7407	39,28571	2	0	7,142857	0	0
M-K	CASE 1-2	2	23	23	11	100	47,8261	47,82609	0	0	0	0	0
OLS	MedOC4	2	22	22	14	100	63,6364	63,63636	0	0	0	0	0
OLS	CASE 1-2	2	21	20	14	95,2381	70	66,66667	1	0	4,761905	0	0
M-K	MedOC4	3	26	25	11	96,15385	44	42,30769	1	0	3,846154	0	0
M-K	CASE 1-2	3	21	21	9	100	42,8571	42,85714	0	0	0	0	0
OLS	MedOC4	3	20	19	11	95	57,8947	55	1	0	5	0	0
OLS	CASE 1-2	3	18	18	9	100	50	50	0	0	0	0	0
Summer trend (input data: summer mean)													
M-K	MedOC4	1	9	7	6	77,77778	85,7143	66,66667	2	2	22,22222	100	22,22222
M-K	CASE 1-2	1	13	12	10	92,30769	83,3333	76,92308	1	0	7,692308	0	0
M-K	MedOC4	2	18	17	8	94,44444	47,0588	44,44444	1	1	5,555556	100	5,555556
M-K	CASE 1-2	2	18	17	13	94,44444	76,4706	72,22222	1	1	5,555556	100	5,555556
M-K	MedOC4	3	20	18	11	90	61,1111	55	2	2	10	100	10
M-K	CASE 1-2	3	25	22	13	88	59,0909	52	3	1	12	33,33333	4

Table 5.1 OC versus *in situ* result. See previous pages for the table description.

The results obtained using either monthly, daily and summer input data indicate that all methods have higher values in columns G, H and I when the test is applied only to data within 1 sigma, independently if the OC product used as input is the standard MED product or the merged case1/2 product. Only for the SMK the statistics are unchanged with the increasing of sigma.

More in details, the values in column G decrease using 2σ and 3σ respect to use 1σ. The same reduction occurs in Column H and in column I. Simultaneously at the increase of sigma corresponds an increment of number of station which have an opposite sign of *in situ* trend and in OC trend. This is probably due to the reduced quality of both in situ (§5.1.1) and satellite data (§5.1.2). Since the identification of possible outliers in both satellite and in situ time series are difficult to achieve, on basis of these results we used only data within the range of 1 sigma in the successive phase of this work.

The next phase aimed to the identification of the most appropriated method to detect the trends, the use of only consistent time series of measurements (satellite-in situ data that falls within 1 sigma) ensure that the error associated to measurements do not perturb the comparison and the subsequent selection of the methodology.

Table 5.2 shows the result of the comparison between the two dataset considering separately the stations having a trend with significance greater than 90% and the stations with a trend significance greater than 75%. Please note that the only difference between table 5.1 and 5.2 is represented by the column C. Indeed in table 5.2 column C represents the significance of the trend. Looking at the results of the monthly trend the SPRC is the method with worse results, indeed there are no stations with significant trend, either considering the significance threshold of 70% or 90%. The SMK has a very low number of stations with significant trend compared to other methods (max 7 stations with significant trends greater than 75% for the algorithm case 1-2). OLS method, either applied to monthly mean or to monthly mean deseasonalized time series, give a number of station with significant trend comparable to that of M-K only considering the level of significance of 75%. The M-K is the method that performs better than the other tests, either using monthly mean or using monthly mean deseasonalized data as input. In fact, we observe the highest number of stations (22 and 28 stations) with trends with confidence limit greater than 90% respect to the other methods (ranging from 0 to 11 stations). More in detail the M-K applied to monthly mean, produced with case 1-2 algorithm, gives the greatest number of stations with significative trend and the better consistence between the in situ and OC data (highest value in column G,H,I, table 5.2).

A	B	C	D	E	F	G	H	I	J	K	L	M	N
Test	OC dataset	Significativity	Number of station	Stations with same sign of trend	Stations with same sign of trend in which the ranges overlap	% E/D	% F/E	% F/D	Stations with opposite sign of trend	Stations with opposite sign of trend in which the ranges overlap	% J/D	% K/J	% K/D
NAdrS													
Montly trend (input data: montly mean)													
M-K	MedOC4	greater than 90	22	22	8	100	36,3636	36,36364	0	0	0	0	0
M-K	CASE 1-2	greater than 90	28	28	19	100	67,8571	67,85714	0	0	0	0	0
OLS	MedOC4	greater than 90	11	11	7	100	63,6364	63,63636	0	0	0	0	0
OLS	CASE 1-2	greater than 90	8	8	7	100	87,5	87,5	0	0	0	0	0
S-M-K	MedOC4	greater than 90	1	1	1	100	100	100	0	0	0	0	0
S-M-K	CASE 1-2	greater than 90	4	4	4	100	100	100	0	0	0	0	0
SPRC	MedOC4	greater than 90	no stations										
SPRC	CASE 1-2	greater than 90	no stations										
M-K	MedOC4	greater than 70	22	22	8	100	36,3636	36,36364	0	0	0	0	0
M-K	CASE 1-2	greater than 70	28	28	19	100	67,8571	67,85714	0	0	0	0	0
OLS	MedOC4	greater than 70	22	22	16	100	72,7273	72,72727	0	0	0	0	0
OLS	CASE 1-2	greater than 70	17	17	14	100	82,3529	82,35294	0	0	0	0	0
S-M-K	MedOC4	greater than 70	6	6	6	100	100	100	0	0	0	0	0
S-M-K	CASE 1-2	greater than 70	7	7	7	100	100	100	0	0	0	0	0
SPRC	MedOC4	greater than 70	no stations										
SPRC	CASE 1-2	greater than 70	no stations										
Montly trend (input data: montly deseasonalized mean)													
M-K	MedOC4	greater than 90	20	20	12	100	60	60	0	0	0	0	0
M-K	CASE 1-2	greater than 90	25	21	11	84	52,381	44	4	0	16	0	0
OLS	MedOC4	greater than 90	7	7	6	100	85,7143	85,71429	0	0	0	0	0
OLS	CASE 1-2	greater than 90	7	7	7	100	100	100	0	0	0	0	0
M-K	MedOC4	greater than 70	20	20	12	100	60	60	0	0	0	0	0
M-K	CASE 1-2	greater than 70	25	21	11	84	52,381	44	4	0	16	0	0
OLS	MedOC4	greater than 70	17	17	15	100	88,2353	88,23529	0	0	0	0	0
OLS	CASE 1-2	greater than 70	14	14	12	100	85,7143	85,71429	0	0	0	0	0
Daily trend (input data: daily mean)													
M-K	MedOC4	greater than 90	26	26	13	100	50	50	0	0	0	0	0
M-K	CASE 1-2	greater than 90	29	28	19	96,55172	67,8571	65,51724	1	1	3,448276	100	3,448276
OLS	MedOC4	greater than 90	9	9	8	100	88,8889	88,88889	0	0	0	0	0
OLS	CASE 1-2	greater than 90	8	8	8	100	100	100	0	0	0	0	0
M-K	MedOC4	greater than 70	26	26	13	100	50	50	0	0	0	0	0
M-K	CASE 1-2	greater than 70	29	28	19	96,55172	67,8571	65,51724	1	1	3,448276	100	3,448276
OLS	MedOC4	greater than 70	20	20	16	100	80	80	0	0	0	0	0
OLS	CASE 1-2	greater than 70	21	21	19	100	90,4762	90,47619	1	0	4,761905	0	0
Summer trend (input data: summer mean)													
M-K	MedOC4	greater than 90	9	7	6	77,77778	85,7143	66,66667	2	2	22,22222	100	22,22222
M-K	CASE 1-2	greater than 90	13	12	10	92,30769	83,3333	76,92308	1	0	7,692308	0	0
M-K	MedOC4	greater than 70	9	7	6	77,77778	85,7143	66,66667	2	2	22,22222	100	22,22222
M-K	CASE 1-2	greater than 70	13	12	10	92,30769	83,3333	76,92308	1	0	7,692308	0	0

Table 5.2 OC versus *in situ* result. See pages 75 and 76 for the table description.

Moreover, when daily case 1-2 data are used as input the M-K test performs better than OLS method. In fact, it has higher power respect to OLS, providing the major number of stations in which the trend has a significance greater than 90%. Furthermore, M-K test has higher values in the columns G,H,I, this indicates that it has a greater number of stations with the same sign of the trend both for *in situ* and for OC data and the majority stations in which the error associated to the trend overlaps. Also for summer trend, case 1-2 algorithm gives better result than MedOC4 algorithm.

The comparison between ocean colour and in situ trend are shown in figure 5.3. The figure shows that the M-K test produces lower standard errors when monthly and daily value are used as input instead to the May-September mean.
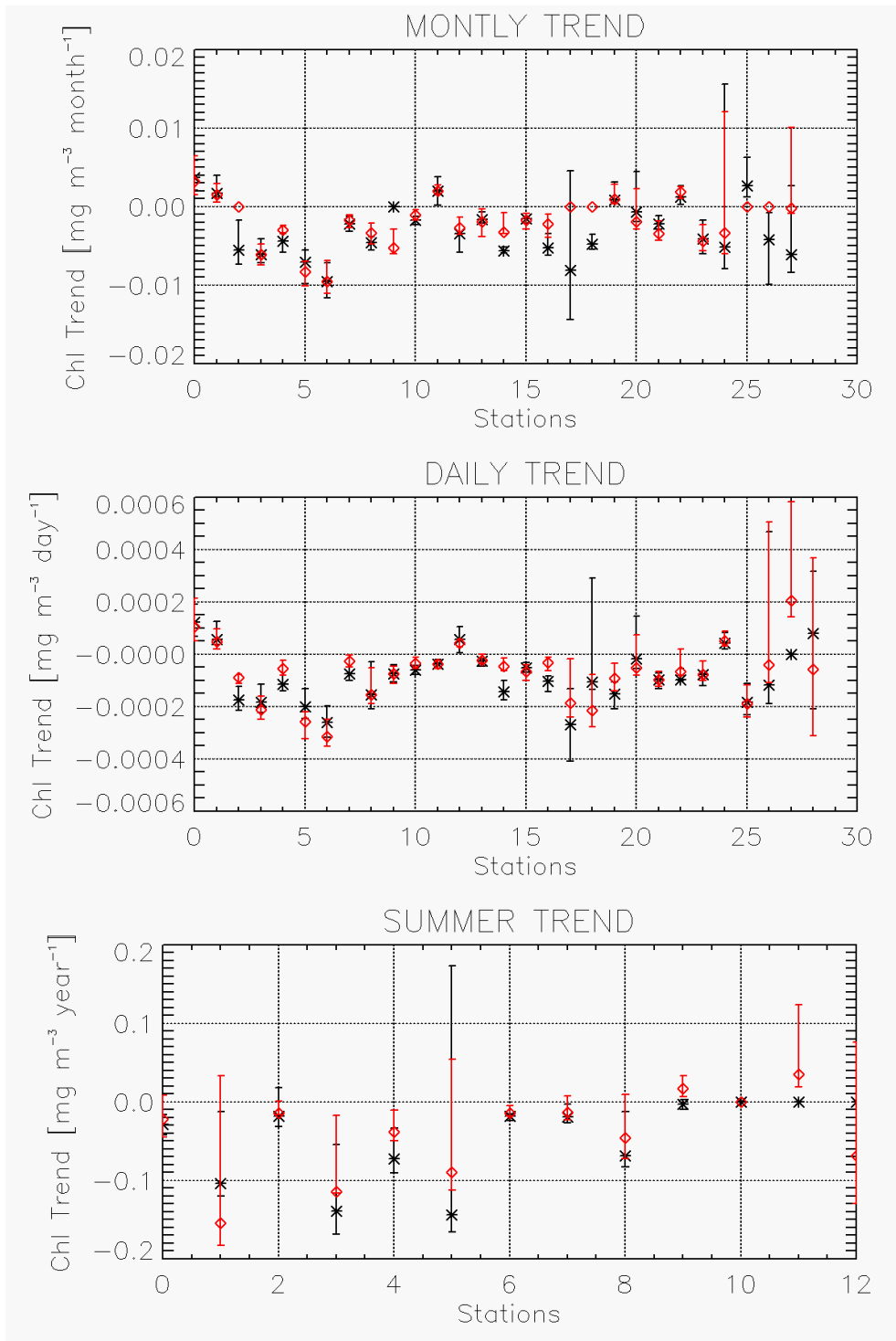
Figure 5.3 OC trend compared with in situ trends in NAdrS area. Each point represents the value of the trend slope for a single station, black are in situ data, red the satellite data sampled over in situ stations. Only trends with confidence limit greater than 90% are plotted. Vertical bar represent the upper and lower range of the trend estimate.

5.3.1.2   Results along the Italian coasts

The results of the comparison between in situ and OC datasets in all stations along the Italian coasts are very similar to those described in section 5.3.1.1 for NadrS. The M-K test applied to daily standard data product ensures the best compromise between an high number of stations with a trend having a significance level above 90% (column C), and the best consistency with in situ observations (higher values in columns F,G,H,I). Respect to the analysis limited to the NAdrS the use of the case-1case-2 merged products does not improve the statistical results but produce values slight lower than those obtained using the standard product. Taking into account that either the case 2 algorithm applied to retrieve the chlorophyll in coastal area and the selection of the case 2 water pixels are based on the bio-optical measurements acquired in the Venice tower located in the northern part of the Adriatic, the observable improvement obtained using this product in the North Adriatic region an indirect confirmation of the improved scientific quality merged case1-case2 product in the Adriatic Sea. The results obtained from the analysis of the trend in overall Italian coastal areas seems to indicate that the case2 algorithm used in the processing does not resolve all the bio-optical characteristics of the Italian coastal regions characterized by different biological and terrestrial components.

For this reason, we decided to use daily OC data obtained with standard MED product as input for Mann-Kendall test to detect trend in all Italian coasts.

Italian Coasts													
A	B	C	D	E	F	G	H	I	J	K	L	M	N
Test	OC dataset	Significativity	Number of station	Stations with same sign of trend	Stations with same sign of trend in which the ranges overlap	% E/D	% F/E	% F/D	Stations with opposite sign of trend	Stations with opposite sign of trend in which the ranges overlap	% J/D	% K/J	% K/D
Montly trend (input data: montly mean)													
M-K	MedOC4	greater than 90	108	95	59	87,96296	62,10526	54,62963	13	1	12,03704	7,692308	0,925926
M-K	CASE 1-2	greater than 90	123	111	76	90,2439	68,46847	61,78862	12	0	9,756098	0	0
OLS	MedOC4	greater than 90	38	38	29	100	76,31579	76,31579	0	0	0	0	0
OLS	CASE 1-2	greater than 90	33	33	29	100	87,87879	87,87879	0	0	0	0	0
S-M-K	MedOC4	greater than 90	3	3	3	100	100	100	0	0	0	0	0
S-M-K	CASE 1-2	greater than 90	7	7	7	100	100	100	0	0	0	0	0
SPRC	MedOC4	no stations											
SPRC	CASE 1-2	no stations											
M-K	MedOC4	greater than 70	108	95	59	87,96296	62,10526	54,62963	13	1	12,03704	7,692308	0,925926
M-K	CASE 1-2	greater than 70	123	111	76	90,2439	68,46847	61,78862	12	0	9,756098	0	0
OLS	MedOC4	greater than 70	87	85	71	97,70115	83,52941	81,6092	2	0	2,298851	0	0
OLS	CASE 1-2	greater than 70	84	80	71	95,2381	88,75	84,52381	5	0	5,952381	0	0
S-M-K	MedOC4	greater than 70	27	23	23	85,18519	100	85,18519	4	1	14,81481	25	3,703704
S-M-K	CASE 1-2	greater than 70	17	17	16	100	94,11765	94,11765	0	0	0	0	0
SPRC	MedOC4	no stations											
SPRC	CASE 1-2	no stations											
Montly trend (input data: montly deseasonalized mean)													
M_K	MedOC4	greater than 90	53	47	43	88,67925	91,48936	81,13208	6	5	11,32075	83,33333	9,433962
M_K	CASE 1-2	greater than 90	46	45	39	97,82609	86,66667	84,78261	1	1	2,173913	100	2,173913
OLS	MedOC4	greater than 90	26	25	20	96,15385	80	76,92308	1	0	3,846154	0	0
OLS	CASE 1-2	greater than 90	32	32	29	100	90,625	90,625			0	0	0
M_K	MedOC4	greater than 70	74	66	59	89,18919	89,39394	79,72973	8	7	10,81081	87,5	9,459459
M_K	CASE 1-2	greater than 70	79	74	66	93,67089	89,18919	83,5443	5	4	6,329114	80	5,063291
OLS	MedOC4	greater than 70	68	66	59	97,05882	89,39394	86,76471	2	0	2,941176	0	0
OLS	CASE 1-2	greater than 70	72	69	62	95,83333	89,85507	86,11111	3	0	4,166667	0	0
Daily trend (input data: daily mean)													
M-K	MedOC4	greater than 90	121	115	69	95,04132	60	57,02479	6	0	4,958678	0	0
M-K	CASE 1-2	greater than 90	119	113	65	94,95798	57,52212	54,62185	6	1	5,042017	16,66667	0,840336
OLS	MedOC4	greater than 90	43	42	37	97,67442	88,09524	86,04651	1	0	2,325581	0	0
OLS	CASE 1-2	greater than 90	38	38	36	100	94,73684	94,73684	0		0	0	0
M-K	MedOC4	greater than 70	121	115	69	95,04132	60	57,02479	6	0	4,958678	0	0
M-K	CASE 1-2	greater than 70	119	113	65	94,95798	57,52212	54,62185	6	1	5,042017	16,66667	0,840336
OLS	MedOC4	greater than 70	102	98	84	96,07843	85,71429	82,35294	4	0	3,921569	0	0
OLS	CASE 1-2	greater than 70	94	92	78	97,87234	84,78261	82,97872	4	0	4,255319	0	0
Summer trend (input data: summer mean)													
M-K	MedOC4	greater than 90	29	26	16	89,65517	61,53846	55,17241	3	2	10,34483	66,66667	6,896552
M-K	CASE 1-2	greater than 90	34	31	22	91,17647	70,96774	64,70588	3	1	8,823529	33,33333	2,941176
M-K	MedOC4	greater than 70	29	26	16	89,65517	61,53846	55,17241	3	2	10,34483	66,66667	6,896552
M-K	CASE 1-2	greater than 70	34	31	22	91,17647	70,96774	64,70588	3	1	8,823529	33,33333	2,941176

Table 5.3 OC versus *in situ* dataset along the Italian Coasts. See pages 75 and 76 for the table description.
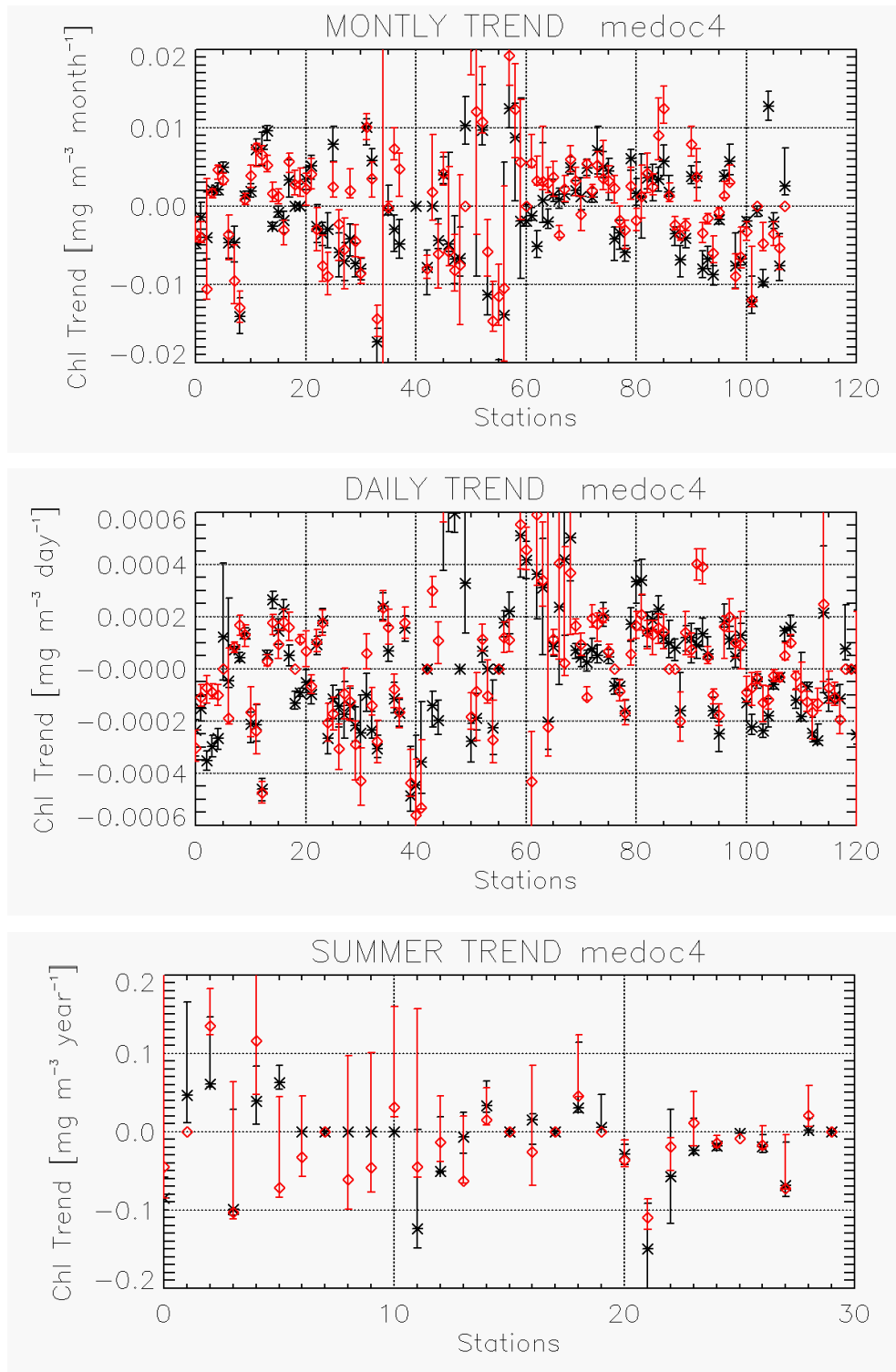
Figure 5.4 OC trend compared with in situ trends along the Italian Coasts. Each point represents the value of the trend slope for a single station, black are in situ data, red the satellite data sampled over in situ stations. Only trends with confidence limit greater than 90% are plotted. Vertical bar represent the upper and lower range of the trend estimate.

5.3.2 Chlorophyll trend along the Italian coastal and shelf region

The Chl trend maps presented in Figure 5.5 describe the Chl trends for the Italian coastal area (defined here as the region between the coastline and 1000 m bottom depth) over the period from 1998 to 2009. As visible in figure 5.5b, most of pixel are characterized by a decreasing trend (blu regions). This is in accordance with the results of many authors (Behrenfeld and al, 2006 Doney 2006, and Greget et al., 2003) who link the general biomass decrease that occurs in the Mediterranean Sea with the enhanced stratification processes resulting from the general warming of the sea surface temperature. Indeed the SST positive trend can be connected to warming of the sea surface layer indicating a reduction of the vertical mixing between the upper and lower layers of the water column with a subsequently reduction of nutrient supply to euphotic layer from the layer below the pycnocline.

The negative trend is more intense in the North Adriatic Sea in correspondence of the Po river discharge 0.18 mg m^{-3} y^{-1} (Fig 5.5 a). Here the trend shows a spatial gradient from the Po delta toward northeast. Indeed, the trend intensity decrease toward offshore and as well as southward, following the path of Western Adriatic Current, WAC, the intense and cold coastal current that flows along the Italian coastlines. This suggests that the oligotrophication of the NAdrS is linked to the outflow of the Po river. Indeed, the reduction in concentration of phosphorus, being banned by Italian law in the mid-1980s, and reduction of ammonia transport by Po occurred during the last 20 years, tanks to the adoption of new Italian regulations and increase of authority control of nutrient loads, probably had determined a progressive reduction these nutrient concentrations in the river outflow (Salidoro et al., 2006). This together with the increase of river transport of total nitrogen, dissolved inorganic nitrogen, reactive silicate, total organic carbon and total suspended matter (Cozzi and Giani, 2010) influence the nutrient concentrations in the coastal area causing a decrease of productivity of the NAdrS. This result confirms the cultural oligotrophication of coastal waters in NAdrS observed by Mozetič and co-authors (2010) and already detected in other estuaries (Jeppesen et al. 2005, Carstensen et al. 2006).

Figure 5.5a shows that the coastal areas impacted by the Tiber and Arno river outflow are characterized by more intense negative trends, -0.06 mg m^{-3} y^{-1} and -0.05 mg m^{-3} y^{-1} respectively, respect to the Tyrrhenian coasts in which the trend values are very low.

Although the trend decrease is less intense of than in the region Po river outflow, it is possible to assume that the causes of the reduction of chlorophyll biomass values are the same, but the impact of law regulation is less evident since the Po river across the Italian territory with the largest concentration of human industry and agriculture activities .

On the contrary the south Adriatic Sea and the North-eastern regions of the Ionian Sea are characterized by an increasing trend (red regions in fig 5.5 b). This increase in phytoplankton concentration is more intense in the Gulf of Manfredonia (0.04 mg m^{-3} y^{-1}). This result is in line with those of Matarrese and co-autors who link the increment of productivity to the increased advection of the Ionian waters, richer in nutrients, attributable to global climatic changes that have influence on the oceanographic phenomena (Marasoviæet al., 1995; Morovic et al., 2004).

Other two regions interested by increasing trend are the Gulf of Gaeta and the Gulf of Naples. The Gulf of Gaeta presents an increasing trend of the order 0.05 mg m^{-3} y^{-1}. The economy of region is based on an intensive agriculture and tourism activities. Moreover, this region is one of the most productive livestock rearing areas in Italy. This determines a very high pollution of the Garigliano and Volturno river discharges that are transported by the Tyrrhenian coastal current into the Gulf, so the increasing trend may be due to the higher nutrient loading from these two rivers.

The Gulf of Naples is the site of an intense antrophic pressure. Human activities range from urban settlements to industrial areas located on the coast and to intense maritime traffic resulting in the discharge of sewage, industrial pollutants and hydrocarbons into the Sea. Moreover, the Gulf is interested by the Sarno river outflow, a very polluted river. The waters off the Gulf obviously experience the effect of this load of pollutant so they are characterized by an increasing trend of 0.04 mg m^{-3} y^{-1} . In the other regions of the Italian coasts the trend value is negligible as close to zero.
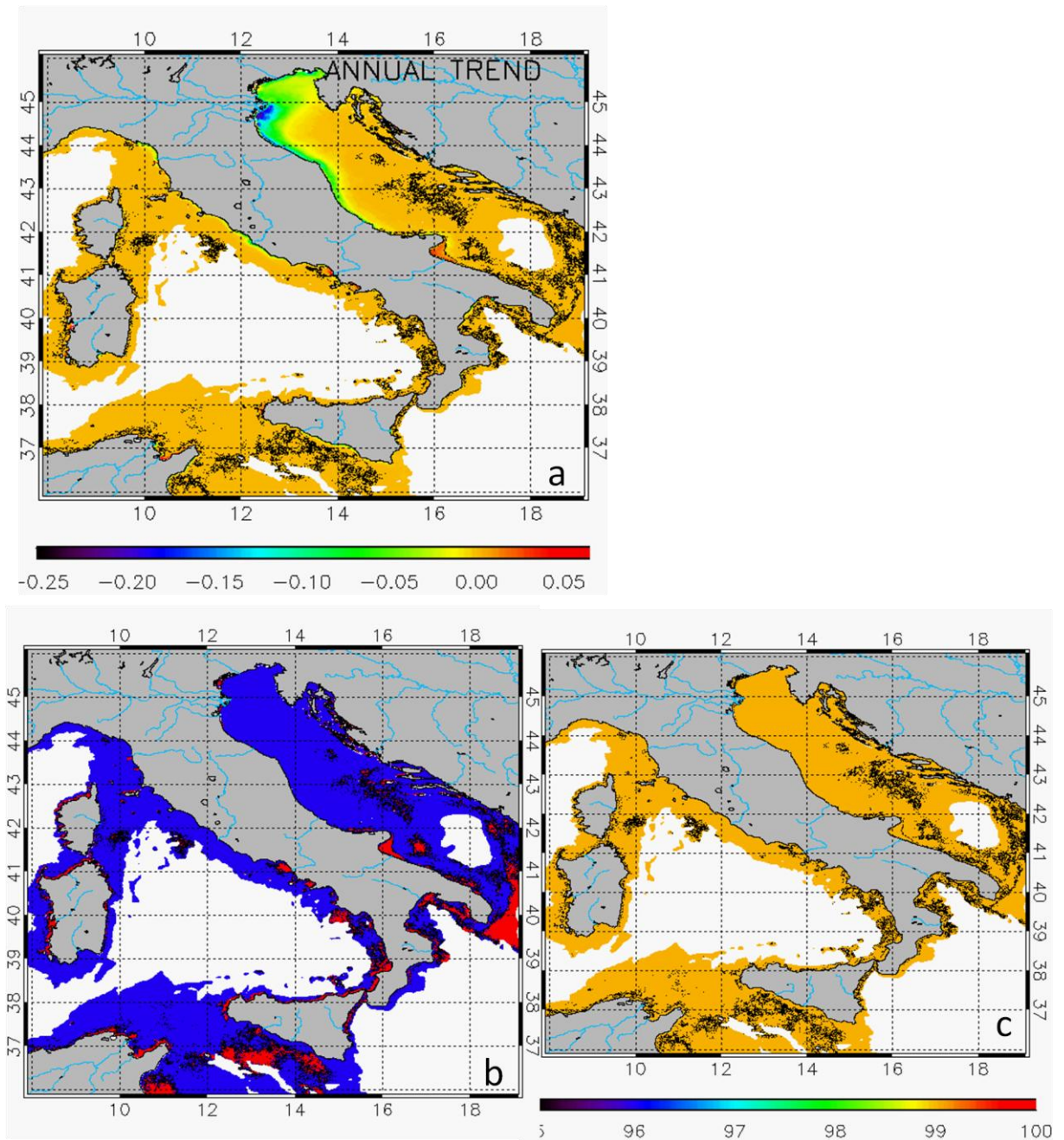
Fig. 5.5 Ocean colour trend over the Italian coastal regions. (a) estimation of the trend slope expressed in mg m^{-3} y^{-1} (a),   (b) map of positive/negative trend (region with negative trend in bleu, regions with positive trend in red; black area indicates regions in which the significance are below threshold limit), Significance of the trend (c).

5.4   Conclusions

Until now chlorophyll trends were estimated by EEA using *in situ* data only, with this study I exploited the potential use of satellite data, which allows a daily monitoring of all Italian coasts for environmental monitoring application. The best methodology for detecting chlorophyll trends along the Italian coasts using OC data has been identified comparing *in situ* data collected by EEA, through Eionet and ICES network, with OC data re-sampled over the *in situ* stations.

Five most commonly methods used for detecting trends was analyzed comparing *in situ* data with OC Mediterranean product (obtained with MedOC4 algorithm for chlorophyll retrieval and with new OC case1/2 merged chlorophyll product). In addition, to highlight the importance of sampling time, the trends are evaluated using daily data, monthly averages and summer mean.

The results show that the best agreement between *in situ* and OC data is achieved using daily data as input instead to monthly or seasonal means. Moreover, the comparison between the possible methods to evaluate trends shows that the MK test applied to the daily OC Mediterranean regional product is more robust than other methods. Indeed it provides more consistency with in situ observations and ensures a significance around 90-100%.

The analysis of Chl data derived from SeaWiFS for the years 1998-2009 has been performed on the Italian coastal domain demonstrating that the use of long-term satellite data is an efficient way to examine water quality trends in the coastal area. As expected, the results show that changes in Chl concentrations along the Italian Coasts follow phytoplankton trend detected in all Mediterranean Sea by many authors (Behrenfeld *et al.* 2006, Barale *et al.*, 2008). The negative trend that characterizes most of the Italian coasts can be attributable not only to the general warming trend of Mediterranean waters that intensify the stratification process limiting the uplift of nutrient from below the nutricline, but also to the assimilation of the new environmental policies aiming to ensure sustainable use of natural resources.

This phenomenon is more evident in NadrS where environmental policies aimed to limiting the nutrient load of the Po river outflow, determine the most intense decreasing trend observable along the entire Italian eastern coastlines. On the contrary, the most evident increasing trends are found in Gulf of Naples and Gulf of Guidonia, these positive trends are mainly due to the release of pollutants caused by an overexploitation of the environmental coastal ecosystems.

This study revealed the importance of satellite data to detecting trend, in particular of the Sea-viewing Wide Field-of-view Sensor, that is able to replace the *in situ* sampling with consistent and well-calibrated data characterized by high frequency of sampling and global coverage. Additionally, the importance to monitor and understand changes in marine coastal ecosystems was highlighted by this work. Indeed the phytoplankton biomass in coastal and shelf regions constitutes an indicator of the water quality that can be potentially linked to terrestrial and human interactions in coastal areas.

Chapter 6

Conclusion

The aim of this thesis was to investigate the space time variability of the marine environment in the Italian Seas using multi-sensors remote sensing data (chlorophyll, sea level, SST). Different approaches and datasets were used to study the marine circulation, the space-time variability of the phytoplankton biomass and to develop indicators of water quality. The analysis aimed also to defined limits and capability of the remote sensing products to investigate the variability of marine environment at short and long term temporal scales.

Regarding the first aspect, the study focused on the Tyrrhenian Sea, region poorly explored by previous studies and in which only the mean large scale surface circulation was well know. The altimeter data in conjunction with Lagrangian surface drifters has been used. The combined use of altimetry and in situ data allowed to quantify the ability of standard interpolated elevation products to detect the sea surface circulation. The pattern of circulation was identify through the analysis of drifters trajectories and of pseudo-Eulerian statistics applied on both dataset. The analysis reveals a complex pattern of the circulation, especially in the southern region of the Tyrrhenian, dominated by semipermanent recirculations and transient features, which sometimes makes it difficult to identify a consistent mean flow. In particular, three persistent structures of circulation was detected for the first time. An anticyclonic gyre between 12°-13°E and 39°-40° N called South Tyrrhenian Anticyclone, a second anticyclonic vortex offshore the Sicilian Coasts and a cyclonic gyre in front of the Calabrian coasts.

The northern region of the basin is characterized by a pair composed of cyclonic and anticyclonic circulations well known in the literature as the North Tyrrhenian Cyclone and North Tyrrhenian Anticyclone. The presence of these structures has been detected both by altimeter both by drifters data. On the contrary, many of the small-scale structures, characterized by short life and a high propagation velocities, identified by the drifters were not present in the altimeter images.

The regular sampling frequency of the satellite and the synoptic measurements, which permit to simultaneously obtain data for the entire basin, has allowed to study the seasonal variability of the circulation. This type of study would not have been possible with in situ data only due

to the limited space/time coverage provided by drifters. The analysis reveals that the mean circulation and consequently the MKE is more subject to the seasonal variations than the eddy fields. In particular, the structures present in the north western section of the basin are stronger in summer than in winter, the contrary happens for the features that characterize the south eastern regions. This behaviour suggests that the seasonal variability is linked to exchanges f the Tyrrhenian Sea with the neighbouring basins rather than local forcing.

This work has demonstrated the difference between altimeter and drifters meaurements. Moreover, the pseudo-Eulerian statistics computed with the two datasets evidenced the representativeness of a joint analysis of altimeter and drifter data and yielded useful indications about proper preliminary preprocessing and resampling procedures, so as to make the comparison statistically sound.

The investigation of the phytoplankton space-time variability and its dependence on physical processes has been conducted in the Channel of Sicily. This is a key region for both physical and biological processes, since it represents a crucial area for both understanding the water mass exchanges between western and eastern Mediterranean Basins and for the important fishery activities carried out by the countries bordering the Channel. The analysis was conducted using a nine years (1998-2006) time series of Ocean Color, SST (Sea Surface Temperature) and MADT (Mediterranean absolute dynamics topography) fields. These last two variables are the best proxy of water column stratification and of the surface circulation dynamics, respectively, while OC data provides information on the phytoplankton biomass. The Empirical Orthogonal Function decomposition applied to the three variables has demonstrate that, depending on the temporal scale considered, the phytoplankton responds to different physical forcing.

At seasonal scale the chlorophyll dynamics are conditioned by surface circulation pattern variability. More specifically, changes in the MAW intensity and displacement inside the Channel are responsible of the phytoplankton biomass abundance variations, that is due to the modifications in the inflow of nutrient and chlorophyll advected by MAW from the North Africa coasts. At annual scale the phytoplankton variability is driven by the annual cycle of water column stratification which determines the nutrient availability in the surface layer. This relation characterizes principally the coastal areas which are less affect by the input of nutrient due to the advection of water by MAW. Finally, only minimally, the variability of phytoplankton was resulted to be influenced by coastal upwelling events that occurs during summer along the southern coasts of Sicily.

This work has demonstrate that satellite data provide unique and important information on surface phytoplankton variability thanks to the sampling frequency and the high spatial resolution, with which they monitor not only the chlorophyll distributions but also the environmental variables capable of influencing phytoplankton production.

One of the challenges of this thesis was to assess the effectiveness and feasibility of using ocean colour data to detecting trend in coastal regions. Until now the environmental monitoring community and governmental agency routinely measure Chlorophyll concentrations using flourometer in situ measurements. The dataset produced have many limitations due to the limited geographic areas sampled and temporal frequency of sampling. The Sea-viewing Wide Field-of-view Sensor offers a nearly continuous, consistent and reliably-calibrated remotely-sensed chlorophyll concentration data which is particularly suitable to identify the patterns of temporal variability (McClain et al., 2004).

The results of comparison between trends estimate with *in situ* and Ocean Colour data shows a good agreement, especially when daily data are used as input to the procedure to detecting trend. The analysis of the results obtained using the four selected no-parametric methods to compute the trends from both in situ and OC data clearly showed that Mann-Kendall test provide the best results. In fact, the value and the sign of the trends are more consistency with those obtained using situ measurements and are more robust in statistical terms, being a significance level of the estimates between 90-100% in all the pixels. The analysis of trend derived from SeaWiFS daily data for the years 1998-2009 has revealed a decreasing trend that characterizes almost all the Italian coastal waters. As suggested by many authors this decrease in chlorophyll concentration can be attributed to the global climate change that is causing water warming in the Mediterranean Sea, with consequent greater stratification of the water column and a lower lift of nutrients from deeper layers. Moreover the effects of the Italian environmental policy taken to reduce the nutrient rivers load on the coastal water are more evident in the North Adriatic Sea where the negative trend is more intense in correspondence of the Po delta. The only regions in which we can observe an positive trend are located in areas subject to intense antrophic pressure (eg, Gulf of Naples, Gulf of Gaeta, Gulf of Manfredonia) in which the increase of pollution and human activity occurred in the last 10 years probably had a direct impact to the chlorophyll trend detected by satellite.

The results of this thesis clearly showed the ability of the satellite data to monitor the environmental changes also in the coastal areas and the method scientifically selected to detect trends from OC data can constitute a new indicator of the water quality. This indicator can be used together with the standard methods by the environmental agencies to

continuously monitoring the environmental state of the Italian shelf and coastal seas covering also areas not sampled by in situ measurements with higher time and spatial scales.

Finally, as already pointed out the satellite data have demonstrated to be an excellent tool for studying the space and time variability of Italian Seas upper ocean ecosystem. New methodologies, that range from the study of surface circulation, to the analysis of the space-time phytoplankton variability and finally to the identification of a new method to detect trends in coastal region, have been developed. The new technique for deriving the surface circulation using standard altimeter interpolated products and drifters data allowed to study and identify all scales of the surface circulation, in addition it revealed that the altimeter products miss a noticeable part of the signal linked to small-scale structures of circulation. The EOF decomposition applied to OC, SST and MADT data permitted to interpret the covariability of physical and biological fields, at different space and time scales, suggesting different mechanisms that link the upper ocean dynamics to the ecosystem functioning. Finally the analysis of long-term SeaWiFS chlorophyl data has demonstrate that they are an efficient way to examine bio-optical trends in the coastal zone.

Appendix A

Deployment and lifetime of drifters analyzed in chapter 3

Deployment	Drifter Number	Deployment Date	Last Transmission
1	33198	14 Dec 2001	2 Jun 2002
1	33199	14 Dec 2001	24 Jan 2002
1	33202	14 Dec 2001	2 Apr 2002
1	33203	14 Dec 2001	31 Dec 2001
1	33204	14 Dec 2001	21 May 2002
1	33252	14 Dec 2001	5 Mar 2002
1	33253	14 Dec 2001	25 Feb 2002
1	33254	14 Dec 2001	2 Feb 2002
2	33207	27 Jun 2002	2 Jul 2002
2	33208	27 Jun 2002	16 Nov 2002
2	33210	27 Jun 2002	29 Aug 2002
2	33211	27 Jun 2002	30 Jul 2002
2	33212	27 Jun 2002	19 Jul 2002
2	33213	27 Jun 2002	29 Jul 2002
2	33214	27 Jun 2002	6 Sep 2002
2	33249	27 Jun 2002	11 Jul 2002
2	33250	27 Jun 2002	10 Jul 2002
2	33251	27 Jun 2002	11 Jul 2002
3	33215	3 Oct 2002	15 Jan 2003
3	33216	3 Oct 2002	21 Apr 2003
3	33217	4 Oct 2002	4 Nov 2002
3	33218	4 Oct 2002	14 Oct 2002
3	33219	4 Oct 2002	21 Jan 2003
4	33222	28 Jan 2003	5 Apr 2003
4	33223	28 Jan 2003	22 Jul 2003
4	33224	28 Jan 2003	8 May 2003
4	33231	31 Jan 2003	5 Sep 2003
4	33235	31 Jan 2003	3 Feb 2003
4	33236	31 Jan 2003	22 Jul 2003
4	33246	28 Jan 2003	8 Jul 2003
4	33247	28 Jan 2003	1 Feb 2003
4	33248	28 Jan 2003	27 Apr 2003
5	34447	17 Apr 2003	27 Oct 2003
5	34448	17 Apr 2003	18 Oct 2003
5	34449	20 Apr 2003	16 May 2003
5	34450	17 Apr 2003	1 Jul 2003
5	39428	17 Apr 2003	8 Sep 2003
5	39429	17 Apr 2003	2 Nov 2003
5	39430	17 Apr 2003	17 Aug 2003
5	39431	17 Apr 2003	20 Sep 2003
6	39432	9 Aug 2003	19 Feb 2004
6	39433	10 Aug 2003	2 Oct 2003
6	39434	9 Aug 2003	8 Dec 2003
6	39435	9 Aug 2003	27 Feb 2004
6	39436	9 Aug 2003	4 Feb 2004
6	39437	10 Aug 2003	9 Oct 2003
6	39438	9 Aug 2003	24 Oct 2003
6	39440	8 Aug 2003	12 Aug 2003
6	39441	10 Aug 2003	15 Oct 2003
6	39442	8 Aug 2003	7 Sep 2003
6	39443	9 Aug 2003	28 Sep 2003
6	39444	8 Aug 2003	12 Dec 2003
6	39445	8 Aug 2003	31 Aug 2003

Bibliography

Agostini, V.N. and A. Bakun, 2002. "Ocean triads" in the Mediterranean Sea: physical mechanisms potentially structuring reproductive habitat suitability (with example application to European anchovy, Engraulis encrasicolus). Fisheries Oceanography, 11: 129-142.

Aliverti G., M. Picotti, L. Trotti, A. De Maio, O. Lauretta and M. Moretti, 1968. Atlante del Mar Tirreno. Isoterme ed Isoaline dedotte dalle misure eseguite durante le crociere per l'Anno Geofisico Internazionale1 957-1958,S tab.T ip. G. Genovese Napoli, 127 pp.

Ayoub N, Le Traon PY, De Mey P, 1998. A description of the Mediterranean surface variable circulation from combined ERS-1 and TOPEX/POSEIDON altimetric data. Journal of Marine Systems 18 (1/3): 3-40

Anati, D. A., 1984. "A dome of cold water in the Levantine Basin". Deep Sea Research, 31, 1251-1257.

Artale, V., Astraldi, M., Buffoni, G., Gasparini, G.P.,1994. Seasonal variability of the gyre-scale circulation in the nor northern Tyrrhenian Sea. Journal of Geophysical Research,99,127-14137.

Artale,V., D. Iudicone, R. Santoleri,V. Rupolo, S.Marullo, and F.D'Ortenzio 2002. The role of surface fluxes in OGCM using satellite SST: Validation of and sensitivity to the forcing frequency of the Mediterranean thermohaline circulation, Journal of Geophysical Research., 107(C8), 3120, doi:10.1029/2000JC000452.

Astraldi M. and Gasparini G. P., 1994. The seasonal characteristics of the circulation in the Tyrrhenian sea. In: La Violette, P. E.(Ed), Seasonal and interannual variability of the Western Mediterranean sea, Coastal and Estuarine Studies, 46, 115-134.

Astraldi, M., Balopulos, S., Candela, J., Font, J., Gacic, M.,Gasparini, G.P., Manca, B., Theorachis, A., Tintore, J., 1999. The role of straits and channels in understanding the characteristics of Mediterranean circulation. Progress in Oceanography 44, 65–108.

Astraldi, M., G. P. Gasparini, A. Vetrano, and S. Vignudelli, 2002. Hydrographic characteristics and interannual variability of water masses in the central Mediterranean: A sensitivity test for long‐term changes in the Mediterranean Sea, Deep Sea Res. Part I, 49(4), 661‐680, doi:10.1016/ S0967-0637(01)00059-0.

Alvera-Azca´rate, A., A. Barth, and R. H. Weisberg, 2009. The surface circulation of the Caribbean Sea and the Gulf of Mexico as inferred from satellite altimetry, Journal of Physical Oceanography, 39, 640 – 657, doi:10.1175/2008JPO3765.1.

Barale, Jaquet, Ndiaye, 2008. Algal blooming patterns and anomalies in the Mediterranean Sea as derived from the SeaWiFS data set (1998–2003), Remote Sensing of Environment, Volume 112, Issue 8, 15, Pages 3300-3313,

Barton, I. J.,1995. Satellite-derived sea surface temperatures: Current status. Journal of Geophysical Research,1 00, 8777-8790

Bauer, S., M. S. Swenson, A. Griffa, A. J. Mariano, and K. Owens ,1998. Eddy‑mean flow decomposition and eddy‑diffusivity estimates in the Tropical Pacific Ocean: 1. Methodology, Journal of Geophysical Research,103,30,855‑30,871..

Behrenfeld, M.J., R.T. O'Malley, D.A. Siegel, C.R. McClain, J.L. Sarmiento, G.C. Feldman, A.J. Milligan, P.G. Falkowski, R.M. Letelier and E.S. Boss. 2006. Climate-driven trends in contemporary ocean productivity. Nature, 444: 752-755.

Bentivegna, F., F. Valentino, P. Falco, E. Zambianchi, and S. Hochscheid 2007. The relationship between loggerhead turtle (Caretta caretta) movement patterns and Mediterranean currents, Mar. Biol. Berlin, 151, 1605–1614, doi:10.1007/s00227-006-0600-1.Benzohra, M., & Millot, C.,1995. Characteristics and circulation of the surface and intermediate water masses off Algeria. Deep Sea Researchearch, *42*, 1803–1830.

Béranger, Mortier, G.P. Gasparini, L. Gervasio, M. Astraldi and M. Crépon., 2004. The dynamics of the Sicily Strait: A comprehensive study from observations and models.. II, Deep Sea Researchearch 51: 411-440.

Birol, F., M. Cancet, and C. Estournel, 2010. Aspects of the seasonal variability of the Northern Current (NW Mediterranean Sea) observed by altimetry, Journal of Marine. Systems, 81, 297‑311, doi:10.1016/j.jmarsys.2010.01.005.

Bouffard, J., S. Vignudelli, M. Herrmann, F. Lyard, P. Marsaleix, Y. Me´nard, and P. Cipollini 2008. Comparison of ocean dynamics with a regional circulation model and improved altimetry in the northwestern Mediterranean, Terrestrial, Atmospheric and Oceanic Sciences., 19, 117–133, doi:10.3319/TAO.2008.19.1-2.117(SA).

Bouffard, J., A. Pascual, S. Ruiz, Y. Faugère, and J. Tintoré, 2010. Coastal and mesoscale dynamics characterization using altimetry and gliders: A case study in the Balearic Sea, Journal of Geophysical Research., 115, C10029, doi:10.1029/2009JC006087.

Budillon, Gasparini, Schroeder, 2009. Persistence of an eddy signature in the central Tyrrhenian basin, Deep Sea Research Part II: Topical Studies in Oceanography, Volume 56, Issues 11-12, Pages 713-724, ISSN 0967-0645, 0.1016/j.dsr2.2008.07.027.

Buongiorno Nardelli B, Santoleri R, Zoffoli S, and Marullo S 1999. Altimetric signal and three-dimensional structure of the sea in the Channel of Sicily. Journal of Geophysical Research 104 (C9): 20585-20603

Buongiorno Nardelli, B., G. Larnicol, E.D'Acunzo, R. Santoleri, S. Marullo, and P. Y. Le Traon, 2002. Near real time SLA and SST products during 2-years of MFS pilot project: Processing, analysis of the variability and of the coupled patterns, Annales Geophysicae, 20, 1–19.

Buongiorno Nardelli B., Santoleri R., 2004. Reconstructing synthetic profiles from surface data, Journal of Atmospheric and Oceanic Technology., vol.21, 4, 693-703.

Buongiorno Nardelli B., Santoleri R., 2005. Methods for the reconstruction of vertical profiles from surface data: multivariate analyses, residual GEM and variable temporal signals in

the North Pacific Ocean, J Journal of Atmospheric and Oceanic Technology. Vol. 22, No. 11, pages 1763 1782.

Buongiorno Nardelli B., S. Colella, R. Santoleri, M. Guarracino, A. Kholod, 2010. A re-analysis of Black Sea Surface Temperature, Journal of Marine Systems.., 79, 1-2, 50-64, doi:10.1016/j.jmarsys.2009.07.001

Cazenave, P. Bonnefond, F. Mercier, K. Dominh, V. Toumazou, 2002. Sea level variations in the Mediterranean Sea and Black Sea from satellite altimetry and tide gauges, Global and Planetary Change, Volume 34, Issues 1-2, Pages 59-86, ISSN 0921-8181.

Challenor, P.G., J.F. Read, R.T. Pollard, and R.T. Tokmakian, 1996.Measuring surface currents in the Drake passage from altimetry and hydrographyd, . Journal of Physical Oceanography.,2 6(12), 2748-2759.

Chelton, D. B., and F. J. Wentz, 2005. Global microwave satellite observations of sea surface temperature for numerical weather prediction and climate research. Bulletin of the American Meteorological Society. , 86, 1097–1115.

Comici, C. and A. Bussani, 2007. Analysis of the River Isonzo discharge (1998‑2005). Bolletino di Oceanologia Teorica ed Applicata 48: 435‑454.

Crépon, M., M. Boukthir, M. Barnier and F. Aikman III, 1989. Horizontal ocean circulation forced by deep water formation. Part I: An analytical study. J. Journal of Physical Oceanography., 19: 1781-1792.

Davis, R. E, 1985. Drifter observations of coastal currents during CODE: The method and descriptive view, Journal of Geophysical Research., 90, 4741‑4755, doi:10.1029/JC090iC03p04741.

De Wit, M. and G. Bendoricchio. 2001. Nutrient fluxes in the Po basin. Science of the Total Environment 273: 147‑161. doi:10.1016/S0048-9697(00)00851-2.

Doney SC, Glover DM,McCue SJ, Fuentes M. 2003. Mesoscale variability of sea-viewing wide field-of-view sensor (SeaWiFS) satellite ocean color: Global patterns and spatial scales. Journal of Geophysical Research. 108(C2):3024

Doney, S. C, 2006. Plankton in a warmer world, Nature, 444, 695-696.

Ducet, N., P. Y. Le Traon, and G. Reverdin 2000. Global high‑resolution mapping of ocean circulation from TOPEX/Poseidon and ERS1 and‑2, Journal of Geophysical Research., 105(C8), 19,477‑19,498, doi:10.1029/2000JC900063.

Elliot A. J. And F. De Strobel, 1978. Oceanographic conditions in the coastal waters of N.W. Italy during the spring of 1977, Bollettino di geofisica teorica ed applicata, XX, 79, 251-262.

Emery, W. J., and R. E. Thomson (1998), Data Analysis Methods in Physical Oceanography, Pergamon, Oxford, U. K.

Fang, W., Hsieh, W.W., 1993. Summer sea surface temperature variability off Vancouver Island from satellite date. Journal of Geophysical Research. 98 _C8., 14391–14400.

Fu, L.-L., and A. Cazenave 2001. Satellite Altimetry and Earth Sciences: A Handbook of Techniques and Applications, 463 pp., Academic, San Diego, Calif.

Gallaudet, T.C., Simpson, J.J., 1994. Empirical orthogonal function analysis of remotely sensed sea surface temperature variability and its relation to interior oceanic processes off Baja California. International Journal of Remote Sensing. Environ. 47, 375–389.

Garc´ıa-Lafuente, J., Vargas, J. M., Criado, F., Garcia, A., Delgado,J., and Mazzola, S., 2005. Assessing the variability of hydrographic processes influencing the life cycle of the Sicilian Channel anchovy, Engraulis encrasicolus, by satellite imagery, Fisheries Oceanography, 14(1), 32–46.

Garcia, 2008. Variability of chlorophyll-*a* from ocean color images in the La Plata continental shelf region. Continental Shelf Research 28:1,568–1,578.

Gascard, J. C., 1978. "Mediterranean Deep Water Formation, Baroclinic Instability and Oceanic Eddies". Oceanologica Acta, 1, 315-330.

Gasparini G.P., Zodiatis G., Astraldi M., Galli C., Sparnocchia S. 1999, Winter Intermediate water lenses in the Ligurian Sea, Journal of Marine Systems. 20 319-332

Goodrum, G., K. B. Kidwell and W. Winston, 2000: NOAA KLM User's Guide September 2000 Revision. NOAA/ NESDIS/NCDC.

Hopkins, T. S., 1985, Physics of the sea, in R. Margalef (ed.), Key Environments: Western Mediterranean (New York: Pergamon Press), pp. 100-125.

Iida, Sei-Ichi Saitoh, 2007. Temporal and spatial variability of chlorophyll concentrations in the Bering Sea using empirical orthogonal function (EOF) analysis of remote sensing data, Deep Sea Research Part II: Topical Studies in Oceanography, Volume 54, Issues 23-26, Pages 2657-2671, ISSN 0967-0645, 10.1016/j.dsr2.2007.07.031.

Ioannone, Catucci, Grasso, Eusebi Borzelli, 2011. Decadal variability and scales of the sea surface structure in the northern Ionian, Continental Shelf Research, Volume 31, Issue 1, 15 Pages 37-46, ISSN 0278-4343, 10.1016/j.csr.2010.11.001.

Iudicone, D., R. Santoleri, S. Marullo, and P. Gerosa, 1998. Sea level variability and surface eddy statistices in the Mediterranean Sea from TOPEX/POSEIDON data, Journal of Geophysical Research., 103(C2), 2995‑3011,doi:10.1029/97JC01577.

Jordi, Wang, 2009.Mean dynamic topography and eddy kinetic energy in the Mediterranean Sea: Comparison between altimetry and a 1/16 degree ocean circulation model, Ocean Modelling, Volume 29, Issue 2, Pages 137-146, ISSN 1463-5003, 10.1016/j.ocemod.2009.04.001

Katara, I., J. Illian, G. J. Pierce, B. Scott, and J. Wang 2008. Atmospheric forcing on chlorophyll concentration in the Mediterranean, Hydrobiologia, 612, 33-48.

Kelly, K.A., and S.T. Gille, 1990. Gulf stream surface transport and statistica 69° W from GEOSAT altimeter. Journal of Geophysical Research,95, 3149-3161.

Bibliography

Kidwell, K. B.1998. NOAA Polar Orbiter Data User's Guide (TIROS-N, NOAA-6, NOAA-7, NOAA-8, NOAA-9, NOAA-10, NOAA-11, NOAA-12, NOAA-13 and NOAA-14) Revision. NOAA/NESDIS/NCDC.

Laggerloef, G.S.E., Berstein, R.L., 1988. Empirical orthogonal function analysis of advanced very high resolution radiometer surface temperature patterns in Santa Barbara channel. Journal of Geophysical Research. 936., 6863–6873.

Larnicol, G., N. Ayoub, and P. Y. Le Traon 2002. Major changes in Mediterranean Sea level variability from 7 years of TOPEX/Poseidon and ERS‑1/2 data, Journal of Marine Systemst., 33‑34, 63‑89, doi:10.1016/S0924-7963(02)00053-2.

Kelly, K.A., 1985. The influence of wind and topography on the surface temperature patterns over the northern California slope. Journal of Geophysical Research. 90, 11783–11798.

Kelly, K.A., 1988. Comment on 'empirical orthogonal function analysis of advanced very high resolution radiometer surface temperature patterns in Santa Barbara channel', in: Laggerloef, G.S.E., Berstein, R.L. Journal of Geophysical Research., 93, C12, pp. 15753–15764.

Korotaev, Oguz, Nikiforov, and Koblinsky. 2003. Seasonal, interannual and mesoscale variability of the Black Sea upper layer circulation derived from altimeter data. Journal of Geophysical Research 108(C4):3122, doi:1029/2002JC001508.

Krivosheya V.G. and I.M. Ovchinnikov, 1973. Pecularities in the geostrophic circulation of the waters of the Tyrrhenian Sea. Oceanology, 13, 822-827.

Lacombe, H., J. C. Gascard, J. Gonella, and B. J. P. 1981. Response of the Mediterranean to the water and energy fluxes across its surface, on seasonal and interannual scales, Oceanologica Acta, 4, 2, 120-130.

Lacombe, H., and P. Tchernia 1972. Characteres hydrologiques et circulation des eaux en Mediterranee, in The Mediterranean Sea: a natural sedimentation ladoratory, edited by D. Stanley, Dowden Hutchinson and Ross, Strousberg.

Larnicol G, Le Traon PY, Ayoub N, De Mey P. 1995. Mean sea level and surface circulation variability of the Mediterranean Sea from 2 years of TOPEX/POSEIDON altimetry. Journal of Geophysical Research 100 (C12): 25163-25177

Lermusiaux, P.F.J. (1999) Estimation and study of mesoscale variability in the Strait of Sicily. Dynamics of Atmospheres and Oceans. 29:255–303.

Lermusiaux, P.F.J. and Robinson, A.R. 2001. Features of dominant mesoscale variability, circulation patterns and dynmics in the Strait of Sicily. Deep Sea Research. I 48:1953–1997.

Le Traon, P.Y., and P. De Mey, 1994. The eddy field associated with the Azores Front east of the Mid-Atlantic Ridge as observed by the GEOSAT altimeter. Journal of Geophysical Research,9 9, 9907-9923.

Marasoviæ, I., Grbec, B. & M. Moroviæ, 1995. Long-term production changes in the Adriatic. Netherlands Journal of Sea Research 34(4): 267-273.

Marullo S., Santoleri R., and Bignami F., 1994. The surface characteristics of the Tyrrhenian sea : historical satellite data analysis. . In: La Violette, P. E.(Ed), Seasonal and interannual variability of the Western Mediterranean sea, Coastal and Estuarine Studies, 46, 135-154.

Marullo, S., R. Santoleri, P. Malanotte-Rizzoli, and A. Bergamasco 1999. The sea surface temperature field in the Eastern Mediterranean from advanced very high resolution radiometer (AVHRR) data: II. Interannual variability, Journal of Marine Systemst, 20, 83– 112.

Mauri, E., and P. ‐ M. Poulain 2004. Wind ‐ driven currents in Mediterranean drifter ‐ data, Tech. Rep. 01/2004/OGA/1, 25 pp., Oceanogr. Geofis. Sper., Trieste, Italy.

Millot C., 1999. Circulation in the western Mediterranean Sea, Journal of Marine Systems, 20, 423-442.

Millot C., Taupier-Letage I., 2004. Circulation in the Mediterranean Sea. The Handbook of Environmental Chemistry, Vol 1.

Morovic M., Grbec B., Marasovic I. 2004. Changed Patterns Of Remotely Sensed Chlorophyll A In The Adriatic-Influence Of Meteorological Conditions. Gayana, 68(2): 405-410

Mozeti´c, P., Solidoro, C., Cossarini, G., Socal, G., Precali, R., Franc´ e, J., Bianchi, F., Smodlaka, N., De Vittor, C., and Fonda-Umani, S. 2010. Recent trends towards oligotrophication of the northern Adriatic: evidence from chlorophyll a time series, Journal of the Coastal and Estuarine Research Federation., 33, 362–375.

Nielsen, J.N., 1912. Hydrography of the Mediterranean and adjacent waters. Rep. Dan. Oceanogr. Exp. Medit., 1: 77-192.

Palacios 2004, Seasonal patterns of sea-surface temperature and ocean color around the Galápagos: regional and local influences, Deep Sea Research Part II: Topical Studies in Oceanography, Volume 51, Issues 1-3, Pages 43-57, ISSN 0967-0645, 10.1016/j.dsr2.2003.08.001.

Pascual A, Buongiorno Nardelli B, Larnicol G, Emelianov M, Gomis D 2002. A case of an intense anticyclonic eddy in the Balearic Sea (western Mediterranean). Journal of Geophysical Research 107 (C11): 3183-3193

Pascual A, Pujol MI, Larnicol G, Le Traon PY, Rio MH 2007. Mesoscale mapping capabilities of multisatellite altimeter missions: first results with real data in the Mediterranean Sea. Journal of Marine Systems65: 190-211

Perilli, A., V. Rupolo, and E. Salusti 1995. Satellite investigations of a cyclonic gyre in the central Tyrrhenian Sea (western Mediterranean Sea), Journal of Geophysical Research. 100, 2487–2500, doi:10.1029/94JC01315.

Poulain, P.M. 2001. Adriatic Sea Surface Circulation as derived from drifter data between 1990 and 1999, Journal of Marine Systems., 29, 3–32, doi:10.1016/S0924-7963(01)00007-0.

Poulain, P.-M. and Zambianchi E, 2007. Near-surface circulation in the central Mediterranean Sea as deduced from Lagrangian drifters in the 1990's, Continental Shelf Research., 27(7), 981–1001.

Poulain, P.‐M., and E. Zambianchi (2007), Near‐surface circulation in the central Mediterranean Sea as deduced from Lagrangian drifters in the 1990s, Continental Shelf Research., 27(7), 981‐1001, doi:10.1016/j.csr.2007.01.005.

Poulain, P.‐M., R. Barbanti, R. Cecco, C. Fayos, E. Mauri, L. Ursella, and P. Zanasca 2004. Mediterranean Surface Drifter Database: 2 June 1986 to 11 November 1999, Tech. Rep. 78/2004/OGA/31, Oceanogr. Geofis. Sper., Trieste, Italy.

Poulain, P.‐M., R. Gerin, E. Mauri, and R. Pennel 2009. Wind effects on drogued and undrogued drifters in the eastern Mediterranean, Journal of Atmospheric and Oceanic Technology., 26, 1144‐1156, doi:10.1175/2008JTECHO618.1

Pujol, M.‐I., and G. Larnicol 2005. Mediterranean sea eddy kinetic energy variability from 11 years of altimetric data, Journal of Marine Systems 58, 121‐142, doi:10.1016/j.jmarsys.2005.07.005

Ralph, E. A., and P. P. Niiler 1999. Wind driven currents in the tropical Pacific, J. Journal of Physical Oceanography., 29, 2121‐2129.

Reynolds, Richard W., Thomas M. Smith, Chunying Liu, Dudley B. Chelton, Kenneth S. Casey, Michael G. Schlax, 2007: Daily high-resolution-blended analyses for sea surface temperature. Journal of Climate, **20**, 5473–5496.

Rhein, M., U. Send, B. Klein, and G. Krahmann 1999. Interbasin deep water exchange in the western Mediterranean, Journal of Geophysical Research., 104(C10), 23,495–23,508, doi:10.1029/1999JC900162.

Rio, M, and F. Hernandez 2004. A mean dynamic topography computed over the world ocean from altimetry, in‐situ measurements and a geoid model, Journal of Geophysical Research., 109, C12032, doi:10.1029/ 2003JC002226.

Rio, Poulain, Pascual, Mauri, Larnicol, 2007. A mean dynamic topography of the Mediterranean sea computed from altimetric data and in-situ measurements. Journal of Marine Systemst. 65, 484–508.

Robinson, A.R., Sellschopp, J., Warn-Varnas, A., Leslie, W.G., Lozano, C.J., Haley Jr., P.J., Anderson, L.A., Lermusiaux, P.F.J., 1999. The Atlantic Ionian Stream. Journal of Marine Research., 20(1-4), 129-156.

Roether, W., and R. Schlitzer 1991. Eastern Mediterranean deep water renewal on the basis of chlorofluoromethanes and tritrium, Dynamics of Atmospheres and Oceans, 15, 333-354.

Ruiz, S., Pascual, A., Garau, B., Faugere, Y., Alvarez, A., Tintoré, J. 2009. Mesoscale dynamics of the Balearic Front, integrating glider, ship and satellite data, Journal of Marine Systems Vol. 78, pp S3-S16.

Smith, T. M., and R. W. Reynolds, 2003: Extended reconstruction of global sea surface temperatures based on COADS data (1854–1997). Journal of Climate, 16, 1495–1510

Sorgente, R., A.F. Drago and A. Ribotti 2003. Seasonal variability in the Central Mediterranean Sea circulation. Annales Geophysicae, 21: 299-322.

Sparnocchia, S., Gasparini, G. P., Astraldi, M., Borghini, M., & Pistek, P. 1999. Dynamics and mixing of the Eastern Mediterranean Outflow in the Tyrrhenian Basin. Journal of Marine Systems, 20, 301–317.

Strub, James, 2000. Altimeter-derived variability of surface velocities in the California Current System: 2. Seasonal circulation and eddy statistics, Deep Sea Research Part II: Topical Studies in Oceanography, Volume 47, Issues 5-6, Pages 831-870, ISSN 0967-0645, 10.1016/S0967-0645(99)00129-0.

Swenson, M. S., and P. P. Niiler 1996. Statistical analysis of the surface circulation of the California Current, Journal of Geophysical Research., 101, 22,631‑22,645, doi:10.1029/96JC02008.

Tait, L., 1984. The physical oceanography of the Tyrrhenian and Ligurian Sea, Proceedings of the 6th Congress of the Associazione Italiana di Oceanologia e Limnologia, 48-84.

Toole and Siegel 2001, "Modes and mechanisms of ocean color variability in the Santa Barbara Channel," Journal of Geophysical Research. **106** (C11), 26985-27000.

Vazquez-Cuervo, J., J. Font, and J. Martinez-Benjamin, 1996: Observations on the circulation in the Alboran Sea using ERS1 altimetry and sea surface temperature data. Journal of Physical Oceanography.,26, 1426–1439.

Vignudelli, S., G. P. Gasparini, M. E. Schiano, and M. Astraldi 1999. A possible influence of the North Atlantic Oscillation on the western Mediterranean circulation, Geophysical Research Letters 26, 623– 626.

Vignudelli, S., P. Cipollini, M. Astraldi, G. P. Gasparini, and G. M. R. Manzella 2000. Integrated use of altimeter and *in situ* data for understanding the water exchanges between the Tyrrhenian and Ligurian seas, Journal of Geophysical Research., 105, 19,649–19,663.

Vignudelli S, Cipollini P, Reseghetti F, Fusco G, Gasparini GP, Manzella G 2003. Comparison between XBT data and TOPEX/Poseidon satellite altimetry in the Ligurian-Tyrrhenian area. Annales Geophys 21: 123-135

Volpe, G., R. Santoleri, V. Vellucci, M. Ribera d'Alcala, S. Marullo, and F. D'Ortenzio 2007. The colour of the Mediterranean Sea: Global versus regional bio-optical algorithms evaluation and implication for satellite chlorophyll estimates, Remote Sensing of Environment, 107, 625-638.

Wilson C, Adamec D. 2001. Correlations between surface chlorophyll and sea surface height in the tropical Pacific during the 1997–1998 El Ni˜ no-Southern Oscillation event. Journal of Geophysical Research. 106(C12):31175–88

Wilson C, Adamec D. 2002. A global view of bio-physical coupling from SeaWiFS and TOPEX satellite data, 1997–2001. Geophys. Res. Lett. 29(8):1257

Wilson, C., and V. J. Coles 2005. Global climatological relationships between satellite biological and physical observations and upper ocean properties, Journal of Geophysical Research., 110, C10001, doi:10.1029/2004JC002724.

Yoder JA, Kennelly MA. 2003. Seasonal and ENSO variability in global ocean phytoplankton chlorophyll derived from 4 years of SeaWiFS measurements. Global Biogeochem. Cycles 17(4):1112

Volkov, Denis L., 2005: Interannual Variability of the Altimetry-Derived Eddy Field and Surface Circulation in the Extratropical North Atlantic Ocean in 1993–2001. J. Journal of Physical Oceanography., **35**, 405–426.

Zanchettin, D., P. Traverso, and M. Tomasino. 2008. Po River discharges: A preliminary analysis of a 200-year time series. Climatic Change 89: 411‑433. doi:10.1007/s10584-008-9395-z.